Geologian tutkimuskeskus, Opas - Geological Survey of Finland, Guide 48

MSF Mini-Symposium

held in conjunction with IMA COM Short Course

"MODERN APPROACHES TO ORE AND ENVIRONMENTAL MINERALOGY"

Espoo Finland, June 11-17, 2000

Extended Abstracts

Edited by

Kari Kojonen, Liisa Carlson, Pentti Hölttä and Seppo Lahti

HELSINKI UNIVERSITY OF TECHNOLOGY

ESPOO
THE CAPITAL OF KNOWLEDGE

GTK

MSF Mini-Symposium, 2000

(Held under the auspices of Mineralogical Society of Finland, Geological Survey of Finland and Helsinki University of Technology in conjunction with IMA COM Short Course: Modern Approaches to Ore and Environmental Mineralogy)

Venue: Sea Park Congress, Training and Exhibition Centre
Tyrskyvuori 4, 02320 Espoo, Finland

ORGANISING COMMITTEE

Kari Kojonen, Research & Development, Geological Survey of Finland
Pentti Hölttä, Research & Development, Geological Survey of Finland
Seppo Lahti, Regional Office for Southern Finland, Geological Survey of Finland
Tegist Chernet, Research & Development, Geological Survey of Finland
Tuija Mäkinen, Laboratory of Engineering Geology and Geophysics, HUT
Bengt Söderholm, Laboratory of Engineering Geology and Geophysics, HUT
Jalle Tammenmaa, Laboratory of Engineering Geology and Geophysics, HUT

ABSTRACT VOLUME
Compiled and edited by
Kari Kojonen, Liisa Carlson, Pentti Hölttä and Seppo Lahti

Front cover: A false coloured optical image of euhedral arsenopyrite grains intergrown with pyrrhotite, sphalerite, galena and chalcopyrite, height of the figure 1.86 mm, reflected light, Rauhala deposit, Finland

CONTENTS

Gold mineralisation at Zarshuran, NW Iran

H.H. Asadi[a,b], J.H.L. Voncken[c], M.Hale[b,c]

[a] *Ministry of Culture and Higher Education, Dr. Beheshti Avenue, Shahid Sabounchi Cross, Tehran, Iran.*
[b] *International Institute of Aerospace Survey and Earth Sciences, Kanaalweg 3, 2628 EB Delft, Netherlands*
[c] *Delft University of Technology, Department of Applied Earth Sciences, Mijnbouwstraat 120, 2628 RX Delft, Netherlands*
Harouni@itc.nl., Hale @itc.nl, J.H.L.Voncken@ta.tudelft.nl

ABSTRACT. At Zarshuran, north of Takab in northwest Iran disseminated gold occurs in Precambrian sedimentary rocks. Detailed investigation of the mineralogy and petrographic relationships give information over the evolution of the hydrothermal fluid in terms of chemistry and temperature. Two phases of mineralization are recognized.

1 INTRODUCTION

At Zarshuran, north of Takab in northwest Iran disseminated gold occurs in Precambrian sedimentary rocks. Recent exploration for gold has established a probable reserve of 2.5 million tonnes of ore with an average grade of 10 g/t gold. Recent studies indicate that the Zarshuran Deposit is of the Carlin-type (Asadi et al., 1999, Mehrabi et al., 1999, Asadi et al. 2000).

Figure 1. Sequence of minerals and temperature ranges in relation to gold deposition

Early Hydrothermal Gold Mineralisation (Arsenian Pyrite) (T > 400 °C)

galena	PbS		
semseyite	$Pb_9Sb_8S_{21}$	T = 350 – 400 °C	***Sb-rich hydrothermal fluid***
plagionite	$Pb_5Sb_8S_{17}$		
twinnite	$Pb(As,Sb)_2S_4$		
geocronite	$Pb_{14}(Sb,As)_6S_{23}$		
baumhauerite	$Pb_3As_4S_9$		
aktashite	$Cu_6Hg_3AsS_4$		**T (°C)**
stibnite	Sb_2S_3		
getchellite	$AsSbS_3$	about 260 °C -300 °C	
lorandite	$TlAsS_2$,		
christite	$TlHgAsS_3$	120 – 250 °C	
orpiment	$As2S_3$		
realgar	AsS		***As-rich hydrothermal fluid***

Late Gold mineralisation (Colloform)

2 RESULTS

The gold occurs mainly in solid solution in arsenian pyrite (HT) and colloform pyrites and sphalerites (LT) (Asadi et al. (1999). Besides the telluride coloradoite (HgTe), several Pb(As,Sb)-sulphosalts, (As,Sb)-sulphides and Tl-minerals occur in the deposit. The telluride indicates a magmatic contribution to the mineralisation, and from the sequence of crystallisation deductions can be made about the formation of the mineralisation. The scheme shown in Figure 1 shows the identified sulphosalt-minerals in their order of crystallisation, and temperature ranges for their stability as mentioned in the literature (Moëlo 1983, Radtke et al. 1977, Weisberg 1965).

REFERENCES

Asadi H.H., Voncken J.H.L., Hale, M. (1999) Invisible Gold at Zarshuran, Iran. Economic Geology, 94, 1367 - 1374

Asadi, H.H., Voncken J.H.L., Kühnel, R.A., Hale, M. (2000) Petrography, Mineralogy, and Geochemistry of the Zarshuran Carlin-like Gold Deposit, NW Iran. Mineralium Deposita, in press.

Mehrabi B., Yardley, B.W.D., Cann, J.R. (1999)Sediment Hosted disseminated gold Mineralisation at Zarshuran, NW Iran. Mineralium Deposita, 34, 673 - 696.

Moëlo Y (1983) Contribution à l'etude des formation des sulpures complexes d'antimoine et plomb. Documents de B.R.G.M., No. 55 (Ph.D. Thesis, Université Pierre et Marie Curie, Paris), 207 pp.

Radtke AS, Dickson FW, Slack JF, Brown KL (1977) Christite, a new thallium mineral from the Carlin gold deposit, Nevada. American Mineralogist, 62, 421-425

Weissberg BG (1965) Getchellite, $AsSbS_3$, from Humboldt County, Nevada. American Mineralogist 50, 1817 – 1826

Mineralogy of ochreous precipitates formed from mine effluents

L. Carlson
Geological Survey of Finland, P.O. Box 96, FIN-02150 Espoo, Finland
Liisa.Carlson@gsf.fi

ABSTRACT. The most important factors affecting the mineralogy of precipitates formed from mine effluents are pH and sulphate concentration. From high-sulphate, low pH effluents jarosite, schwertmannite or SO_4-rich goethite are formed. At near-neutral pH and low sulphate concentrations ferrihydrite is favoured by the presence of silicate whereas goethite is favoured by the presence of carbonate in solution. These minerals often occur as mixtures.

1 INTRODUCTION

Sulphide minerals exposed in mines and tailings decompose in the presence of H_2O and O_2 to yield an acid effluent high in dissolved SO_4^{2-}, Fe^{2+} and other contaminants. Dilution with surface waters or influence of adjacent carbonaceous rocks may change the pH, as exemplified by the range of pH values from 2.6 to 7.8 observed by Bigham et al. (1992) in 37 sulphide and coal mine effluent sites in Finland and the United States.

Oxidation of Fe^{2+} usually leads to the formation of an ochreous precipitate, familiar in streams, ditches and ponds. The rate of abiotic oxidation of iron is negligible at pH < 4.5 but acidophilic bacteria such as *Thiobacillus ferrooxidans* catalyse the oxidation (Singer & Stumm, 1970). The bacteria use the energy of Fe oxidation for growth but do not actively participate in mineral formation, which is controlled by geochemical parameters (pH, $[SO_4^{2-}]$, etc).

2 MINERALOGY

A variety of minerals are found in ochreous precipitates from mine drainage:

Schwertmannite, $Fe_8O_8(OH)_6SO_4$, is the most common mineral formed from acid effluents. It was first described by Bigham et al. in 1990 and accepted by IMA in 1992 (Bigham et al., 1994). Optimal conditions for its formation are pH values in the range 3 to 4 and sulphate concentrations of 1000 to 3000 mg/L. Schwertmannite is poorly crystalline, with high specific surface area and strong yellow colour (Munsell hue 10YR–2.5YR). Structurally it is related to akaganéite (β-FeOOH), but instead of Cl the tunnels are occupied by SO_4. Natural schwertmannites contain 10–14% (w/w) SO_4.

At the closed Paroistenjärvi Cu-W-As mine in SW Finland, schwertmannite was found to contain 7 wt% As and only 3.8 wt% SO_4. In response to this finding, mineral synthesis and adsorption experiments were conducted to determine if AsO_4 is capable of substituting for SO_4 in the structure of schwertmannite. An oxyhydroxyarsenate of Fe could not be synthesised and schwertmannite structure was only formed when enough SO_4 was present in solution. AsO_4, however, competed successfully with SO_4 for surface adsorption sites even at much lower concentrations (0.4 mg/L As against 900 mg/L SO_4; Carlson & Bigham, 1992).

Jarosite, $(Na,K)Fe_3(OH)_6(SO_4)_2$, is formed at pH 1-3 and sulphate concentrations > 3000 mg/L. Such extreme conditions occur only occasionally in mine drainage environments and

jarosite is thus mostly found as a minor component together with schwertmannite or goethite. Jarosite is well crystalline and the colour is straw yellow (Munsell hue 2.5YR-5YR).

Ferrihydrite, $Fe_5HO_8 \cdot 4H_2O$, is a major component of ochreous precipitates from mine effluents with pH > 5. It is produced by rapid oxidation (which may be abiotic) and hydrolysis of iron. Dissolved silica favours ferrihydrite formation (Carlson & Schwertmann, 1981) and it is also known to be formed in organic-rich environments. Ferrihydrite is poorly crystalline, has high specific surface area and its colour is redder than that of schwertmannite (Munsell hue 5YR-7.5YR). Ferrihydrite preferentially scavenges silica from solution, which may lower its point of zero charge from pH 8 (pure synthetic ferrihydrite) to around pH 5 (natural ferrihydrite with 6.8 wt% Si)(Schwertmann & Fechter, 1982).

Goethite, α-FeOOH, is often present in mine drainage precipitates as a minor compound together with schwertmannite or ferrihydrite. Because goethite is thermodynamically the only stable mineral of those mentioned here, e.g. schwertmannite and ferrihydrite tend be transformed via dissolution to goethite. Bigham et al. (1992) found goethite as a major compound where low-pH effluents are neutralized by carbonate-charged waters. Recently, Carlson & Kumpulainen (2000) described a SO_4-rich goethite (7.5-10.5 wt% SO_4) from the Hammaslahti Cu-Zn-Au mine in eastern Finland that is formed at conditions typical for schwertmannite (pH 3.5-3.8, SO_4 1000-1500 mg/L). Webster et al. (1998) found goethite with SO_4-content ranging from 5.6 to 11.3 wt% from the former Tui Pb-Zn mine in New Zealand.

Lepidocrocite, γ-FeOOH, was reported by Milnes et al. (1992) to occur in mine drainage precipitates in Australia. It is a common mineral in certain types of ochreous precipitates in Finland but has not been found in mine effluents.

3 REFERENCES

Bigham, J.M., Schwertmann, U., Carlson, L., & Murad, E. 1990. A poorly crystallized oxyhydroxysulfate of iron formed by bacterial oxidation of Fe(II) in acid mine waters. Geochimica et Cosmochimica Acta, 54, 2743-2758.

Bigham, J.M., Schwertmann, U., & Carlson, L. 1992. Mineralogy of precipitates formed by the biogeochemical oxidation of Fe(II) in mine drainage. In: Biomineralization. Processes of Iron and Manganese. (H.C.W Skinner & R.W. Fitzpatrick, Eds.) Catena Supplement, 21, 219-232.

Bigham, J.M., Carlson, L., & Murad, E. 1994. Schwertmannite, a new iron oxyhydroxysulfate from Pyhäsalmi, Finland, and other localities. Mineralogical Magazine, 58, 641-648.

Bigham, J.M., Schwertmann, U., Traina, S.J., Winland, R.L., & Wolf, M. 1996. Schwertmannite and the chemical modelling of iron in acid sulfate waters. Geochimica et Cosmochimica Acta, 60, 2111-2121.

Carlson, L. & Bigham, J.M. 1992. Retention of arsenic by precipitates from acid mine drainage. W.M. Goldschmidt Conference, Reston, Virginia. Abstracts, pp. A-16-A-17.

Carlson, L. & Kumpulainen, S. 2000. Mineralogy of precipitates formed from mine effluents in Finland. Tailings and Mine Waste 2000, Fort Collins, Colorado. Balkema, Rotterdam, pp. 269-275.

Carlson, L. & Schwertmann, U. 1981. Natural ferrihydrites in surface deposits from Finland and their association with silica. Geochimica et Cosmochimica Acta, 45, 421-429.

Carlson, L. & Schwertmann, U. 1990. The effect of CO_2 and oxidation rate on the formation of goethite versus lepidocrocite from an FeII system. Clay Minerals, 25, 65-71.

Milnes, A.R., Fitzpatrick, R.W., Self, P.G., Fordham, A.W., & McClure, S.G. 1992. Natural iron precipitates in a mine retention pond near Jaribu, Northern Territory, Australia. In: Biomineralization. Processes of Iron ans Manganese. (H.C.W Skinner & R.W. Fitzpatrick, Eds.) Catena Supplement, 21, 233-262.

Schwertmann, U. & Fechter, H. 1982. The point of zero charge of natural and synthetic ferrihydrites and its relation to adsorbed silicate. Clay Minerals, 17, 471-476.

Singer, P.C. & Stumm, W. 1970. Acid mine drainage: the rate-determining step. Science, 167, 1121-1123.

Webster, J.G., Swedlund, P.J., & Webster, K.S. 1998. Trace metal adsorption onto an acid mine drainage iron(III) oxy hydroxy sulfate. Environmental Science & Technology, 32, 1361-1368.

Skarn textures

Cristiana L. Ciobanu, Nigel J. Cook
Geological Survey of Norway, N-7491 Trondheim, Norway
Cristiana.Ciobanu@ngu.no, Nigel.Cook@ngu.no

ABSTRACT. Skarn deposits carry useful information on primary and overprinting processes through their textures. Although no textures are skarn-specific, the prevalence of non-equilibrium conditions allows certain key textural patterns to be well-preserved in many deposits. This paper examines the theoretical background for dissipative textures in relation to specific instabilities at skarn-forming fronts in order to show their patterning potential. Phenomena including Liesegang-Ostwald banding, competitive particle growth and oscillatory zoning in minerals are reviewed, citing relevant examples. The Ocna de Fier Fe-Cu-(Zn,Pb) deposit, Romania is used as a case study.

1 INTRODUCTION

Various series of textures of primary and/or overprinting character occur in skarn deposits. None of them are exclusively skarn-specific as such, but sets of sequential space/ time textures are instructive and sometimes unique windows to the individual combination of prograde-retrograde paths followed by mineralising processes in given skarn-forming systems. Zonation patterns are nevertheless intimately associated with skarn formation and thus represent intrinsic variations on the theme within any type of skarn deposit. Deposit-scale zonation is a useful exploration tool for skarn deposits (Meinert, 1997). Patterns seen in hand specimen, and various crystal zonation patterns, are instructive in placing constraints on the evolution of mineralising processes.

Metasomatism is defined as the mineralising process realised by reactions of a fluid moving through a porous solid, and requires an initial disequilibrium between fluid and solid. Formation of skarns, classically defined at the contact of intrusives with carbonate protholiths, is one of the most successful applications of metasomatic theory. Skarn-forming systems lie, however, within the broader metamorphic domain (Meinert, 1992), with various settings regarding nature of the fluids and protolith (e.g. silty limestone, BIF, dolomite, or pure limestone).

2 HISTORICAL PERSPECTIVE

The pioneering work of Korzhinskii (1970) established the differential equations of metasomatic zoning, assuming local equilibrium conditions at reaction front. Korzhinskii differentiated between two mechanisms of fluid transport in metasomatism: infiltration, driven by pressure gradients, and diffusion, dependent upon chemical potentials and thus an order of magnitude more sluggish than infiltration. By neglecting kinetic phenomena, he concluded that the metasomatic column realised through infiltration has sharp reaction fronts, whereas diffusion zoning would be represented by transitory limits. This conclusion led to the basis of chromatographic modelling or phase diagrams equilibria as valid methods to study skarn assemblages. Predicted bimetasomatic skarn zoning columns were obtained experimentally, reproducing different types of natural skarn-forming systems (Zaraisky, 1991).

Field evidence, however, indicates that fluid-rock interaction in the contact aureole is expressed in more complex crystal growth patterns and associated textures in mineral assemblages than can be predicted from petrogenetic grids, which assume static equilibrium. Liesegang banding (Liesegang, 1913), patterns of mineral coarsening (Ostwald, 1925), metamorphic banding (Turing, 1952), calc-silicate nodules/ rims of calc-silicate on chert nodules in

limestone (Joesten, 1974; 1991) and widespread oscillatory zoning in garnet, all in contact aureoles, were the basis for interpretations which consider mineral kinetics in a non-equilibrium environment (Joesten, 1991; Kerrick et al., 1991). Metastability and non-equilibrium are drawn into kinetic isotherms and overstepping parameters. They are considered as either imposed on the system by variation in parameters (e.g. pressure, temperature, infiltration) or are functions of kinetic barriers in relation to diffusion-controlled growth and nucleation. A whole suite of extrinsic parameters are thus defined as inherent to the various textures resulting from metasomatic growth, implying that reaction sequences cannot be modelled in terms of conventional phase equilibria theory.

Nevertheless, the rich potential of skarns as fertile ground for 'oscillatory textures' or other non-inherited mineral patterns is revealed in the larger context of revolutionary concepts regarding non-linear evolution of systems at far-from-equilibrium conditions (Glansdorff & Prigogine, 1971; Nicolis & Prigogine, 1977). Skarn-forming systems are included in this general picture of processes based on non-linear functions, either by the model of chromatography applied to metasomatic zoning theory (Guy, 1993) or by models of reaction-infiltration feedback addressed to skarn front hydrodynamics (Dipple & Gerdes, 1998).

3 DISSIPATIVE STRUCTURES AT REACTION FRONTS

The main characteristic of far-from-equilibrium systems is their potential to evolve into dissipative structures by amplifying, up to macroscopic scale, the small perturbations present in any given system, i.e., the background noise at the boundary, initial conditions, and rates of operating processes. If the system is sufficiently far-from-equilibrium, and at least two processes are coupled into a looping or feedback manner, such dissipative structures are initiated by self-organising phenomena, without external templates. Dissipative structures are therefore the expression of instabilities promoted into types of order attainable in non-equilibrium systems, e.g., chemical waves, multiple steady states, limit cycle, tori, knots and spontaneous morphological transformations. They are common in natural systems and are traced by the presence of oscillatory, periodic/non-periodic ordered patterns with increasing complexities, dependant upon the number of variables involved in the system. The variance of these descriptive variables can be analysed in multi-dimensional space and define the attractor of the evolving structure, e.g., steady state, periodic limit cycle, knotted, spiral, toroidal, strange, etc., of the evolving structure. Ortoleva (1994) demonstrated reaction fronts in geochemical systems to be highly predictable in promoting dissipative structures as spontaneous modes of patterning, coupling instabilities, e.g., oscillations, chaos, waves, with reaction-diffusion non-linear dynamics. Guy (1981) discussed mineral patterns from skarns in terms of dissipative structures.

According to Ortoleva et al. (1987a), the potential for self-organising phenomena in geochemical systems is linked to the fact that several well-established isothermal reaction-mass transport feedbacks exist in such systems. Examples include reactive-infiltration instability (Ortoleva et al., 1987b), supersaturation-nucleation-depletion cycle, competitive particle growth (CPG), autocatalytic crystal growth, mechanochemical coupling, etc., which can produce chemical, mineral and textural patterning in rocks. Such self-organisation feedback loops have direct application to skarns and may produce a wide variety of self-organised patterns, e.g., dissolution fingering or scalloping of reaction front, repeated precipitation in bands, spots, or other 2D or 3D precipitate patterns, multiple interacting mineral banding. The positive loop describes a sequences of processes that is closed on itself, e.g., reactive infiltration feedback; a negative loop involving time delays, e.g., the supersaturation-nucleation-depletion cycle, can also induce temporal oscillatory order. Contrary to traditional views, self-organisation analysis may be applied to observed mineral and textural patterns which cannot be explained in terms of inheritance from initial conditions, e.g., skarns formed in BIF environments, original bedding or other inhomogenities in the protholith, chert nodules in limestone etc., or imposed templates, e.g., variation of pressure, temperature or fluid fluxes.

4 LIESEGANG-OSTWALD BANDING

Mineral banding, clots and orbicules described in skarns (Table 1) and other rocks were interpreted as related to Liesegang banding, believed to form at the junction of two distinct lithologies, or when a fluid percolates through a rock with which the fluid is in disequilibrium. The

first examples came from skarn deposits, e.g., *Tiegererz*; magnetite bands in limestone from Ocna de Fier, Romania (von Cotta, 1864), and the spectacular and complex mineral banding from Hopunwaara-Pitkäranta, Karelia (Trüstedt, 1907). Liesegang phenomena is the spontaneous formation of banded patternslocalised rings of precipitate in 2D, and corkscrew patterns in 3D, obtained by interdiffusion of two co-precipitates. Ostwald (1925) showed that the mechanism for band formation may be produced without precipitation before the initiation of interdiffusion, as a result of sequential events involving supersaturation-nucleation-depletion in the zone where co-precipitate concentration profiles meet. Turing (1952) discussed spontaneous pattern formation in metamorphic rocks as a reaction-diffusion mechanism.

Ortoleva et al. (1987a) demonstrated that spatially periodic structures may result in rocks from the repetitive succession of supersaturation-nucleation-depletion (the Ostwald-Liesegang cycle; OLC), in which events are offset with respect to time. This is a time-delayed, negative loop oscillation which can explain e.g., Fe-oxide banding associated with uranium roll-type deposits (Ortoleva et al., 1986). The bifurcation of flow-driven OLC was investigated analytically for precipitate banding in a pyrite-goethite system (Sultan et al., 1990). Numerical simulations show that unsteady pulses of mineral deposition are obtained and develop in a variety of patterns, e.g., unsteady pulse, undulating patterns and discrete bands, with appropriate variance of parameters within the system.

5 COMPETITIVE PARTICLE GROWTH

Ortoleva (1994) discussed CPG as another type of feedback instability, which may form macroscopic patterns at reactive fronts in rocks undergoing changes in stress, temperature or gradients of composition. Precipitate banding and other self-patterning phenomena occur after cessation of nucleation with many small precipitate particles remaining in the system. Experiments with initially uniform sols evolved into self-organised patterns such as mottled, halos and spiral, which can not be explained by a simple OLC (Ortoleva, 1978). To account for post-nucleation pattern formation, the CPG model was started based on a feedback involving the dependence of the dissolution equilibrium constant on particle radius of curvature. The CPG phenomenon is in fact a competitive type of Ostwald ripening process. The CPG model of post-nucleation precipitate patterning states that also the competition can be co-operative, so that deviation of the local average particle size tends to amplify themselves and promote the appearance of what are termed 'greedy giants'. The CPG theory is promising with respect to many types of patterning involving crystal size, distribution, morphology, mineralogy and composition. For example, alternating banding of calcite and aragonite can be predicted. The theory may also be applied to zoning of minerals in solid solution.

6 SKARN-MARBLE CONTACT S

Analysis of reaction-infiltration feedback mechanisms indicate the reaction front to be predictable for disequilibrium and other non-linear phenomena, favouring the appearance of complex morphology also in relation to self-organising phenomena (Ortoleva et al., 1987b; Ortoleva, 1994) and examples of reaction fronts marked by inter-fingering morphologies quoted therein. Direct implication for skarn environments are that the marginal reaction front is highly likely to develop patterning in the form of dissipative structures, Liesegang-Ostwald banding and CPG patterning. As a direct consequence of reaction-infiltration feedback mechanism, the reaction front is characterised by specific morphologies reflected in cm-scale scalloped banded skarns or km-scale scalloped dolomitisation fronts. Such features are characteristic for skarn deposits (Meinert, 1997).

Analysis of reactive infiltration applied to skarn systems (Dipple & Gerdes, 1998) shows that infiltration-reaction feedback at skarn fronts can define two reaction parameters impacting on mineral reaction and fluid production: over-pressure potential and change in porosity. Observed stacking of mineral reaction reflected in banded skarn patterns (Table 1; Meinert, 1997) and isotopic fronts at the skarn-marble contact (Gerdes & Valley, 1994) may be produced by large increases in porosity at the skarn front, coupled with focused flow parallel to the contact, assuming reactive-infiltration instabilities provide for this.

Yardley & Lloyd (1995) have shown that similar complex oscillatory patterns may develop in skarn-reaction zones within metamorphic terranes, which, in reality, represent metasomatic 'sides' of reactive fronts, providing that a focused fluid flux is established. Metamorphic secondary porosity is generated by rapid decar-

bonation reaction at high lithostatic gradients under far-from-equilibrium conditions.

7 OSCILLATORY ZONING IN MINERALS

Oscillatory zoning is a common phenomenon in minerals, having been recorded from 75 species (Shore & Fowler, 1996). Reported examples of oscillatory zoning among ore minerals are, however, rare. Numerous imaging techniques exist to investigate fluctuations in zone thickness, composition and patterns of inclusions, dislocations and point defects; all are described collectively as 'oscillatory'. However the term accounts for a variety of grading, periodic, harmonic or more complicated patterns.

Crystal growth processes during skarnification may undergo sensitive adjustments to fluctuating parameters. These may be extrinsic (e.g., episodic fluid flow; Yardley et al., 1991; Jamtveit et al., 1993), rates of infiltration (Jamtveit et al., 1995), fluid fluxes etc. (Holten et al., 1997) or intrinsic (e.g., strain within growing layers because of unit cell differences in solid solution minerals; Jamtveit, 1991; Putnis et al., 1992.). Zoning patterns in minerals (Table 1) may be related to variation of major components in minerals from solid solution series, order-disorder phenomena in polysomatic or accretional series, trace elements, adsorption of impurities, as well as point defects.

Zoning pattern within individual minerals may be correlated to the mineralising processes in the surrounding environment. Some of the best examples are given by zonation patterns in skarn minerals from the Oslo Paleorift. Jamtveit (1991) suggested non-ideal solid solution between end-members in the grossular-andradite mineral series as an explanation for the chaotic type of oscillatory zonation patterns. He interpreted such chaotic patterns in immiscible solids as induced by periodic changes in fluid composition. Zonation patterns of major and trace elements (e.g., As, W) in garnet from the same location were further found to relate to the evolution of the hydrothermal system (Jamtveit et al., 1993). Intracrystalline zoning patterns in garnets and vesuvianite were analysed by statistical methods in order to investigate fractal behaviour and were tested against simulation of external fluctuation on diffusion and local growth kinetics (Holten et al., 1997). Zoning patterns indicate the influence of external fluctuation in open system and factors operating at scales much larger than the local interface processes were found responsible for the zonation.

Ortoleva (1994) related oscillatory zonation in crystals from geological systems to several models of self-organisation related to far-from-equilibrium theory, assuming that the oscillations during growth are time-independent in relation with the medium. Other published models, especially for minerals from igneous rocks, explain zonation as a result of internal crystal growth processes. Holten et al. (1997) questioned the applicability of such models to natural systems by inferring that fluctuations in the environment, i.e. external influences, cannot readily be considered in terms of time scales very different to crystal growth rates.

An opinion reconciling the two standpoints was presented by Jamtveit et al. (1995), who investigated the grandite solid solution relative to aqueous solution equilibrium in order to establish correlations between zonation patterns of grossular-andradite and skarn-forming fluids. Zonation patterns are considered as mainly externally controlled; by fluctuations in Al/Fe-ratios of the pore fluid caused by variable rates of infiltration and kinetic dispersion in the hydrothermal system. Minor variations in garnet composition may relate to surface kinetics and local transport processes near the crystal surface and may also relate to self-organisation.

The importance of oscillatory zoning in metamorphic minerals is underlined by Yardley et al. (1991), indicating that it could be a key parameter to identify mineral growth due to infiltration processes. This would have important application in distinguishing between skarn environments and regional metamorphic terrains. Schumacher et al. (1999), however, report oscillatory zoning in garnet from metamorphic terrains as a function of complex growth-and-resorbtion histories related to subtle, small-scale variations in the rate of decompression during regional metamorphism. No evidence to support an open-system fluid phase influence on the oscillatory pattern was found.

8 OVERPRINTING TEXTURES

Skarn deposits are characterised by prograde stages and superimposed, retrograde events; the latter reflecting contributions from hydrothermal or meteoric waters in shallow environments (Meinert, 1992). Fluctuation of chemical parameters during the retrograde event, mixing of fluid types and possible boiling and collapse of the skarn system will impact upon skarn textures. Shock-induced textures and brecciation are widespread, overprinting primary, i.e. pro-

grade, textures. Abrasion of refractive minerals is enhanced by the presence of ductile sulphides. Annealing and healing of brecciated, hydraulically-reworked assemblages are evidenced by equilibration reactions and recementation along grain boundaries and by welding of fragments. Microtextures show distinct parallels to both hydrothermal breccia and regionally metamorphosed deposits and relate to depth of formation. Study of skarn textures offers an often-neglected additional key for tracing zoning patterns during deposit evolution.

Table 1: Some published examples of mineral and textural patterns in skarn environments.

Type & Reference	Locality	Features described
Banded textures and scalloped skarn fronts:		
Bussel et al. (1990)	Uchucchacua, Peru	Ag-Mn-Pb-Zn vein replacements & skarn
Gower et al. (1985)	Mount Reed- Mount Haskin, Canada	W-Mo skarn; wrigglite textures
Guy (1981)	Costabonne, French Pyrenees	Banded, W-bearing skarns
Jahns (1944)	Iron Mountains, New Mexico, USA	Lenses/masses of ribbon-textured Beryllium-bearing 'tactite'
von Cotta (1864), Kissling (1967)	Ocna de Fier, Romania	Classic locality of 'Tiegererz'.
Kwak & Askins (1981)	Moina, Tasmania, Australia	F-Sn-W-(Be-Zn) skarn; wrigglite
Nakano (1978)	Kamaishi Mine, Shinyama, Japan	Fe-Cu skarn, monomineralic bands
Ochiai (1987)	Kamaichi, Nippo, Japan	Cu skarn; alternating layers
Trüstedt (1907)	Pitkäranta, Karelia	Banded & orbicular textures in magnetite
Ortoleva et al. (1986, 1987a)	Several examples are mentioned, including from Mn ores in Brasil / Gabon	
Oscillatory zoning in crystals:		
Ciobanu & Cook (2000a, b)	Ocna de Fier, Banat, Romania	Silicate inclusion trails in magnetite, order-disorder phenomena in Bi-sulphosalts
Guy (1981)	Costabonne, French Pyrenees	Garnet
Jamtveit (1991), Jamtveit et al. (1993, 1995), Holten et al. (1997)	Oslo Paleorift, Norway	Andradite-grossular, diopside-hedenbergite, trace elements; garnet, vesuvianite
Katchan (1984)	Ertsberg, Irian Jaya, Indonesia	Monticellite
Nakano (1989)	Shinyama, Japan	Clinopyroxene
Nakano et al. (1989a, 1989b)	Chichibu Mine & Yaguki, Japan	Garnet (with individual textures); epidote
Shore & Fowler (1996)	Review of oscillatory zoning; includes reference to examples from skarn environments	
Sitzman et al. (2000)	Adirondack Mts., New York	Impurity adsorption, dislocations in magnetite
Yardley et al. (1991)	Connemara, Ireland (and others)	Pyroxene
Clots and orbicules in contact aureoles:		
Tilley (1951), Hoersch (1981)	Beinn an Dubhaich, Skye, Scotland	Orbicular chert nodules in contact dolostone
Joesten (1991)	This review Includes reference to several examples in contact aureoles	
Joesten & Fisher (1988)	Christmas Mountains, Texas	Chert, calc-silicates, wollastonite, tilleyite
Knopf (1908)	Seward Peninsula, Alaska, USA	Orbicular textures, Sn deposits
Leveson (1966)	Includes reference to several examples in contact aureoles	
Moore (1984)	Palabora, South Africa	Layers/bands in metasomatised carbonatitite
Moore & Kerrick (1976)	Alta, Utah, USA	Orbicular nodules, rimmed by calc-silicates
Patterson et al. (1981)	Rennison Bell, Tasmania	Orbicular textures in Sn-skarn deposits
Puga & Fontboté (1980)	Santa Olalla, Spain	Zoned silicate nodules in brucite marble

9 CASE EXAMPLE: OCNA DE FIER

The classic Fe-Cu-(Zn-Pb) calcic skarn deposit of Ocna de Fier, S.W. Romania, contains examples of the textures described in this paper. Scalloped fronts at the marble-skarn contact are marked by cm- to dm-scale well-zoned mineral assemblages of distal type: garnet-wollastonite-marble, garnet-tremolite-marble, garnet–hedenbergite-marble. The marble-skarn contact is also well marked by a range of diffusion-related dissipative structures. Mineral banding, orbicular, nodular, spotted and mottled patterns are recorded in a variety of skarn-ore minerals associations. In order to explain their formation, both Liesegang banding and CPG mechanisms may be invoked, relating to chemical instabilities manifested at the distal skarn front.

Central parts of the ore are characterised by infiltration-related oscillatory patterns. Widespread oscillatory zoning in garnet, magnetite, and garnet-magnetite composite crystals points to the manifestation of an active infiltration-reaction feedback driven by focused flow parallel to the skarn-forming front. Ciobanu & Cook (2000b) have proposed that comparable dissipative structures may be initiated by small chemical fluctuations in relation to variable rates of diffusion/infiltration to explain observed patterns among certain Bi-sulphosalts. These minerals, via their structural modularity, or ability to accommodate order-disorder phenomena, are able to adjust to small, incremental random and/or patterned compositional variations. Concepts such as polysomatism and modularity among accretional series (Makovicky, 1998) and the ability to ooperate via modular coordination polyhedra are echoed in different types of minerals within skarn deposits. Carbonate-quartz piercing and cracking, blown-apart textures (garnet, magnetite) and shock-induced anisotropy (garnet) are evidence for interruption of prograde skarnification by build-up of volatile-rich fluids. Explosive boiling, dissipated by fluid-pumping and milling, resulted in repeated collapse within the 5 km deep system, and marked the onset of retrograde events. Oscillatory variation in fO_2 during the retrograde episode is expressed by microscopic repetitive patterns of magnetite-hematite.

Primary prograde assemblages overprinted by hydraulic reworking, produce a wide range of brecciation and deformation textures. Microtextural adjustments, abrasion and overgrowth during microshear-assisted fracture are especially common in refractory magnetite. Rhythmically intergrown composite magnetite-garnet crystals or associations of refractive minerals document adjustment in the form of jigsaw borders. Syn-deformational hooks and pressure shadows are preserved as relics despite recrystallisation. Abrasion of refractive minerals is enhanced by ductile sulphides present. Annealing and healing of brecciated, hydraulically reworked assemblages are evidenced by equilibration reactions and recementation along grain boundaries and by welding of fragments.

10 REFERENCES

Bussell, M.A., Alpers, C.N., Petersen, U., Shepperd, T.J., Bermudez, C. & Baxter, A.N. 1990. The Ag-Mn-Pb-Zn vein replacement, and skarn deposits of Uchucchacua, Peru; studies of structure, mineralogy, metal zoning, Sr isotopes, and fluid inclusions. Economic Geology, 85, 1348-1383.

Ciobanu, C.L. & Cook, N.J. 2000a. An ore textural approach to evolution of mineralising processes: the case of a classic Fe-(Cu) skarn deposit at Ocna de Fier, Banat, Romania. Geonytt 1/2000, 49.

Ciobanu, C.L. & Cook, N.J. 2000b. Intergrowths of bismuth sulphosalts from the Ocna de Fier Fe-skarn deposit, Banat, S.W. Romania. European Journal of Mineralogy (in press)

Dipple, G.M. & Gerdes, M.L. 1998. Reaction-infiltration feedback and hydrodynamics at the skarn front. In: Mineralized Intrusion-related Skarn Systems (D.R. Lentz ed.). Mineralogical Association of Canada Short Course Volume 26, 71-97.

Gerdes, M.L. & Valley, J.W. 1994. Fluid flow and mass transport at the Valentine wollastonite deposit, Adirondack Mountains, New York State, Journal of Metamorphic Geology, 12, 589-608.

Glansdorff, P. & Prigogine, I. 1971. Thermodynamic Theory of Structure, Stability and Fluctuations. Wiley, New York, 288pp.

Gower, S.J., Clark, A.H. & Hodgson, C.J. 1985. Tungsten-molybdenum skarn and stockwork mineralization, Mount Reed – Mount Haskin District, Northern British Columbia, Canada. Canadian Journal of Earth Sciences, 22, 728-747.

Guy, B. 1981. Certaines alternances recurrentes recontrees dans les skarns et les structures dissipatives au sens de Prigogine: un rapprochement. Comptes Rondes, Academie de Science de Paris, 292, 413-416.

Guy, B. 1993. Mathematical revision of Korzhinskii's theory of infiltration metasomatic zoning. European Journal of Mineralogy, 5, 317-339.

Hoersch, A.L. 1981. Progressive metamorphism of the chert-bearing Durness limestone in the Beinn an Dubhaich aureole, Isle of Skye, Scotland: A reexamination. American Mineralogist, 66, 491-506.

Holten, T., Jamtveit, B., Meakin, P., Cortini, M., Blundy, J. & Austrheim, H. 1997. Statistical characteristics and origin of oscillatory zoning in crystals. American Mineralogist, 82, 596-606.

Jahns, R.H. 1944. 'Ribbon rock', an unusual beryllium-bearing tactite. Economic Geology, 39, 173-205.

Jamtveit, B. 1991. Oscillatory zonation patterns in hydrothermal grossular-andradite garnet: Nonlinear dynamics in regions of immiscibility. American Mineralogist, 76, 1319-1327.

Jamtveit, B., Ragnarsdottir, V. & Wood, B.J. 1995. On the origin of zoned grossular-andadite garnets in hydrothermal systems. European journal of Mineralogy, 7, 1399-1410.

Jamtveit, B., Wogelius, R.A. & Fraser, D.G. 1993. Zonation patterns of skarn garnets: Records of hydrothermal system evolution. Geology, 21, 13-116.

Joesten, R.L.1974. Local equilibrium and metasomatic growth of zoned calc-silicate nodules from a contact aureole, Christmas Mountains, Big Bend Region, Texas. American Journal of Science, 274, 876-901.

Joesten, R.L. 1991. Kinetics of coarsening and diffusion-controlled mineral growth. In: Contact Metamorphism, Reviews in Mineralogy, 26, 507-582.

Joesten, R. & Fisher, G.W. 1988. Kinetics of diffusion-controlled mineral growth in the Christmas Mountains

(Texas) contact aureole. Geological Society of America Bulletin, 100, 714-732.
Katchan, G. 1984. Zoned monticellite-glaucochroite from the Gunung Bijih (Ertsberg) skarn, Irian Jaya, Indonesia. 27th IGC Abstracts, 5, 70.
Kerrick, D.M., Lasaga, A.C. & Raeburn, S.P. 1991. Kinetics of heterogeneous reactions. In: Contact Metamorphism, Reviews in Mineralogy, 26, 583-671.
Kissling, A. 1967. Studii mineralogice i petrografice in zona de exoskarn de la Ocna de Fier (Banat). Editura Academiei Republicii Socialiste România, 127 pp..
Knopf, A. 1908. Geology of the Seward Peninsula tin deposits. U.S. Geological Burvey Bulletin, 358, 71 pp..
Korzhinskii, D.S. 1970. Theory of Metasomatic Zoning. Carendon Press, Oxford, 162 pp.
Kwak, T.A.P. & Askins, P.W. 1981. Geology and genesis of the F-Sn-W (-Be-Zn) skarn (Wrigglite) at Moina, Tasmania. Economic Geology, 76, 439-467.
Leveson, D.J. 1966. Orbicular Rocks: A review. Geological Society of America Bulletin, 77, 409-426.
Lisegang, R.E. 1913. Geologische Diffusion. Steinkopf, Dresden/Leipzig, 180 pp..
Makovicky, E. 1998. Modularity – different types and approaches. EMU Notes in Mineralogy, 1, 315-343.
Meinert, L.D. 1992. Skarns and skarn deposits. Geoscience Canada Reprint Series, 6, 117-134.
Meinert, L.D. 1997. Application of skarn deposit zonation models to mineral exploration. Exploration and Mining Geology, 6, 185-208.
Moore, A.C. 1984. Orbicular rhythmic layering in the Palabora carbonatite, South Africa. Geological Magazine, 121, 53-60.
Moore, J.N. & Kerrick, D.M. 1976. Equilibria in siliceous dolomites of the Alta aureole, Utah. American Journal of Science, 276, 502-524.
Nakano, T. 1978. The zoned skarn developed in diorite porphyry in the Shinyama area, Kamaishi Mine, Japan. Mining Geology, 28, 99-109.
Nakano, T. 1989. Fluctation model for compositional heterogeneity in skarn clinopyroxenes. Geochemical Journal, 23, 91-99.
Nakano, T., Takahara, H. & Norimasa, N. 1989a. Intracrystalline distribution of major elements in zoned garnet from skarn in the Chichibu Mine, Central Japan; illustration by color-coded maps. Canadian Mineralogist, 27, 499-507.
Nakano, T., Takahara, H. & Fujii, T. 1989b. Development of compositionally-zoned epidote from the Yaguki skarn deposit, Northeastern Japan. Mining Geology, 39, 1-8.
Nicolis, G. & Prigogine, I. 1977. Self-organization in Non-equilibrium Systems. Wiley, New York, 491 pp.
Ochaiai, K. 1987. A reaction model relating skarn zones and ore formation at the Nippo copper ore deposit, Kamaishi Mine, Northeastern Japan. Economic Geology, 82, 1001-1018.
Ortoleva, P.J. 1978. Theoretical Chemistry, Periodicities in Chemistry & Biology, IV. Academic Press, New York.
Ortoleva, P.J. 1984. The self-organization of Liesegang Bands and other precipitate patterns. In: Chemical Instibilities (G. Nicolis & F. Baras, eds.), NATO Advanced Science Ser. C, 120, 289-297.
Ortoleva, P.J. 1994. Geochemical Self-Organization. Oxford Monographs on Geology & Geophysics 23, 411 p.
Ortoleva, P.J., Auchmuty, G., Chadam, J., Merino, E., Hettmer, J., Moore, C. & Ripley, E. 1986. Redox front propagation and banding modalities. Physica D, 334-354.
Ortoleva, P.J., Merino, E., Moore, C. & Chadam, J. 1987a. Geochemical self-organization I. Reaction-transport feedbacks and modeling approach. American Journal of Science, 287, 979-1007.
Ortoleva, P.J., Chadam, J., Merino, E. & Sen, A. 1987b. Geochemical self-organization II. The reactive-infiltration instability. American Journal of Science, 287, 1008-1040.
Ostwald, W. 1925. Kolloid Zeitschrift, 36, 330.
Patterson, D.J., Ohmoto, H. & Solomon, M. 1981. Geological setting and genesis of cassiterite-sulfide mineralization at Renisson Bell, Western Tasmania. Economic Geology, 76, 393-438.
Puga, E. & Fontboté, L. 1980. Zoned silicate nodules in brucite marble, Santa Olalla, western Sierra Morena, Spain. Schweiz. Mineral. Petrogr. Mitt., 60, 69-80.
Putnis, A., Fernandez-Dias, L. & Prieto, M. 1992. Experimentally produced oscillatory zoning in the $(Ba,Sr)SO_4$ solid solution. Nature, 358, 743-745.
Schumacher, R., Rötzler, K. & Maresch, W.V. 1999. Subtle oscillatory zoning in garnet from regional metamorphic phyllites and mica schists, Western Erzgirirge, Germany. Canadian Mineralogist, 37, 381-402.
Shore, M. & Fowler, A.D. 1996. Oscillatory zoning in minerals: A common phenomenon. Canadian Mineralogist, 34, 1111-1126.
Sitzman, S.D., Banfield, J.F. & Valley, J.W. 2000. Microstructural characterization of metamorphic magnetite crystals with implications for oxygen isotope distribution. American Mineralogist, 85, 14-21.
Sultan, R., Ortoleva, P., DePasquale, F. & Tartaglia, P. 1990. Bifurcation of the Ostwald-Liesegang supersaturation-nucleation-depletion cycle. Earth Science Reviews, 29, 163-173.
Tilley, C.E. 1951. The zoned contact-skarns of the Broadford area, Skye: a study of boron-fluorine metasomatism in dolomites. Mineralogical Magazine, 29, 621-666.
Trüstedt, O. 1907. Die Erzlagerstätten von Pitkäranta. Bulletin Commission géologique Finlande, 19, 1-333.
Turing, A.M. 1952. The Chemical Basis of Morphogenesis. Philosophical Transactions of the Royal Society of London, ser. B, 237, 37-72.
von Cotta, B. 1864. Erzlagerstätten im Banat und in Serbien. W. Braunmuller, Wien, 105 pp..
Yardley, B., Bottrell, S.H.& Cliff, R.A. 1991. Evidence for a regional-scale fluid loss during mid-crustal metamorphism. Nature, 349, 151-154.
Yardley, B.W.D. & Lloyd, G.E. 1995. Why metasomatic fronts are really metasomatic sides. Geology, 23, 53-56.
Yardley, B.W.D., Rochelle, C.A., Barnicoat, A.C. & Lloyd, G.E. 1991. Oscillatory zoning in metamorphic minerals: an indicator of infiltration metasomatism. Mineralogical Magazine, 55, 357-365.
Zaraisky, G.P. 1991. Experimental modeling of bimetasomatic calcareous skarn zoning. In: Skarns – their

Genesis and Metallogeny (A.M. Aksyuk ed.). Theophrastus Publications S.A., Athens, 467-495.

LA-ICP-MS analysis techniques in mineralogical studies

Paul Ek
Process Chemistry Group, c/o Laboratory of Analytical Chemistry, Åbo Akademi University, Biskopsgatan 8, FIN-20500 Åbo, Finland. e-mail: paul.ek@abo.fi

ABSTRACT. Laser ablation (LA) is a sample introduction technique used for direct analysis of solid materials. Normally it is used in combination with an inductively coupled plasma mass spectrometer for multi-elemental microanalysis. By reducing the inner volume of the laser ablation sample cell a faster analyte signal response and better spatial resolution can be obtained. For this purpose a special Geo-Sampling Cell was constructed to evaluate the suitability and performance of the analytical equipment for analysis of geological thin sections. This can be done for instance by elemental mapping of certain structurally well defined mineral grains occurring in the rock matrix.

1 INTRODUCTION

In geochemical studies of rocks and minerals there is a need to estimate the concentration of main and trace elements, to survey incorporated foreign elements in the lattices of different key minerals, to study elemental zonation in individual mineral grains and spatial distribution of minor and trace elements. These studies give valuable information about the history and the prevailing physical- and chemical conditions when the rock was formed. Such data are of great importance in geo-chemical research in general and for instance in geo-chemical prospecting for ore deposits.

To gather this kind of analytical data by direct analysis of solid samples, micro-analytical techniques with a high spatial resolution must be used.

2 INSTRUMENTATION

During the last few decades the development of different micro-beam techniques such as the electron microprobe, micro-pixe and the coupling of laser ablation (LA) and more recently laser ablation microprobe (LAM) to the high sensitive ICP-MS instrument has resulted in a huge increase of new analytical data for geo-chemists.

In geological applications the samples are mostly polished thin-sections prepared from rock samples. The analytical instrumentation used in our laboratory is a Perkin-Elmer Elan 6000 inductively coupled plasma mass spectrometer equipped with the Cetac LSX 200 UV (266nm) laser ablation instrument. The laser ablation system is provided with polarizing lenses as a geo-option.

3 LASER ABLATION SAMPLING CELL

An important feature of laser ablation is the ability of spatial resolved analysis, which enables elemental mapping of very small mineral grains (100 x 100 μm).

By replacing the standard ablation sampling cell with a smaller cell[1] with an inner volume of 2 cm^3 a good resolution, a higher sensitivity and a faster response signal could be obtained. An in-house made ablation sampling cell Fig.1 has been constructed especially for analysis of geological thin-section samples. The cell has an open bottom and can be fixed by cramps directly on the smooth surface of the sample. As a result of this construction the thin-sections can be viewed under crossed polarized light, which

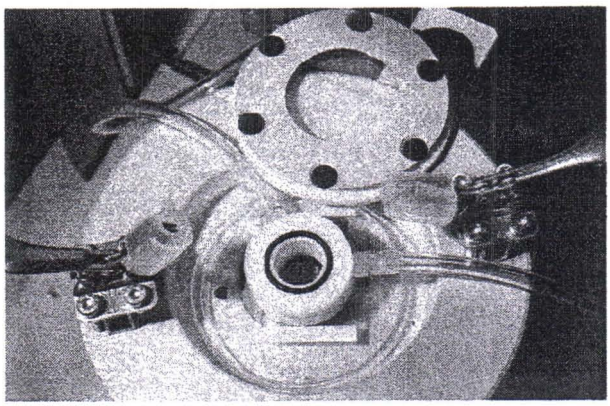

Figure 1. Geo- Sampling Cell

facilitates identification of the individual minerals, by their interference colours.

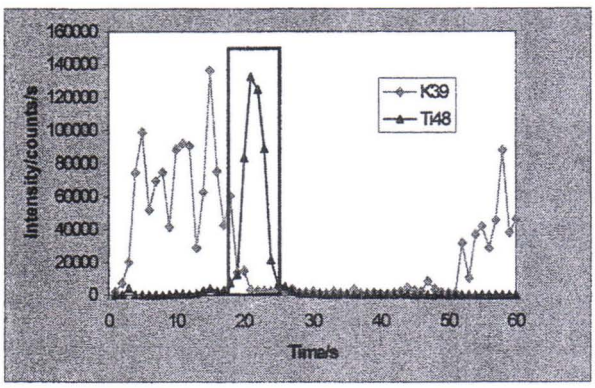

Figure 2. Single line scan profile across an ilmenite grain using the Geo- Sampling Cell. The rectangular box indicates the ilmenite grain in the K-feltspar matrix.

The suitability and performance of this new ablation cell for element distribution studies (Fig.2) will be demonstrated and compared with results obtained with the standard ablation sampling cell (Fig.3). The peak profiles obtained by the Geo-Sampling Cell are much narrower (ca 60 μm at the sampling point) and they return nicely to the base line with no tailing, thus demonstrating a fast response and good spatial resolution of the analytical system.

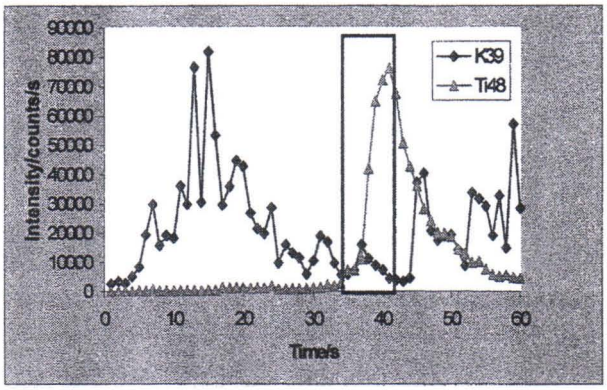

Figure 3. Single line scan profile using the standard sampling cell.

This analysis technique makes it possible to study the trace elemental distribution in the micro-structure of the target materials, by moving the laser beam in the x-y directions on the sample surface. By reducing of the profiling speed of the laser beam to a few μm/sec and simultaneously increasing the measuring rate on the ICP-MS instrument a very high resolution of the elemental distribution can thus be achieved. This can be visualised by preparation of topographic images of the examined samples.

4 REFERENCES

Hulden, S., Ek, P., Effcts of using a reduced scale ablation cell on analyte response in spatial element distribution studies of rock forming minerals by LA-ICP-MS. 2000 Winter Conference on Plasma Spectrochemistry, January 10-15. 2000, 191 p.

Some ore textures of selective replacement

Alexandr D. Genkin
Institute of geology of ore deposits, petrography, mineralogy and geochemistry. Russian Academy of Sciences. Staromonetny 35, Moscow, Russia

ABSTRACT. The significance of replacement and especially of selective replacement textures for understanding the hydrothermal ore formation is shown. The different types of selective replacement are illustrated by the examples from some Russian deposits. Among these types are the replacement of regular intergrowths of ore minerals by later 1) pyrite, 2) quartz and 3) carbonate and 4) the replacement of quartz and silicates by later sulfides. First three types permit to establish the sequence of formation of minerals and show the different behaviour of sulfides under subsequent replacement of sulfide ores by pyrite and quartz. Sphalerite and stannite remain stable while chalcopyrite is unstable and undergo replacement. The described textures lead to an interesting conclusion that in all cases, the chalcopyrite is the most unstable mineral, stannite is more stable, and sphalerite – the most difficult for dissolution. The fourth type, a selective replacement of quartz by sulfides (stannite and fahlore) that facilitates a significant change in the composition of the later solution with its enrichment in alkalies is suggestive of the replacement of quartz.

1 INTRODUCTION

Replacement, or metasomatism is a dominant process in the formation of most sulfide ore deposits. The replacement textures have been attracting attention for a long time. But according to correct opinion of Hubert Barnes (1979, p.438) "replacement is a major area of ignorance in understanding hydrothermal ore genesis."

2 REPLACEMENT TEXTURES

The textures that result from replacement are variable. Among them, peculiar and surprising are the textures of selective replacement, where some minerals show a distinct preference to one of the replacing minerals. Selective replacement of earlier formed sulfides by non-opaque minerals and vice versa, is of great interest. A separate type is the replacement of quartz and silicates (tourmaline) by sulfides (fahlore and stannite). The different types of selective replacement will be illusrated here by the examples from some Russian deposits.

The textures arising during the replacement of regular intergrowths of ore minerals, when the host mineral with oriented inclusions of other ore mineral is replaced and the inclusions are left intact, permit unequivocally establish the sequence of formation of minerals.

3 EXAMPLES OF DEPOSITS STUDIED

In the Bukuka tungsten deposit (Transbaikalia) starlike inclusions of sphalerite are distributed in chalcopyrite. The same inclusions occur in idiomorphic crystals of pyrite (Fig. 1). Chalcopyrite from the Sinancha deposit (Far

East) contains many laminar inclusions of stannite and isometric inclusions of sphalerite. These inclusions with the same orientation are found in idiomorphic crystals of pyrite (Fig.2). These examples show the later formation of pyrite porphyroblasts.

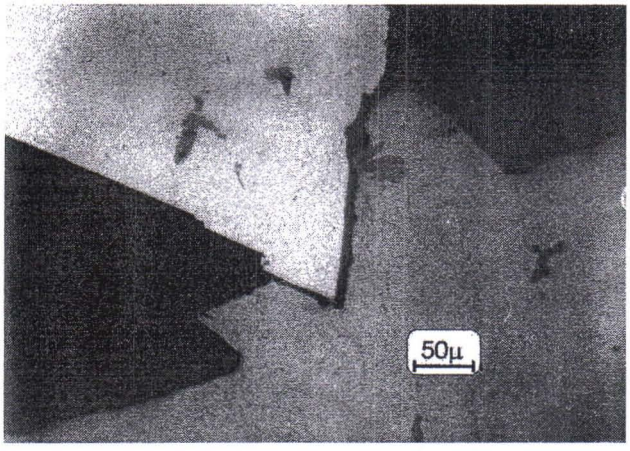

Figure 1. Inclusions of sphalerite (dark grey) in pyrite crystal (white) and chalkopyrite (light grey).

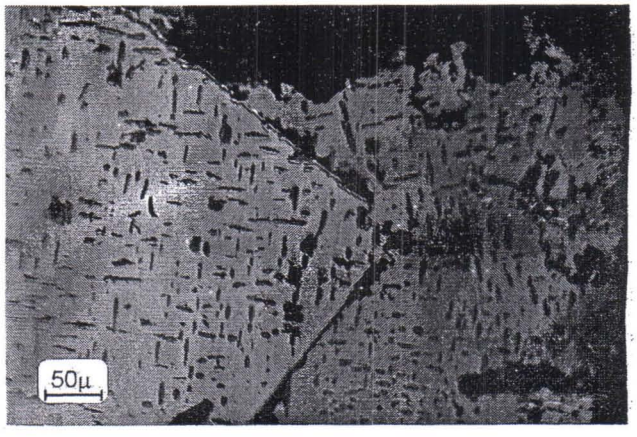

Figure 2. Inclusions of stannite and sphalerite (dark grey) in pyrite crystal (light grey) and chalkopyrite (grey).

Most interesting case of selective replacement was described by P. Ramdohr (Ramdohr, 1980, p. 204) from the Carrick Dhu-Quarry mine, Cornwall. Ramdohr writes "chalcopyrite with well-developed small exsolution bodies of stannite is replaced by perfectly idiomorphic quartz. The observation that the stannite bodies are completely intact and in their old orientation within quartz provides the only clue, but a conclusive one of the replacement nature of the quartz. Both the chemistry and mechanism of this sparing and selective replacement are enigmatic".

Analogous phenomena were observed in the samples of the Bukuka tungsten deposit. During the replacement of chalcopyrite by metacrystals of quartz the linearly distributed inclusions of stannite with the same orientation as in chalcopyrite were preserved in quartz.

The presented data testify to different behaviour of sulfides under subsequent replacement of sulfide ores by pyrite and quartz: sphalerite and stannite remain stable while chalcopyrite unstable and undergo replacement. Hence the solutions interacting with earlier sulfide association were undersaturated with copper or the physico-chemical conditions were changed and the solution became unequilibrated with sulfide paragenesis. The described phenomenon is obviously connected with the different solubility of chalcopyrite, sphalerite and stannite.

The selective replacement of ore minerals by carbonates also occurs in some deposits. In the Deputatskoe tin deposits (Yakutia) the starlike inclusions of sphalerite in chalcopyrite were replaced by carbonate. During the carbonate replacement of the pyrrhotite-pentlandite exsolution textures in copper-nickel ores of Norilsk deposit, the exsolution lamellar of pentlandite (Fig.3) were preserved.

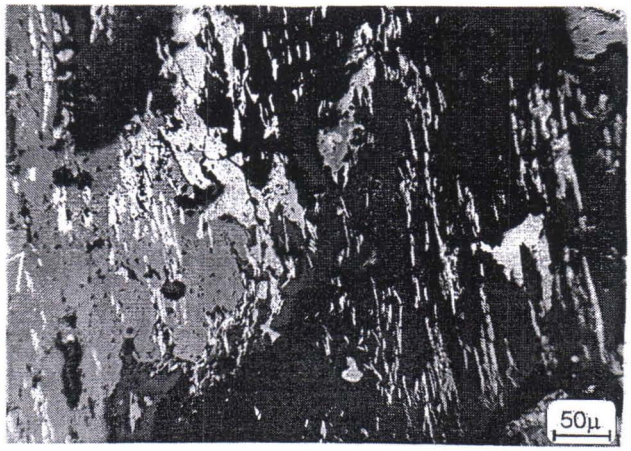

Figure 3. Inclusions of pentlandite (white) in pyrrhotite (grey) and carbonate (black).

The described textures lead to an interesting conclusion that in all cases, the chalcopyrite is the most unstable mineral, stannite is more stable and sphalerite is most difficult to dissolution. This is caused by different behaviour of copper, tin and zinc. As it has

been shown, copper is a metal which is more easily soluble under the action of later sulfides precipitation solutions. Noteworthy is that the sequence of solution of sulfides under transformation do not coincide with the sequence of their crystallization from the solutions. The observed phenomena represent a unique data for understanding the behaviour of ore forming sulfides and metals during retrograde processes.

The next type of replacement of quartz by sulfides is especially significant because quartz is very stable in chemical respect and can be dissolved only by solutions rich in alkalies and fluoric acid. Therefore the facts of its solution in sulfide ores are important for understanding a chemical composition of ore forming solutions. The replacement of quartz is shown in the examples of the sulfide-cassiterite Valkumei (Chukotka) and the gold-sulfide Darasun (Transbaikalia) deposits. In the Valkumei deposit the idiomorphic quartz crystals in sphalerite are replaced on their periphery by stannite (Fig. 4).

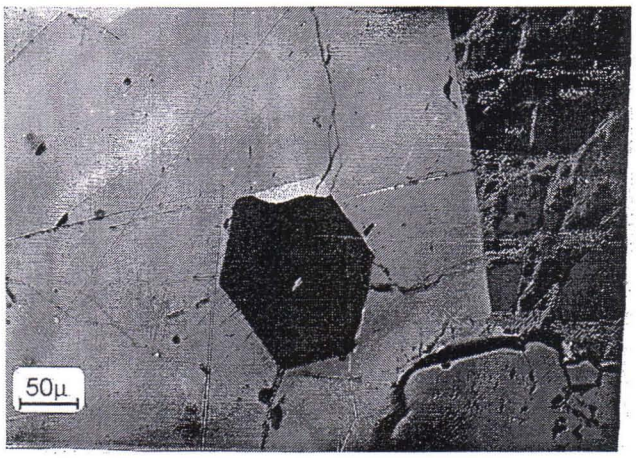

Figure 4. Stannite (white) replacing quartz crystal (black) in sphalerite (grey).

The relatively late formation of stannite is demonstrated by its thin veinlents is sphalerite. All stages of replacement of idiomorphic quartz crystal in chalcopyrite by fahlore (Fig.5) were observed in Darasun deposit. A false impression of the existence of perfectly formed crystals of fahlore in chalcopyrite (Fig. 6) could arise in the case of full pseudomorphs of fahlore. Tourmaline as needle crystals often occurs in Darasun deposit in quartz, chalcopyrite and fahlore.

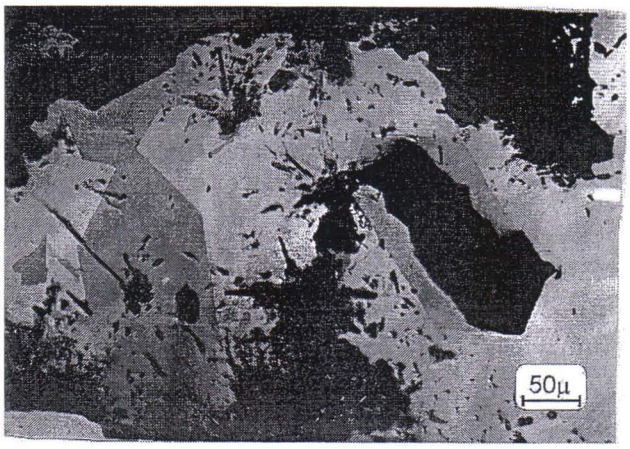

Figure 5. Fahlore (grey) replacing quartz crystal (black) in chalkopyrite (light grey).

Figure 6.Hexagonal pseudomorph of fahlore (grey) in chalkopyrite (light grey).

Needle crystals of fahlore sometimes with relics of tourmaline testify that tourmaline also underwent a pseudomorph replacement by fahlore. These examples show that the formation of stannite and fahlore occur in later moments of ore formation process.

4 CONCLUSIONS

The described different types of selective replacement lead to the conclusion that in the process of ore formation such replacement events took place in later stage of this process. The textures of selective replacement permit to establish: 1) the sequence of formation of minerals; 2) the different behavior of sulfides under subsequent replacement of sulfide ores; 3) a singnificant change in the composition of ore forming solutions.

The textures formed during the replacement of regular intergrowths of ore minerals, when the host mineral with oriented inclusions of other ore mineral is replaced and the inclusions are left intact, permit unequivocally establish the sequence of formation of minerals.

During the replacement of chalcopyrite, sphalerite and stannite by pyrite and quartz, the chalcopyrite is the most unstable mineral, stannite is more stable and sphalerite is most difficult for dissoluyion. This is caused by different behavior of copper, tin and zinc.

The replacement of quartz, a mineral very stable in chemical respect by sulfides (stannite, fahlore) can help in understanding the chemical composition of orefoming solutions. This replacement could be explained by the enrichment of later solutions by alkalies.

5 REFERENCES

Barnes, H. 1979. Solubilities of ore minerals. In: Geochemistry of hydrotermal ore deposits. Second edition. Ed. H. L. Barnes.

Ramdor, P. 1980. The ore minerals and their intergrowths. 2n^{d} Edition. Volume 1.

Microbial sulfide oxidation in tailings from Boliden

M.M. Gleisner
Department of Geology and Geochemistry, Stockholm University, S-106 91 Stockholm, Sweden
magdalena.gleisner@geo.su.se

ABSTRACT. Batch experiments containing freshly processed sulfide tailings, were performed at different degrees of oxygen saturation and in the presence of *Thiobacillus* species. These investigations concluded that microbial sulfide oxidation could proceed at low oxygen (dysoxic) levels.

1 INTRODUCTION

In mine tailings impoundments containing sulfide minerals, sulfide oxidation is a significant problem resulting in acidification and the mobilization of heavy metals to natural waters. The factors which most greatly affect this process in the waste rock environment are microbial activity, oxygen concentration, water accessibility, ferric iron concentration, temperature and pH. Among the microbial populations in sulfide rich environments, bacteria of the genus *Thiobacillus* (Figure 1) are associated with acid mine water. They are rod shaped microaerophilic acidophiles, and catalyze sulfide oxidation reactions as they gain energy from the transformations of sulfur and iron.

This work is focused on freshly processed sulfide tailings from Boliden's tailings mill in northern Sweden. Previous studies have shown that microbial oxidation of tailings at oxic conditions results in the most rapid oxidation rates. A task of this study was to investigate if microbial oxidation of tailings could be carried out at dysoxic conditions (oxygen concentrations greater than 0.1 mg/L and less than 0.5 mg/L), which are probably more representative of oxygen levels in covered tailings impoundments.

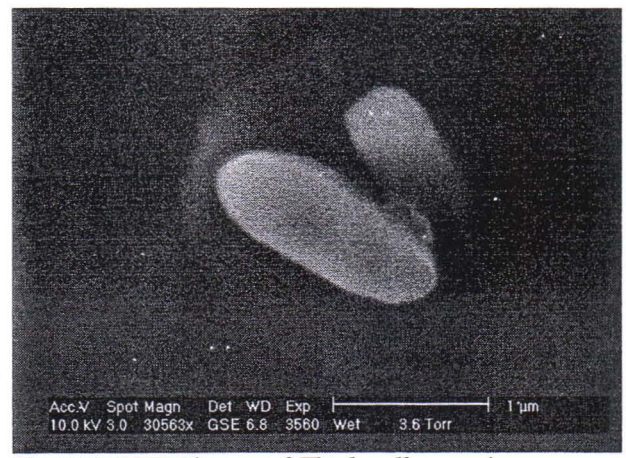

Figure 1. ESEM image of *Thiobacillus* species.

2 MATERIALS AND METHODS

Characterization of the Boliden tailings displayed that the most common minerals were pyrite, chalcopyrite, sphalerite, quartz and chlorite, according to optical microscopy analysis. Sulphur and iron content were 9.27 (±0.16) and 7.69 (±0.70) %, respectively, according to total chemical analysis. Particle size distribution was 20 - 60 µm according to grain size analysis. Environmental scanning electron microscopy (ESEM) analysis of the tailings indicated the presence of relatively heavy minerals (i.e. sulfides) in contrast to relatively light minerals (e.g. quartz) (Figure 2).

Figure 2. ESEM image of the Boliden tailings in back-scattered electron mode. The BSE images show minerals containing heavier elements (e.g. metal sulfides) as white, while relatively lighter minerals are shown less brightly.

Batch experiments containing the tailings were performed at room temperature under different conditions for about four months, and studied with respect to the various oxidation rates. Experiments executed were: microbial oxidation at oxic conditions (0.21 atm O_2), microbial oxidation at dysoxic conditions (0.01 atm O_2), and abiotic oxidation by dissolved oxygen at low and high pH.

3 RESULTS

The results showed that microbial oxidation proceeded at both oxic and dysoxic conditions, and the rates were 2.5 times more rapid in the oxic (2.0×10^{-8} mol m^{-2} pyrite s^{-1}) than in the dysoxic (7.9×10^{-9} mol m^{-2} s^{-1}) experiments. Microbial oxidation was also faster than abiotic oxidation. At oxic microbial conditions, the rate was 5 times more rapid than at oxic abiotic conditions by dissolved oxygen at low pH (4.2×10^{-9} mol m^{-2} s^{-1}), which was the fastest oxidation rate among the abiotic experiments. Tailings oxidized abiotically by dissolved oxygen at high pH, i.e. the pH of the tailings when discharged from the tailings mill, showed an even slower rate (1.4×10^{-9} mol m^{-2} s^{-1}).

The results also showed that the oxidation rates decreased toward the end of the experimental period in all batch experiments. Presumably, different amorphous ferric hydroxides started to precipitate and covered the sulfide grains, leading to slower oxidation rates as the free sulfide surfaces became less available.

The nickel minerals in chromitites of the Kapitanov Deposit, Ukrainian Shield

S.S. Gornostayev, K. Laajoki,
Department of Geosciences, University of Oulu, P.O.BOX 3000, FIN-90401, Oulu, Finland
ssg@cc.oulu.fi

S.E. Popovchenko
National Mining University of Ukraine, 19 Karl Marx Avenue, Dnepropetrovsk, 49027, Ukraine

P.K. Kornienko
Pravoberezhnaya Geological Expedition, 9/16 Geologicheskaya Street, Fursy, 256400, Ukraine

ABSTRACT. The nickel minerals in chromitites of the Kapitanov chromite deposit, Ukrainian Shield are represented by gersdorffite, maucherite, millerite, nickeline, pentlandite, As-bearing tucekite and violarite. The minerals occur as inclusions in chromite and distributed in interstitial matrix. The formation of nickel sulphides, arsenides, sulpharsenides and antimonides in the deposit took place within several stages, starting from high temperature crystallization of some varieties of nickeline, millerite and gersdorffite followed by relatively low-temperature formation of these and other phases and by origin of secondary mineral assemblages.

1 INTRODUCTION

The most important chromite deposits of the Ukrainian Shield named Kapitanov and Lipovenki are known since 1952 (N.T. Vadimov, unpubl.). The deposits represent potential target for mining operations and are located closely to the Pobugskoe town, which was one of the major producers of lateritic nickel ores in former USSR. However, very limited data exist on mineralogy of Ukrainian chromite deposits. In this paper we present data on nickel minerals found in chromitites of the Kapitanov deposit.

2 GEOLOGIC BACKGROUND

The Kapitanov chromite deposit is hosted by a 1.96–2.1 Ga layered fault-bounded massif 2500 m long and 260 m wide, located within the Golovanev suture zone, which separates the Western and Central geoblocks of the Ukrainian Shield (Kanevskii 1981, 1996; Gornostayev et al., 1999). The deposit consists of massive and disseminated chromitite bodies (2–16 m thick and 40–250 m long) enriched in Al and hosted by serpentinized and carbonatized dunite and harzburgite. The chromitites are composed of chromite enriched in Al, ilmenite (euhedral to subhedral grains in silicate matrix and lamellae in chromite), olivine (Fo_{80-90}), serpentine, orthopyroxene and clinopyroxene. Opaque minerals in serpentine matrix and in chromite grains comprise chalcopyrite, galena, gersdorffite, maucherite, millerite, nickeline, pentlandite, As-bearing tucekite and violarite. Among platinum-group minerals (PGM) found in the ores are anduoite, irarsite, laurite, ruarsite, sperrylite and unidentified Ru-Rh-Ir-As, Pd-Sb and Pd-As phases. They occur as small (mostly 1-5 μm) irregular grains attached to chromite edges or within interstitial silicates and as euhedral crystals in chromite.

3 NICKEL MINERALS

3.1 *Gersdorffite, NiAsS*

Gersdorffite occurs in the ores as negative inclusions in chromite in association with millerite (Fig. 1a, Table 1. anal. 1; Fig. 1b). It also occurs in chromite as a component of three-phase inclusions (Fig. 1c) with nickeline and millerite.

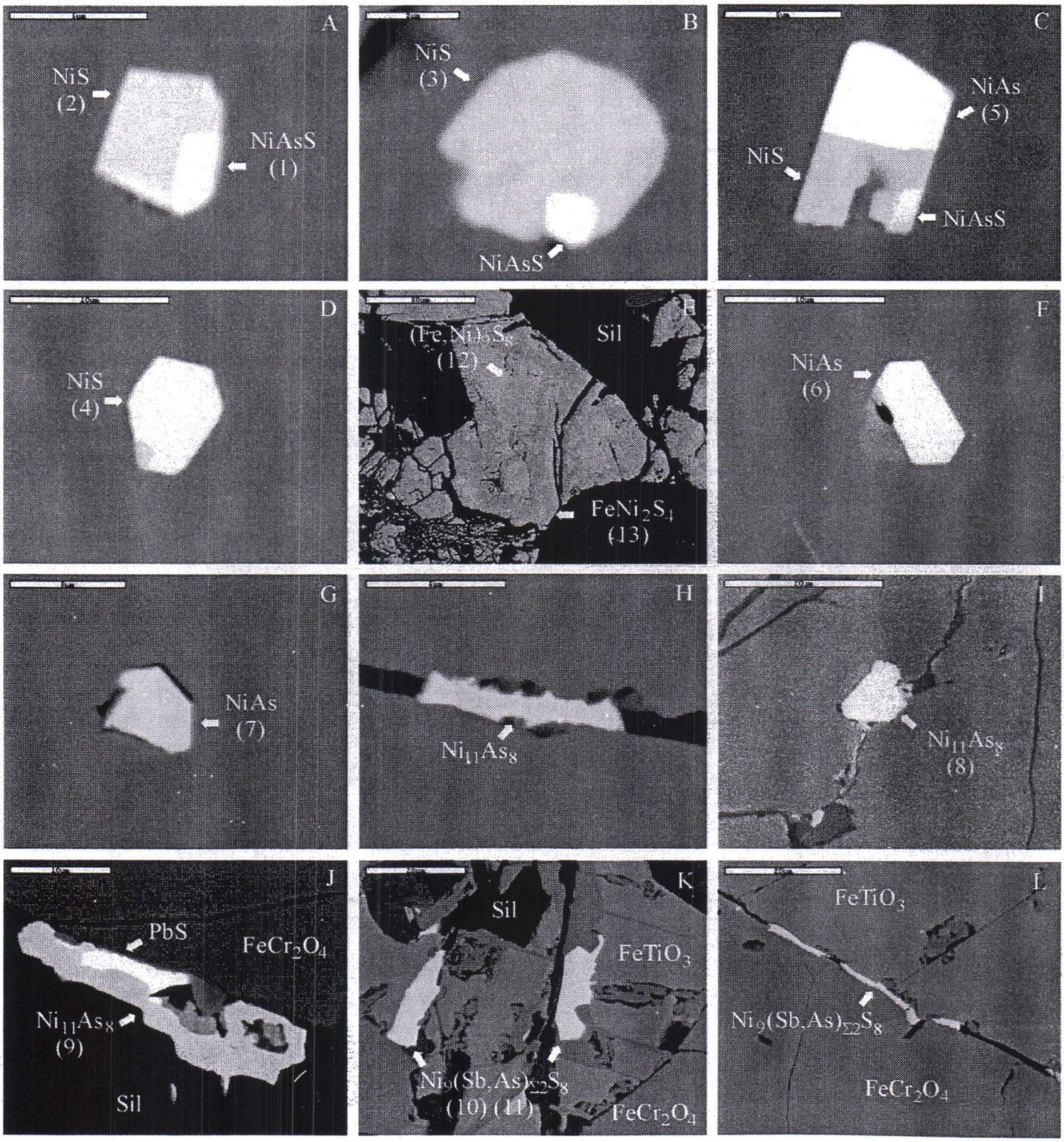

Figure 1. BSE images of nickel minerals from Kapitanov. Bar scale: 2 μm in Figure 1b; 5 μm in Figures 1a, 1c, 1f, 1g and 1h; 10 μm in Figure 1j; 20 μ m in Figures 1I, 1k and 1l; 50 μm in Figure 1E. Digits in brackets correspond to analysis in Table 1.

Table 1. Representative electron-probe analyses* on nickel minerals from Kapitanov.

	S	Fe	Co	Ni	As	Sb	Σ
				Weight %			
1	19.22	0.00	0.00	35.61	45.55	0.00	100.38
2	34.60	1.46	0.00	64.06	0.07	0.00	100.19
3	32.50	4.46	0.00	62.34	0.15	0.00	99.45
4	34.89	0.00	0.09	64.82	0.00	0.00	99.80
5	0.45	1.88	0.00	43.12	55.01	0.00	100.46
6	0.44	1.59	0.00	42.56	54.30	0.00	98.89
7	0.00	0.00	0.00	43.51	56.61	0.00	100.12
8	0.32	1.56	0.00	50.22	46.53	1.46	100.09
9	0.00	0.00	0.00	53.43	48.92	0.00	102.35
10	22.53	3.18	1.91	45.30	1.24	21.38	95.54
11	22.78	3.41	1.52	47.29	2.70	18.29	95.99
12	30.64	25.13	0.89	42.70	0.00	0.00	99.36
13	39.14	13.45	0.81	44.53	0.00	0.00	97.93
				Formulae units**			
1	0.99			1.00	1.01		3.00
2	0.98	0.02		0.99			2.00
3	0.94	0.07		0.98			2.00
4	0.99			1.01			2.00
5	0.02	0.04		0.97	0.97		2.00
6	0.02	0.03		0.97	0.97		2.00
7				0.99	1.01		2.00
8	0.12	0.04		10.65	7.73	0.15	19.00
9				11.06	7.94		19.00
10	7.60	0.62	0.35	8.35	0.18	1.90	19.00
11	7.55	0.65	0.27	8.55	0.38	1.60	19.00
12	7.56	3.56	0.12	5.76			17.00
13	3.82	0.75	0.12	2.38			7.00

* JEOL JSM–6400 scanning electron microscope equipped with a LINK eXL energy dispersive spectrometer. Analytical conditions: 15 kV, 1.2 nA, 100s counting time. 1 – gersdorffite; 2 – 4 - millerite; 5 – 7 - nickeline; 8, 9 - maucherite; 10, 11 - As-bearing tucekite; 12 - pentlandite; 13 – violarite.

** Totals for formula unit are given for ideal stoichiometry.

3.2 *Millerite, NiS*

Millerite is found in three associations: (1) in a two-phase negative crystal association with gersdorffite (Fig. 1a; Table 1, anal. 2 and Fig. 1b; Table 1, anal. 3), (2) in three-phase inclusions with gersdorffite and nickeline (Fig. 1c), (3) as euhedral "primary" inclusions in chromite (Fig. 1d, Table 1, anal. 4). It should be noted that the single-phase inclusion contains detectable amount of Co, while other varieties of millerite are enriched in Fe and show presence of As.

3.3 *Pentlandite, (Fe,Ni)$_9$S$_8$ and violarite, FeNi$_2$S$_4$*

Pentlandite and violarite (Fig. 1e; Table 1, anals. 12 and 13) are most abundant nickel minerals in the ores. They are located in silicate matrix and violarite forms secondary rims after pentlandite. Pentlandite occurs as broken grains of some 50×100 μm, as small irregular aggregates or as veinlets.

3.4 *Nickeline, NiAs*

Nickeline is a common inclusion in chromite from Kapitanov. In addition to three-phase inclusions (Fig. 1c; Table 1, anal. 5) with millerite and gersdorffite, it occurs as euhedral "primary" crystals (Fig. 1f; Table 1, anal. 6) enclosed in the chromite, which contains lamellae of ilmenite. Nickeline also occurs as single negative crystals in chromite (Fig. 1g; Table 1, anal. 7).

3.5 *Maucherite, Ni$_{11}$As$_8$*

Maucherite represents typical "secondary" association and is found in the ores as irregular grains and veinlets filling cracks and cavities in ilmenite (Fig. 1h) and in chromite (Fig. 1i; Table 1, anal. 8). In the latter case, it contains detectable amount of Sb. In some cases, the mineral has been found attached to chromite grains associated with galena (Fig. 1j; Table 1, anal. 9).

3.6 *As-bearing tucekite, Ni$_9$(Sb,As)$_2$S$_8$*

Tucekite, ideally $Ni_9Sb_2S_8$, is a rare mineral of the hauchecornite group. It was described in a mineralized Archaean chlorite schist at Kanowna, Western Australia, and in the gold-bearing conglomerates of Witwatersrand, South Africa (Just & Feather, 1978). As-bearing tucekite is only found in the copper-nickel sulphide ore hosted by a mafic-ultramafic pluton of the Voronezh crystalline massif (Kasatov et al., 1988). As-bearing tucekite from Kapitanov occurs as irregular aggregates of some 5×20 μm (Fig. 1k; Table 1, anals. 10, 11) or 35 – 40 μm long veinlets (Fig. 1l) filling the cracks between chromite and ilmenite. It shows sharp boundaries and has no signs of alteration or replacement by other minerals.

4 CONCLUSIONS

The nickel minerals in chromitites of the Kapitanov chromite deposit, Ukrainian Shield are gersdorffite, maucherite, millerite, nickeline, pentlandite, As-bearing tucekite and violarite.

Some mineral species were found in various assemblages also showing differences it their composition. The formation of nickel sulphides, arsenides, supharsenides and antimonides in Kapitanov took place within several stages, starting from high temperature crystallization of some varieties of nickeline, millerite and gresdorffite followed by relatively low-temperature formation of these and other phases and, finally, by origin of secondary mineral assemblages.

5 ACKNOWLEDGEMENTS

This study is a contribution to the GEODE project. The financial support from the Society of Economic Geology, CIMO and the Academy of Finland (grants to S.S.G.) is gratefully acknowledged.

6 REFERENCES

Gornostayev, S.S., Laajoki, K., Popovchenko, S.E., Pikarenya, D.S. and Poloskov, I.M. (1999). Mineral resources of the Pobugskoe Region, Ukranian Shield. In: Mineral Deposits: Processes to Processing (Stanley C.J. et al., eds.). Proc. of the 5th SGA Meeting and the 10th IAGOD Symp., London, 1999. Rotterdam: Balkema, 2: 1101-1104.

Just, J. and Feather, C.E. (1978). Tucekite, a new antimony analogue of hauchecornite. Mineralogical Magazine, 42, 278: M21-22.

Kanevskii, A.Ya. (1981). Accessory chromian spinels as an indicators of formation types of ultramafic rocks. Sovetskaya Geologiya, 4: 98-106 (in Russian).

Kanevskii, A.Ya. (1996). Chromite ores of Ukraine. Mineral Resources of Ukraine 3: 12-13 (in Ukrainian).

Kasatov, A.S., Plaksenko, A.N., Polezhaeva, L.I. and Rezhenova, S.A. (1988). New data on copper-nickel sulphide ore minerals from Voronezh crystalline massife. Zapiski Vsesoyuznogo Mineralogicheskogo Obshchestva, 117: 351-359 (in Russian).

X-ray diffraction methods in determining quantitative mineral composition of chromite ore and metallurgical products

Säde Harle
Outokumpu Research Oy, P.O. Box 60, FIN-28100 Pori, Finland
sade.harle@outokumpu.com

ABSTRACT. The possibility of using x-ray diffraction (XRD) to quantify mineral composition of chromite ore and metallurgical products was tested both with the classical method, which is based on calibrations with standard samples, and the Rietveld method. The best results were obtained in the determination of chromite in the ore samples with the classical method. The average relative error was 2.9 %. The Rietveld-method proved to be less accurate and the relative errors were around 30 %. The inaccuracy of the Rietveld-calculations is due to difficulties in talc determinations. The Rietveld-method is more suitable for pyrometallurgical products, in which the amount of amorphous material is substantial. Sample preparation, especially grinding, is the main limitation in utilizing quantitative XRD methods. The grindabilities of the minerals are very different, e.g. soft clay-like minerals are easily overground.

1 INTRODUCTION

Quantification of phases is one of the most important tasks in process mineralogy. Traditionally, phases have been quantified by point counting. The method is neither the most economical nor the fastest. For this reason other methods have been developed for quantification. The most important ones are chemical methods (based on mass balance calculations), image analysis and quantitative X-ray diffraction (XRD).

This paper deals with the quantification for phases of chromite ore and metallurgical products by the classical absorption-diffraction method that requires a large number of calibration samples and the standardless Rietveld method. The results are presented in detail in an unpublished report and thesis (Harle 1999 and 2000).

2 RESEARCH METHODS

2.1 Samples

The calibration and validation samples for the classical method were compiled from pure mineral samples: chromite ($FeCr_2O_4$), talc ($Mg_3Si_4O_{10}(OH)_2$), clinochlore ($(Mg,Fe)_5Al(Si_3Al)O_{10}(OH)_8$), phlogopite ($KMg_3Si_3AlO_{10}(F,OH)$), calcite ($CaCO_3$) and dolomite ($Ca,Mg)(CO_3)_2$)

Chromite pellets were compiled from the same chromite and talc samples as the calibration and validation samples.

2.2 Sample preparation

For the calibration samples, pure minerals were milled for 15 s in a swing-mill. The desired weight fraction of each mineral was added to a calibration sample with a total mass of 10 g. The calibration samples covered a wide compositional range from 11 to 93 % chromite, 0-27.8 % chlorite, 1.8-57.0 % talc, 0-23 % calcite, 0-27 % dolomite and 0-5 % phlogopite. The calibration samples were swing-milled for 15 s before measurement.

The quality of the calibrations was checked with validation samples. They were prepared from a distinct grain size range of each mineral so that different minerals were as identical in grain size as possible. The grain size ranges were 180/315, 90/180, 45/90, 20/45 and <20 μm. The validation samples were then swing-milled for 30 s.

In metallurgical test, 80 % chromite and 20 % talc was mixed and made to pellets. The pellets were sintered at five temperatures using two different heating times. The sintered pellets were then crushed and 20 wt-% of corundum powder (Al_2O_3) was added to it and the mixture was then milled in Retsch laboratory mill for 25 s. Adding corundum enables estimation of amorphous material in the samples.

2.2 XRD measurements

The XRD measurements were done using Philips PW1820 diffractometer PC-APD 3.6 software and a Siemens D500 diffractometer and Brukers Siroquant™ 2.0 was used for the Rietveld-calculations.

3 QUANTIFICATION OF MINERAL COMPOSITION IN ORE

3.1 Effect of grinding on minerals

In quantitative XRD, the grain size of the material should preferably be less than 10 µm (Buhrke et al. 1998). XRD is very sensitive to sample preparation, in particular grinding, and the risk of overgrinding often occurs with soft clay-like minerals.

Grindabilities of pure minerals are often very different from each other. The grain size distribution graph in Figure 1 demonstrates the differences in the grindabilities of the minerals occurring in chromite ore.

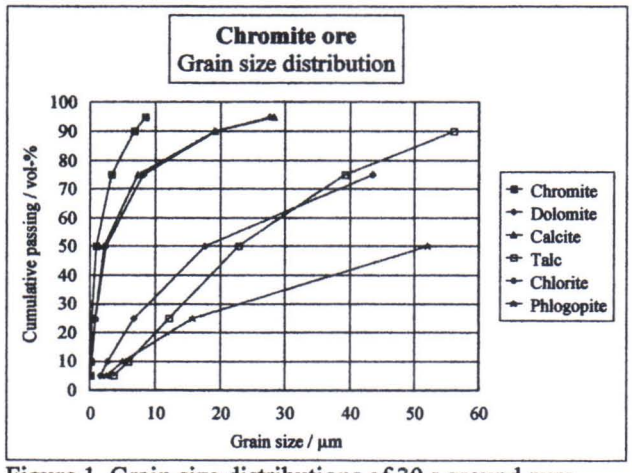

Figure 1. Grain size distributions of 30 s ground pure mineral samples.

The effects of grinding are even more complex in normal process samples, where interactions between hard and soft minerals affect the grain size. In the ore case, chromite grains behave like grinding balls that diminish the grain size of the softer minerals e.g. talc and carbonates.

Overgrinding of soft minerals is likely to happen while preparing samples for quantitative XRD. Figures 2 and 3 show the different behaviour of a hard mineral (chromite) and a soft one (talc) in a same sample. The peak intensity of chromite increases slightly with grinding time whereas the peak intensity of talc collapses to one third of the original value. The calibration curves were done with 30 s. ground samples which in case of talc, means clearly overgrinding.

Overginding is not the only possible problem in the sample preparation. Schmitz et al. (1994) had difficulties in getting fine enough grain sizes in quartz-bearing lignite samples. In this study such difficulties were not detected.

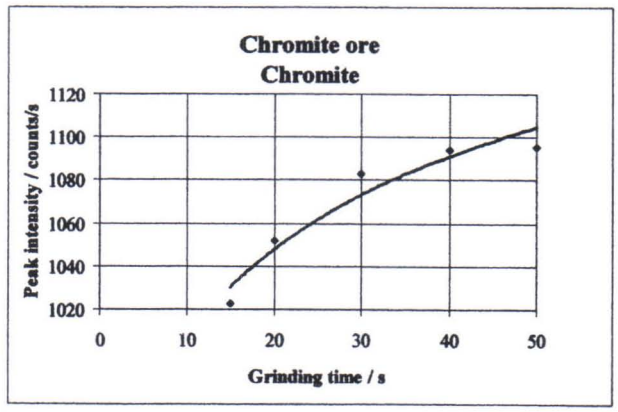

Figure 2. Effect of grinding on the XRD-peak intensity of chromite.

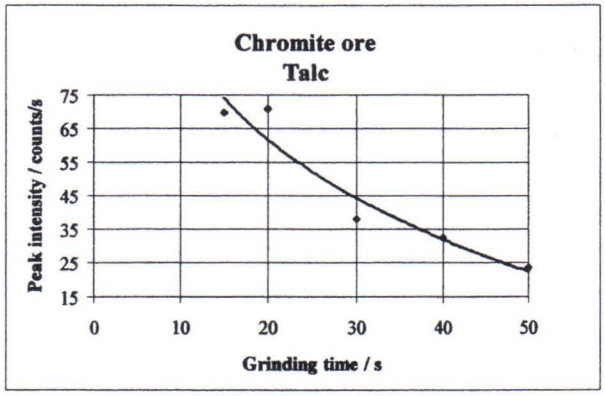

Figure 3. Effect of grinding on the XRD-peak intensity of talc.

3.2 Accuracy of the measurements

Mineral compositions obtained by the classical XRD and the Rietveld method were compared to the weighted compositions to validate the determinations.

Table 1. Weighted mineral composition of the validation samples.

	180/315	90/180	45/90	20/45	-20	Bulk
Chromite	63.0	56.0	49.0	42.0	35.0	52.7
Chlorite	7.0	8.4	9.9	11.3	12.8	9.1
Talc	19.0	22.2	25.4	28.6	31.8	23.7
Dolomite	7.0	8.5	10.0	11.5	13.0	9.2
Phlogopite	4.0	4.8	5.6	6.4	7.3	5.2

The classical XRD method proved to be a very accurate method to determine chromite composition in the ore regardless of the grain size of the original sample (Table 2). The relative error (difference between weighted and obtained mineral composition) of the determination as low as 2.9 % is on average. The relative errors for the other minerals are considerably higher. This is mainly due to two factors: the low absolute amounts of these minerals and overgrinding.

Table 2. Measured composition (classical XRD method) of samples in comparison to weighted composition (relative error).

Determined mineral composition / wt-%						
	180/315	90/180	45/90	20/45	-20	Bulk
Chromite	61.2	55.9	49.2	39.7	35.5	49.0
Chlorite	5.5	6.8	9.3	9.4	8.2	5.9
Talc	14.0	14.1	17.1	20.9	35.5	29.0
Dolomite	4.3	6.6	8.5	10.3	11.9	9.6
Phlogopite	1.6	3.1	4.1	4.3	4.3	5.4
Total	86.5	86.4	88.1	84.6	95.4	98.9
Relative error / %						
	180/315	90/180	45/90	20/45	-20	Bulk
Chromite	2.9	0.3	0.4	5.4	1.5	7.0
Chlorite	21.4	18.9	5.7	16.9	35.7	35.1
Talc	26.4	36.6	32.5	26.9	11.8	22.5
Dolomite	38.1	22.9	15.3	10.8	8.3	4.7
Phlogopite	59.5	34.2	27.5	32.4	41.4	4.4

The Rietveld method proved to be less accurate than the traditional one (Table 3). The reason for inaccurate results is the difficulty in the determination of talc and chlorite. Because the Rietveld method assumes the sum of the calculated phases to be 100 %, determination of every mineral suffers if one of the phases cannot be determined accurately. The goodness of fit (GOF) is a numerical value for the quality of the calculation. In an ideal case it should less than three (Anonymous 1996). The obtained compositons in this particular case should only be considered as trendsetting, because the GOF exeeds five.

Table 3. Measured composition (the Rietveld method) of samples in comparison to weighted composition (relative error).

Determined mineral composition / wt-%						
	180/315	90/180	45/90	20/45	-20	Bulk
Chromite	77.5	73.8	67.8	61.7	57.4	71.1
Chlorite	2.5	3.7	5.3	5.8	4.9	4.2
Talc	9.4	8.7	8.5	9.7	11.9	9.3
Dolomite	6.2	8.8	12.5	15.8	17.9	9.6
Phlogopite	4.4	5.1	5.9	7.0	7.9	5.9
Total	100.0	100.1	100.0	100.0	100.0	100.1
Goodness of fit	6.20	6.46	5.80	5.81	5.88	5.67
Relative error / %						
	180/315	90/180	45/90	20/45	-20	Bulk
Chromite	23.0	31.8	38.4	46.9	64.0	34.9
Chlorite	64.1	56.0	46.2	48.7	61.6	53.8
Talc	50.4	60.7	66.5	66.0	62.5	60.7
Dolomite	11.4	4.1	25.0	37.4	37.7	4.3
Phlogopite	11.1	6.6	5.2	8.8	8.8	14.1

4 QUANTIFICATION OF PHASE COMPOSITION IN SINTERED PELLETS

Chromite pellets are a feed material in the ferrochrome process. The effects of sintering on the phase compositions of the pellets were studied by using five different temperatures and different original mineral composition (Harle 1999). The Rietveld method was used in composition calculations. Chromite + 20 % talc is used in this paper as an example of the method.

The main phases in the sintered chromite-talc pellets are chromite, sesquioxide (eskolaite, $(Cr,Fe)_2O_3$) and an amorphous silicate phase. Minor amounts of enstatite ($Mg_2Si_2O_6$) and cristobalite (SiO_2) are also formed in the pellets (Figure 4). The phase composition of the products reflects the oxidation stage of the pellets.

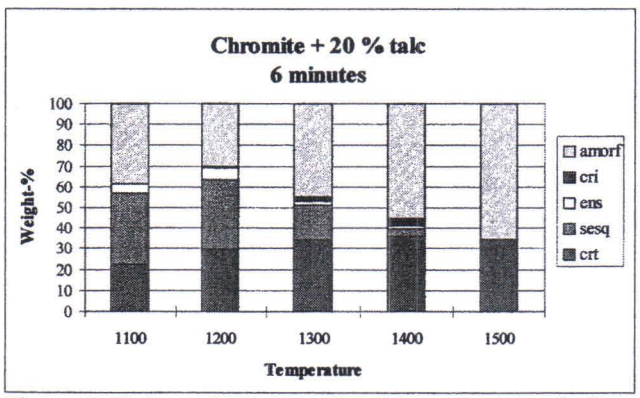

Figure 4. Estimated phase composition of sintered chromite pellets.

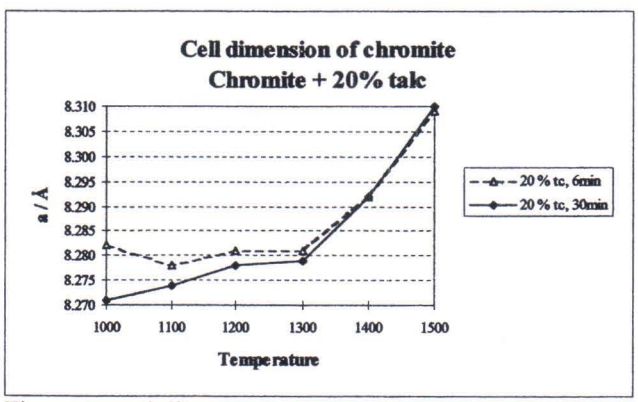

Figure 5. Cell dimension variation of chromite in sintered chromite+talc pellets.

One obvious advantage of the Rietveld method is the possibility to determine crystal structure (cell parameters) simultaneously with composition calculations. Figure 5 shows the increase of the cell dimension of chromite with the heating temperature. In the case of chromite, the cell dimension reflects the composition of chromite.

5 CONCLUSIONS

The results of this study show that quantitative XRD methods are suitable for many types of process mineralogical determinations. The best available technique depends on the mineral assemblage. The classical method is more suitable for the talc-containing ore samples, because talc is very difficult to determine with the Rietveld method. In contrast, the Rietveld method is better for pyrometallurgical products, in which the amount of amorphous material is substantial.

Sample preparation, especially grinding, is the main limitation in utilising quantitative XRD methods. Minerals behave in grinding in a very different manners and this should always be taken in concideration. Selection of the best possible method depends on the mineral assamblage and the type of the sample.

7 REFERENCES

Anonymous 1996. Siroquant™, Version 2.0 (June 1996). Operation Manual. Sietronics, Australia.

Buhrke, Victor E., Jenkins, Ron and Smith Diane K. (editors) 1998. A Practical Guide for the Preparation of Specimens for X-Ray Fluorescence and X-Ray diffraction Analysis. Wiley-VCH, New York. 333 p.

Harle, Säde 1999. Sintrattujen pellettien faasikoostumuksen määrittäminen XRD-menetelmällä. Outokumpu Research Oy, Unpublished research report 99108-ORC-T. 34 p.

Harle, Säde 2000. Kvantitatiivisen röntgendiffraktion soveltaminen prosessinäytteiden mineraalikoostumuksen määrittämiseen. University of Helsinki, Department of Geology. Unpublished licentiate thesis. 104 p.

Schmitz, W., Zahn, A., Geissler, S., and Straube, K.1994. Comparison of multiphase Rietveld and classical quantitative X-ray analysis. Materials Science Forum Volumes 166-169, 699-704.

Microbial sulfide oxidation and secondary mineral formation

R. B. Herbert Jr.
Department of Geology and Geochemistry, Stockholm University, S - 106 91 Stockholm, Sweden
Roger.Herbert@geo.su.se

ABSTRACT. Mine waste deposits contain an abundance of bacteria, including iron- and sulfur-oxidizing bacteria such as *Thiobacillus ferrooxidans*. The presence of *T. ferrooxidans* and other bacteria can accelerate the rate of Fe^{2+} and pyrite oxidation by several orders of magnitude, relative to the abiotic rates. In addition to their effect on sulfide oxidation, bacteria in mine waste deposits are reactive solids providing effective nucleation sites for metal adsorption and precipitation. The interaction of dissolved metals and surface functional groups results in the adsorption of metals to the bacterial surfaces, and may subsequently provide discrete sites for mineral nucleation and the precipitation of secondary iron phases (*e.g.* ferric oxyhydroxides; ferrous sulfides). Mineral phases that nucleate and precipitate on bacterial surfaces are notoriously difficult to characterize because of their poor crystallinity and intimate relationship with biological membranes.

1 INTRODUCTION

Where ever mining activities expose sulfide mineral deposits and extract base and precious metals from sulfidic ore bodies, the atmospheric oxidation of sulfide minerals is a potential source of acid mine drainage. Pyrite (FeS_2) is the most common sulfide mineral present in sulfide ore deposits, and is thus the most common source of acid mine drainage from mine workings and mine waste deposits. In the presence of atmospheric oxygen, pyrite oxidation can be written as:

$$FeS_{2(s)} + 7/4O_{2(g)} + H_2O_{(aq)} \Rightarrow Fe^{2+}_{(aq)} + 2SO_4^{2-}{}_{(aq)} + 2H^+_{(aq)} \quad (1)$$

In addition to atmospheric oxygen, other oxidants may contribute to the oxidative dissolution of sulfide minerals. Ferric iron is a strong oxidant of pyrite, such that at low pH (< 4.5) and under sterile conditions, it is widely accepted that Fe^{3+} oxidizes pyrite much faster than O_2 (*cf.* equation 1):

$$FeS_{2(s)} + 14Fe^{3+}_{(aq)} + 8H_2O_{(aq)} \Rightarrow 15Fe^{2+}_{(aq)} + 2SO_4^{2-}{}_{(aq)} + 16H^+_{(aq)} \quad (2)$$

This reaction proceeds more rapidly than the abiotic oxidation of dissolved Fe^{2+} to Fe^{3+}. For this reason, ferrous iron oxidation is considered the rate-limiting step in abiotic pyrite oxidation. A recent review of sulfide oxidation in mine wastes has been presented in Nordstrom & Alpers (1999).

2 BACTERIAL MEDIATION OF SULFIDE OXIDATION

Mine waste deposits possess a complex microbial ecology consisting of numerous auto- and heterotrophic microorganisms, as well as fungi and prokaryotes (*e.g.* yeast). Within this ecosystem, there is an abundance of bacteria, including iron- and sulfur-oxidizing bacteria such as *Thiobacillus ferrooxidans*. This bacteria is chemolithotrophic (autotrophic), oxidizing reduced inorganic compounds including ferrous iron and sulfides with oxygen as an electron acceptor, in order to gain energy for carbon dioxide fixation. The presence of *T. ferrooxidans* and other bacteria can accelerate the rate of Fe^{2+} oxidation by O_2 by up to six orders of magnitude (Singer & Stumm 1970). However, *T. ferrooxidans* activity is a function

of pH, with an optimal growth pH of < 3 (Nordstrom & Southam 1997). At very low pH, pyrite oxidation is diminished because of physiological limitations on the bacterial production of Fe^{3+}, while above pH 3.5, the pyrite oxidation rate is limited by the decreasing solubility of Fe hydroxides. For both the abiotic and microbial processes, sulfide oxidation will be limited by the availability of oxygen as either a direct oxidant of sulfide (equation 1) or for the oxidation of ferrous iron.

Although *T. ferrooxidans* is often considered the primary bacterial mediator of pyrite oxidation in mine wastes, a variety of other iron- and/or sulfur-oxidizing bacteria such as *T. thiooxidans* and *Leptospirillum ferrooxidans* may be present, depending on mineral composition and geochemical conditions in the oxidative environment. For example, in studies of tailings deposits where neutral pH conditions persist because of carbonate dissolution, populations of the neutrophilic species *T. thioparus* were 1 - 6 orders of magnitude higher than the population of acid-tolerant *T. thiooxidans* and acidophilic *T. ferrooxidans* (Blowes *et al.* 1998).

Since the oxidation of S in pyrite requires the transfer of many electrons, various S species with progressively greater oxidation states are produced during the intermediate steps. Examples of intermediate species include elemental sulfur (S^0), thiosulfate ($S_2O_3^{2-}$), sulfite (SO_3^{2-}), and tetrathionate ($S_4O_6^{2-}$; see Figure 1). Elemental sulfur has been identified in mine waste deposits, but is generally associated with the oxidation of monosulfides such as pyrrhotite ($Fe_{1-x}S$; Bhatti *et al.* 1993) and not with pyrite. As shown in Figure 1, sulfur anions of higher oxidation state than S^0 (*e.g.* sulfite, thiosulfate, polythionates) may also be produced in intermediate steps during bacterial oxidation (Moses *et al.* 1987), but these are metastable and will rapidly oxidize to sulfate in the presence of the Fe^{3+}.

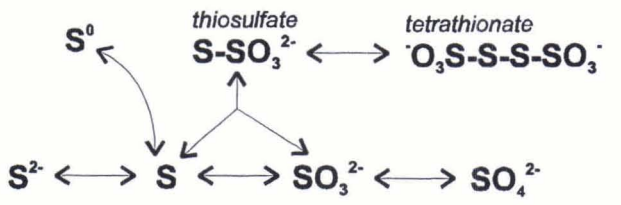

Figure 1. Bacterial oxidation of sulfide to higher oxidation states. Adapted from Suzuki *et al.* (1994).

In recent years, the production of oxidation products on pyrite and other sulfide surfaces has been investigated using surface-sensitive techniques such as X-ray photoelectron spectroscopy (XPS). Buckley and Woods (1987) concluded that iron tends to be easily leached from a pyrite surface producing an iron-deficient surface that does not have the properties of elemental sulfur unless prolonged strong acid attack is used. The presence of surficial elemental sulfur was confirmed in studies by Sasaki *et al.* (1995). Other studies (*e.g.* Nesbitt & Muir 1994) have shown that initial dissolution under acidic conditions releases iron and produces a surface layer containing disulfide, monosulfide, and polysulfides. With increased oxidation, the levels of monosulfide decrease relative to disulfide and polysulfides, and thiosulfate and sulfate begin to form (Guevremont *et al.* 1998). This sulfur-rich surface should be energetically favorable for *T. thiooxidans*, and may explain their association with *T. ferrooxidans* (Sasaki *et al.* 1995).

3 OXIDATION PATHWAYS

The oxidation of sulfide minerals in mine waste deposits can proceed via a number of pathways, as illustrated in Figure 2. Solid-phase sulfide may be abiotically oxidized by O_2 (pathway 1, equation 1). It should be apparent here that this abiotic oxidation mechanism has limited relevance, because iron- and sulfur-oxidizing bacteria are ubiquitous in ground and surface waters and are omnipresent mediators in sulfide oxidation reactions (*i.e.* pathways 2 – 5). In systems containing iron, *T. ferrooxidans* may exclusively oxidize Fe^{2+} to Fe^{3+} to gain energy, although reduced S is also a potential source of energy, with O_2 used as an electron acceptor (pathway 2). Ferric iron may oxidize pyrite (equation 2) with or without microbial mediation (Figure 2, pathways 4 and 3, respectively). Finally, other oxidants may be present in the mining environment, such as nitrate (pathway 5), and nitrate-reducing bacteria may contribute to pyrite oxidation.

Much of the debate on sulfide oxidation centers on the evidence for an indirect or direct oxidation mechanism (*e.g.* Wakao *et al.* 1984; Sand *et al.* 1995). Free-floating bacteria can catalyze the oxidation of ferrous to ferric iron in aqueous solution, with ferric iron as the electron

acceptor in the abiotic oxidation of pyrite (Figure 2, pathway 3). This is the 'indirect mechanism'. The 'direct contact mechanism' works by direct bacterial adhesion to the pyrite surface (Figure 2, pathway 2), where the sulfide surface is solubilized through hypothesized enzymatic oxidation reactions (Ehrlich 1981). Extracellular polymeric substances, composed primarily of lipopolysaccharides, mediate the contact between the bacterial cell and sulfide energy source, and play an important role in organic film formation and bacterium-substratum interactions.

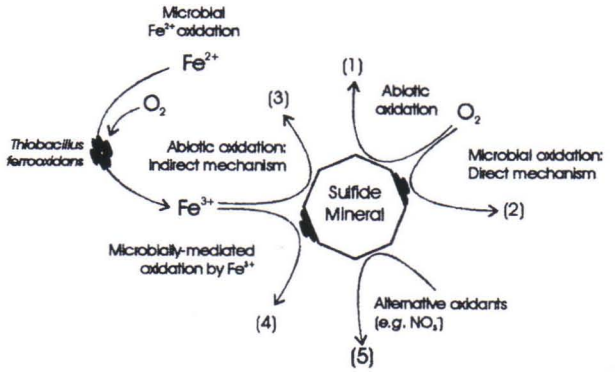

Figure 2. Alternative pathways in the oxidative weathering of sulfide minerals.

Nordstrom & Alpers (1999) contend that the indirect mechanism is dominant, as abiotic Fe^{3+} oxidation rates generally exceed biotic rates, but there is evidence to the contrary. In a study by Bennett & Tributsch (1978), they confirmed that the chemical processes taking place on the pyrite surface due to oxidizing bacteria occur mainly in the region of contact between bacteria and pyrite. They also suggested that the bacterial distribution on the surface is dependent on the crystal structure and the diversity in the crystal order (fracture lines, dislocations) of the pyrite. This suggests that it is more favorable for the bacteria to obtain their energy from solid surfaces that are characterized either by weaker chemical bonding or by an increased surface area along cracks or polycrystalline regions. It appears that *T. ferrooxidans* is capable of distinguishing between favorable and less favorable sites for energy extraction, selecting the site of attack according to the availability of nutrient.

In the discussion of direct or indirect sulfide oxidation mechanisms, it may be that both groups are correct, as both bacterial attachment and Fe^{3+} are required (Figure 2, pathway 4). A recent study by Gehrke *et al.* (1998) indicated that extracellular polymeric substances, which are apparently necessary for bacterial attachment to solid substrates, are important in the first steps in metal sulfide dissolution. Charge effects are involved in the attachment. Primary attachment to pyrite is mediated by Fe^{3+} ions complexed with the bacterial exopolymers, which allows for an electrochemical interaction with a negatively charged pyrite surface ($pH_{i.e.p.}$ ~ 1.5, Bebie *et al.* 1998). *T. ferrooxidans* regenerates the Fe^{3+} ions and uses the energy for growth. Thus, although direct bacterial contact is required for this oxidation mechanism, the main bacterial contribution is to keep the iron ions in the oxidized state. The actual sulfide oxidation proceeds chemically. Consequently, the indirect leaching mechanism is supported by the data of Gehrke *et al.* (1998), in addition to other studies such as Sand *et al.* (1995).

4 MINERAL NUCLEATION ON BACTERIAL SURFACES

Evidence for microbial ferrous iron oxidation is usually pervasive at mine sites: the formation of yellow-red iron precipitates is readily apparent in the upper horizons of mine deposits and in near-lying surface water. These precipitates are often composed of ferric oxides and oxyhydroxides (*e.g.* goethite, α-FeOOH; ferrihydrite, $Fe_5HO_8 \cdot 4H_2O$) and ferric sulfates [*e.g.* jarosite, $KFe_3(SO_4)_2(OH)_6$; schwertmannite, $Fe_{16}O_{16}(OH)_y(SO_4)_z \cdot nH_2O$]. The precipitation of secondary oxides from solution is usually initiated by the nucleation of poorly – ordered relatively soluble ferric oxides (*e.g.* ferrihydrite). These poorly - crystalline phases will, with time, crystallize to less soluble phases (*e.g.* goethite) through a loss of water from the structure and a refinement in crystal order. The initial nucleation of soluble Fe oxides directly from solution requires a certain degree of supersaturation. Alternatively, nucleation can be facilitated by organic and inorganic surfaces, with nucleation initiated as the surface adsorption of iron (Warren & Ferris 1998).

In addition to their effect on sulfide oxidation and dissolution, bacteria in mine waste deposits are reactive solids providing effective nucleation sites for metal adsorption and precipitation (Schultze-Lam *et al.* 1996; Fortin & Beveridge 1997b). The reactivity of the

bacterial surfaces is derived from the presence of amphoteric surface functional groups (e.g. carboxyl, phosphoryl, and amino groups) that are associated with structural polymers in the cell walls and external sheaths or capsules of individual cells (Beveridge *et al.* 1997). The point of zero net proton charge is generally quite low for bacterial surfaces, such that even at low pH, many of these functional groups will be deprotonated and thus negatively charged (Beveridge 1989). The interaction of dissolved metals and these surface functional groups results in the adsorption of metals to the bacterial surfaces, and may subsequently provide discrete sites for mineral nucleation and precipitation reactions (Warren & Ferris 1998). The adsorption of anions such as silicate ($H_3SiO_4^-$) may also be enhanced by the presence of bacterial surfaces (Fortin & Beveridge 1997b), leading to the formation of surface layers of amorphous silica.

For iron-oxidizing bacteria (*e.g. T. ferrooxidans*, *Gallionella ferruginea*), high concentration gradients of ferric iron will exist close to the cell surfaces as a direct consequence of metabolic ferrous iron oxidation; ferric iron adsorption and oxide nucleation should thus be promoted on these bacterial surfaces. Indeed, iron oxyhydroxide precipitates have been observed in intimate association with *T. ferrooxidans* surfaces and other bacteria in a number of studies (*e.g.* Southam & Beveridge 1992; Fortin & Ferris 1998). These fine-grained precipitates provide a large surface area for the further nucleation and the adsorption of other heavy metals. In contrast, iron sulfide may precipitate on the surfaces of sulfate-reducing bacteria under anoxic conditions below the water table or below a hard pan (Fortin & Beveridge 1997a), also providing a large surface area for trace metal adsorption. Secondary metal sulfides of lower solubility (*e.g.* CuS, ZnS) may also precipitate in the tailings, or may form by cation substitution for iron in pre-existing iron sulfides.

Mineral phases that nucleate and precipitate on bacterial surfaces are notoriously difficult to characterize due to their poor crystallinity and intimate relationship with biological membranes. Most traditional methods of mineralogical characterization, such as X-ray diffractometry, suffer from a lack of near – surface resolution and will only provide a bulk composition. In general, successful methods for the characterization of biominerals rely on imaging techniques coupled with elemental and/or mineralogical analysis. Transmission electron microscopy coupled with energy - dispersive spectroscopy (EDS) is commonly used for imaging biofilms and providing chemical analyses, while selected area electron diffraction can yield data on mineralogical composition (*e.g.* Fortin & Ferris 1998). Low vacuum techniques, such as those utilizing environmental scanning electron microscopy (ESEM), are often very effective, as cellular membranes are preserved in the water saturated analytical chamber. Surface analyses are generally not possible by ESEM – EDS analysis, as the electron beam excites a rather large sample volume. Surface analyses of biogenic minerals and bacteria require high vacuum techniques, which generally dehydrate and destroy bacterial membranes. Nevertheless, surface methods such as XPS can provide much information on the composition, valence state, and ligand binding in bacterial precipitates.

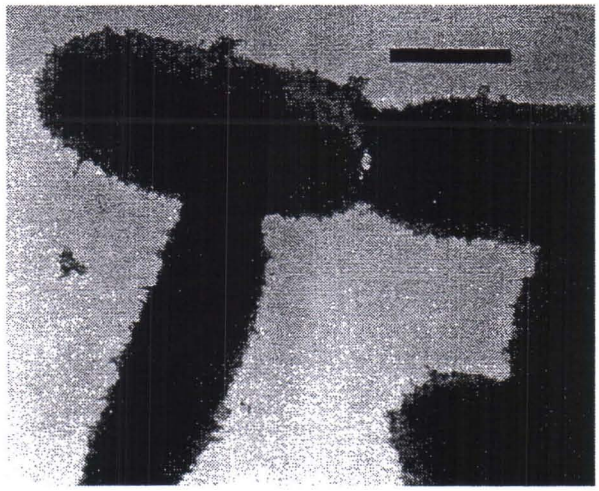

Figure 3. Transmission electron micrograph of *Pseudomonas aeruginosa* with surface precipitates of poorly ordered two-line ferrihydrite (selected area electron diffraction analysis). Solution conditions: pH 4, 10^{-4} M Fe. Scale bar = 500 nm. Reprinted with permission, from Warren & Ferris (1998). © 1998 American Chemical Society.

5 ACKNOWLEDGMENTS

The data presented in this paper has been collected and reviewed within the Swedish research program *Mitigation of the Environmental Impact from Mining Waste* (MiMi) under funding by the *Foundation for Strategic Environmental Research* (MISTRA).

6 REFERENCES

Bebie, J., Schoonen, M.A.A., Fuhrmann, M. & Strongin, D.R. 1998. Surface charge development on transition metal sulfides: An electrokinetic study. Geochimica et Cosmochimica Acta, 62, 633 - 642.

Bennett, J. & Tributsch, H. 1978. Bacterial leaching patterns on pyrite crystal surfaces. Journal of Bacteriology, 134, 310-317.

Beveridge, T.J. 1989. Metal ions and bacteria. In: Metal ions and bacteria (T.J. Beveridge & R.J. Doyle, Eds.). Wiley, New York, pp. 1 – 30.

Beveridge, T.J., Hughes, M.N., Lee, H., Leung, K.T., Poole, P.K., Savvaidis, I., Silver, S. & Trevors, J.T. 1997. Metal – microbe interactions: Contemporary approaches. Advances in Microbial Physiology, 38, 177 – 243.

Bhatti, T., Bigham, J., Carlson, L. & Tuovinen, O. 1993. Mineral products of pyrrhotite oxidation by Thiobacillus ferrooxidans. Applied & Environmental Microbiology, 59, 1984-1990.

Blowes, D.W., Jambor, J.L., Hanton-Fong, C.J., Lortie, L. & Gould, W.D. 1998. Geochemical, mineralogical and microbiological characterization of a sulphide-bearing carbonate-rock gold-mine tailings impoundment, Joutel, Québec. Applied Geochemistry, 13, 687 - 705.

Buckley, A.N. & Woods, R.W. 1987. The surface oxidation of pyrite. Applied Surface Science, 27, 437 - 452.

Ehrlich, H.L. 1981. Geomicrobiology, Dekker, New York.

Fortin, D. & Beveridge, T.J. 1997a. Microbial sulfate reduction within sulfidic mine tailings: Formation of diagenetic Fe sulphides. Geomicrobiology Journal, 14, 1-21.

Fortin, D. & Beveridge, T.J. 1997b. Role of the bacterium Thiobacillus in the formation of silicates in acidic mine tailings. Chemical Geology, 141, 235 – 250.

Fortin, D. & Ferris, F.G. 1998. Precipitation of iron, silica, and sulfate on bacterial cell surfaces. Geomicrobiology Journal, 15, 309 – 324.

Gehrke, T., Telegdi, J., Thierry, D. & Sand, W. 1998. Importance of extracellular polymeric substances from Thiobacillus ferrooxidans for bioleaching. Applied & Environmental Microbiology, 64, 2743 – 2747.

Guevremont, J.M., Bebie, J., Elsetinow, A.R., Strongin, D.R. & Schoonen, M.A.A. 1998. Reactivity of the (100) plane of pyrite in oxidizing gaseous and aqueous environments: Effects of surface imperfections. Environmental Science & Technology, 32, 3743 - 3748.

Moses, C.O., Nordstrom, D.K., Herman, J.S. & Mills, A. 1987. Aqueous pyrite oxidation by dissolved oxygen and by ferric iron. Geochimica et Cosmochimica Acta 51, 1561-1571.

Nesbitt, H.W. & Muir, I.J. 1994. X-ray photoelectron spectroscopic study of a pristine pyrite surface reacted with water vapour and air. Geochimica et Cosmochimica Acta, 58, 4667 – 4679.

Nordstrom, D.K. & Alpers, C.N. 1999. Geochemistry of acid mine waters. In: The Environmental Geochemistry of Mineral Deposits. Part A: Processes. techniques, and health issues (G.S Plumlee & M.J. Logsdon, Eds.). Reviews in Economic Geology, 6A, 133 - 160.

Nordstrom, D.K. & Southam, G. 1997. Geomicrobiology of sulfide mineral oxidation. In: Geomicrobiology: Interactions between microbes and minerals (J.F. Banfield and K.H. Nealson, Eds). Reviews in Mineralogy, 35, 361 – 390.

Sand, W., Gerke, T., Hallmann, R. & Schippers, A. 1995. Sulfur chemistry, biofilm, and the indirect attack mechamism - a critical evaluation of bacterial leaching. Applied Microbiology & Biotechnology, 43, 961 - 966.

Sasaki, K., Tsunekawa, M., Ohysuku, T. & Konno, H. 1995. Confirmation of a sulfur-rich layer on pyrite after oxidative dissolution by Fe(III) ions around pH 2. Geochimica et Cosmochimica Acta, 59, 3155-3158.

Schultze-Lam, S., Fortin, D., Davis, B.S. & Beveridge, T.J. 1996. Mineralization of bacterial surfaces. Chemical Geology, 132, 171-181.

Singer, P.C. & Stumm, W. 1970. Acidic mine drainage: The rate-determining step. Science, 167, 1121-1123.

Southam G. & Beveridge T.J. 1992. Enumeration of Thiobacilli within pH-neutral and acidic mine tailings and their role in the development of secondary mineral soil. Applied and Environmental Microbiology, 58, 1904-1912.

Suzuki, I., Chan, C.W. & Takeuchi, T.L. 1994. Oxidation on inorganic sulfur compounds by Thiobacilli, In: Environmental Geochemistry of Sulfide Oxidation (C.N. Alpers & D.W. Blowes, Eds.). American Chemical Society symposium series 550, Washington, D.C. pp. 60 – 67

Wakao, N., Mishina, M., Sakuri, H. & Shiota, H. 1984. Bacterial pyrite oxidation, III. Adsorption of Thiobacillus ferrooxidans cells on solid surfaces and its effect on iron release from pyrite. Journal of General & Applied Microbiology, 30, 63 - 77.

Warren, L.A. & Ferris, F.G. 1998. Continuum between sorption and precipitation of Fe(III) on microbial surfaces. Environmental Science & Technology, 32, 2331 – 2337.

Optical absorption spectroscopy - the method and applications in mineral science

U. Hålenius
Department of Mineralogy
Swedish Museum of Natural History
Box 50007, SE-104 05 Stockholm
ulf.hålenius@nrm.se

ABSTRACT. Optical absorption spectroscopy is a mature method, which has found a wide range of applications in mineral science during the last four decades. It has with considerable success been applied to determine cation valence in minerals, intracrystalline cation distribution in structurally complex phases, quantitative cation concentrations and stabilisation energies of cations in minerals. The integration of the petrographic microscope and the optical spectrophotometer represents a major improvement from the Earth Sciences point of view, which allows studies of fine-grained anisotropic minerals directly in petrographic thin sections at comparably high resolution.
The information retrieved by optical absorption spectroscopy is largely limited to the character of transition metal cations and their structural environment, primarily the first coordination sphere. This limitation is explained by the fact that the method is mainly used to detect electronic transitions in the cation valence shell. In spite of this, geochemically relevant information can be obtained on, e.g., the speciation of members of the first transition element series, of which some occur in high crustal abundance (e.g. Fe) or are otherwise of interest from an economic or environmental point of view (e.g., Cu, Ni or Cr).

1 INTRODUCTION

Optical absorption spectroscopy may in a popular way be defined as a method for the analysis of colours in matter. In combination with theoretical model concepts as, e.g., crystal field theory, ligand field theory or molecular orbital theory, which relate to quantum mechanics and group theory, it provides a means to gather detailed information on the valence and structural incorporation of cations in substances. In Earth Sciences the method has also been applied as an analytical technique, which allows quantitative *in situ* determination of cation concentrations in minerals. In addition, it has been used to determine thermodynamically relevant parameters as, e.g., the crystal field stabilisation energy of cations.

Classically, optical absorption spectra record the colour of a mineral or other substance by measuring its transmission of light at all the wavelengths which make up the visible part of the electromagnetic spectrum. A large number of different effects may contribute to the recorded spectrum. Just to mention a few, we may encounter interference effects, as in opal and some feldspar minerals or electron defects contributing to the formation of colour centre as in sodalite. In many ore minerals colours relate to transitions in electronic band structures. A very useful compilation of causes for mineral colours is given by Burns (1993) in his comprehensive work on crystal field studies of minerals.

The most frequent cause for coloration in transparent minerals is related to transfer of electrons in cations of the transition elements. Several of these elements are of geochemical importance as they may be common in the Earth's crust or they may be of economic or environmental importance. Specifically, this applies to the cations of the first transition element series (3d-elements), which comprise Sc, Ti, V, Cr, Mn, Fe, Mn, Co, Ni, Cu and Zn. REE-cations (4f-elements) also represent geochemically interesting species, which may be studied by means of optical absorption spectroscopy.

The electron transfers occur between different orbitals in the valence shell of the cation and they normally produce discrete bands in the recorded optical absorption spectrum. The character of the absorption bands in terms of, e.g., energy, intensity, widths, anisotropy etc., is related to the electron configuration of the absorbing cation as well as the character of the surrounding ligand sphere (number of ligands, ligand charge distribution and symmetry of the ligand arrangement). Consequently, optical absorption spectroscopy can provide information on cation valences as well as on the nature of the interacting local ligand sphere. In contrast to common bulk methods , e.g., XRD-techniques, optical absorption spectra can provide this type of local information even in weakly 3d-element substituted minerals. In addition, the information may be recorded with an areal resolution almost comparable to, e.g., electron microprobe techniques.

2 PHYSICAL BACKGROUND

2.1 *Transitions and absorption band character*

As cations of the first transition series (3d-elements) are of major interest from a geochemical point of view, they have been chosen to examplify the nature of electron transitions and resulting absorption bands.

The electrons in the incompletely filled d-shell of a 3d-cation are distributed over five different d-orbitals. In the free ion, all five orbitals are energetically degenerate, but in a crystalline phase, where ligand charges act on the central cation, this degeneracy is lifted. This allows transitions of different energy to occur through transfer of electrons between different d-orbitals. Such electronic d-d transitions may be of two main types, *spin-forbidden* or *spin-allowed*. In the first case, which applies to cations with half-filled d-orbitals ($3d^5$-cations) as, e.g., high-spin ferric iron or divalent manganese, any d-d electron transfer will involve a change of the number of orbitals with unpaired electron population. This violates fundamental transition selection rules and the resulting probability of such a transition becomes very low. For spin-allowed electronic d-d transitions, the number of unpaired d-electrons are the same in the ground state and in the excited electronic state. The transition is consequently allowed according to spin-multiplicity rules. The probability for such transitions are orders of magnitude higher than for the spin-forbidden transitions. Consequently, spin-allowed electronic transitions result in absorption bands which are much more intense than those caused by spin-forbidden ones.

The number of spin-allowed d-d transitions occurring in a 3d-cation is dependent on the symmetry of the surrounding ligand field. In a cation placed in a regular octahedral or tetrahedral field only one transition may be observed, but at decreasing point symmetry of the field an increasing number (for 3d-cations, maximum of four) of energetically different transitions occur.

Additional prolific features (IVCT-bands) caused by electron transfer in homonuclear or heteronuclear cation clusters are often encountered in spectra of rock-forming minerals. Numerous examples of Fe^{2+}-Fe^{3+} charge transfer bands have for instance been observed in spectra of many common Mg-Fe silicates. The processes causing these bands bend the selection rules and consequently resulting band intensities are anomalous, often being orders of magnitude higher than those observed for spin-allowed d-d bands.

Absorption bands in optical spectra are not sharp lines, bur rather broad features of approximately Gaussian shape. In addition to the obvious effect of closely spaced bands, broadening is related to thermal lattice vibrations. Consequently, bands become sharper in spectra measured at low temperatures. In general, broadening is more pronounced for bands caused by transitions involving electronic states arising from the same ground state. This explains why absorption bands caused by spin-allowed transitions are often distinctly broader than spin-forbidden bands. Intervalence charge transfer transitions, which involve electron transfer between nuclei at larger distances are even more effected by lattice vibrations, which is one reason for the very large band widths observed for IVCT-bands.

2.2 *Coordination and polarisation*

The occurrence of transition metal cations in coordination polyhedra of low-symmetry leads not only to a splitting of the d-orbital energy levels but also to crystallographic dependencies of the transition probabilities. In polarised light, spectra of non-cubic minerals will show strong

band anisotropy, which is related to the point symmetry of the ligand field at the absorbing 3d-cation. The interpretation of band polarisation is based on group theory, which considers the symmetry of the involved ground and excited electronic states and the electric vector of the polarised light transmitted through the crystal. In addition to this, the symmetry of vibrational modes must be considered in the interpretation.

2.3 *Cation concentration and band intensity*

The measured intensity or optical density (OD) of an absorption band is related to three factors: the thickness of the absorber (t), the concentration of the absorbing cation species (C) and the molar extinction coefficient (ε) of the absorption band:

$$OD = t \cdot C \cdot \varepsilon.$$

Provided that the ε-value for a specific absorption band has been established, the concentration of a cation may be measured by recording the optical spectrum and the thickness of the mineral absorber. Unfortunately, ε-values are not only different for different cations but they also vary with mineral matrices and polarisation. In fact, one could say that each d-d band has its own ε-value and directional dependency. Nevertheless, a large number of useful ε-values for bands related to different 3d-cations in various mineral polyhedra have been established during the years. These allow quantitative determinations of cation concentrations in geologically important minerals directly from recorded optical absorption spectra. For kinetic studies or other applications focusing on changes in cation concentrations over very small distances, optical absorption spectroscopy represents an interesting method and its potential has so far not been fully realised.

3 THE TECHNIQUE

3.1 *Instrumentation*

As with all resonance methods, optical absorption spectroscopy relies basically on two technical devices; a radiation source and a detector. The radiation source must of course cover, with as high brilliancy as possible, the range of energies at which the phenomena of interest occur and likewise the detector system must be as sensitive as possible to radiation of these energies. Optical absorption spectroscopy covers a relatively large range of the electromagnetic spectrum, from the low-energy UV over the visible range (VIS) to the near infrared (NIR). This range extends roughly from 250 to 2,500 nm (40,000 - 4,000 cm^{-1}) and this makes it necessary to use a number of different light sources and detectors to ensure high instrumental efficiency in all parts of the spectrum.

In order to obtain information of high spectral resolution different strategies may be employed. In the conventional and so far most frequently used instruments, this is achieved by placing monochromators in the light beam. Monochromators may be prisms or gratings.

With the aim to improve the spatial resolution, optical absorption spectra may be recorded through the lens system of a petrographic microscope. This enables measurements of particles down to approximately 5 μm in diameter, and ideally spectra may be recorded on single crystals of minerals in a standard petrographic thin-section.

As most minerals are optically aniostropic, polarisers, which allow spectral recordings with the E-direction of the incident light beam parallel to the optical main axes, are integral parts of the instruments. Commonly, calcite-based Glan-Thompson prisms are used as polariser, but also different types of polarising films are in use. The latter provide efficient polarisation only in restricted spectral ranges, and consequently at least three different coated filters have to be employed in order to ensure adequate polarisation of the light-beam in the entire UV-VIS-NIR range.

In addition to the briefly mentioned major components of the instrumentation, a number of alternative accessories complete the measuring system. Details on these and other matters are given in Piller (1977) and further details are also provided by Langer & Frentrup (1978).

3.2 *Samples and preparation*

In principle, useful optical absorption spectra may be obtained from mineral grains in standard petrographic thin sections. There are, however, some limitations which need to be considered. Primarily, polished thin sections should be used. This minimises the distance which the light beam needs to travel through embedding material etc. They also ensure smooth and parallel mineral surfaces for light entrance and exit,

which minimises stray light effects. As thin sections normally are just 30 μm thick, there may occur detection problems. This is specifically true for samples which contain very low concentration of the absorbing species or cations which are characterised by bands with low ε-values. The problem is obvious for minerals containing $3d^5$-cations as, e.g., Fe^{3+} or Mn^{2+}, which only produce spin-forbidden d-d absorption bands. A further limitation, which is specifically problematic for analytical applications, is related to optical anisotropy, which characterises a large fraction of all known minerals. Provided that the mineral of interest occurs abundantly in the thin section, suitably oriented single crystals are most likely present. This needs, however, to be ascertained, for instance, through optical interference figures using conoscopic microscopy.

In those cases where spectra may not be recorded, with full crystallographic control, from mineral grains in a thin section, one normally relies on absorbers prepared from selected single crystals. Selected mineral grains may be oriented on the basis of crystal habitus, cleavages or preferentially by conoscopic microscopy or XRD-methods. Subsequently, the grains are transferred, with retention of the orientation, to a glass slide covered with a suitable embedding material (e.g., thermoplastic resin). After resin hardening and grinding to an appropriate sample thickness, two carefully polished and parallel surface should be produced.

4 SOME APPLICATIONS

4.1 *Valence determinations*

Iron and manganese are frequent elements in many common minerals. They may occur as nominal constituents or as substituting elements at lower concentration levels. They often interact with other common elements as, e.g., Al, Mg or Ca through exchange processes in solid solution series. Intercrystalline distribution of Fe between Fe-Mg phases as members of the pyroxene, mica, garnet or spinel groups may provide information on the conditions for mineral formation.

Iron as well as manganese occur in the divalent and trivalent state in several of these minerals. Consequently, it is essential for the calculation of partioning coefficients, which constitute the basis for thermal or barometric interpretations, that not only elemental concentration but also valency information is available. Many mineral investigations by means of optical absorption spectroscopy has focused on the question on 3d-cation speciation. Burns (1993) presents a comprehensive compilation of these studies.

4.2 *Concentration determinations*

Ordering of 3d-cations among available cation sites is often depending on the temperature and/or pressure prevailing during mineral crystallisation or on the thermal history of the mineral. Information on cation order may be obtained by a number of bulk methods, e.g., XRD single crystal refinements. Optical absorption spectroscopy provides an alternative method, which allows data collection at a high spatial resolution. In this category of studies, the investigation on Fe-Mg distribution among M1- and M2-sites in orthopyroxene by Goldman & Rossman (1978) is a pioneering work.

4.3 *Crystallographic information*

The physical properties of a mineral may be strongly effected by substituting 3d-cations already at low concentrations. As crystal structures of many minerals are complex and comprise a large number of different structural sites, it is not trivial to relate the physical changes to a particular exchange process. Through careful analyses of optical absorption spectra of minerals as well as synthetic equivalents it is possible to obtain qualitative as well as quantitative data on 3d-cation distribution in structurally and chemically complex minerals.

5. REFERENCES

Burns, R.G. 1993. Mineralogical Applications of Crystal Field Theory. Cambridge Topics in Mineral Physics and Chemistry 5. Cambridge University Press.

Goldman, D.S. & Rossman, G.R. 1978. Determination of quantitative cation distribution in orthopyroxene from electronic absorption spectra. Physics and Chemistry of Minerals 4, 43-55.

Langer, K. & Frentrup, K.R. 1979. Automated microscope-absorption-spectrophotometry of rock forming minerals in the range 40,000-5,000 cm^{-1} (250-2000 nm). Journal of Microscopy 116, 311-320.

Piller, H. 1977. Microscope Photometry. Springer-Verlag, Berlin.

Sulphide minerals in carbonatites from Turiy alkaline complex (Turiy-Kovdor-Sokli ancient rift system): mineralogical features and the model of formation

P. I. Karchevsky
Mineralogy Department, St-Petersburg University, 199034 St-Petersburg, Russia
pavel@pk5298.spb.edu

ABSTRACT. Our petrographic and microprobe analyses of sulphide minerals that occur in phoscorites carbonatites from Turiy alkaline complex (Kola Peninsula, Russia), have revealed the presence of hexagonal and monoclinic pyrrhotite, chalcopyrite, sphalerite, galena, pyrite and marcasite. Sulfides are late minerals in the carbonatites and phoscorites of Turiy alkaline complex and have hydrothermal origin. Evolution of Eh and pH conditions had great influence to the sulfide formation in the phoscorites and carbonatites. The changes of Eh and pH conditions has "wave-like" trend and all types of sulfide assemblages have occured at the strictly determined intervals of "Eh-pH wave".

1 GEOTECTONIC POSITION

The Turiy complex forms part of the Kola Alkaline Province (Russia). Its origin is due to the Paleozoic rifting zone represented by the Kandalaksha graben. The Kandalaksha fracture zone is considered to control the spatial distribution of the Sokli carbonatite complex in Finland and Kovdor, Kandagubskii and Turiy complexes further to east extending across the White Sea to Archangelsk (Bell et. al., 1996).

2 SULFIDE MINERALS

The phoscorite-carbonatite rocks of the Turiy complex contain up to 13 volume % of sulfide minerals. Among them are found sulfides of iron, copper, zinc and lead. All observed sulfides form three paragenetical associations:

1) High-temperature sulfides - hexagonal pyrrhotite, chalcopyrite-I, and sphalerite-I;
2) Low-temperature sulfides - monoclinic pyrrhotite, calcopyrite-II, sphalerite-II, galena and pyrite-I;
3) The products of pyrrhotite oxidation - pyrite-II and marcasite.

Each of the phoscorite-carbonatite rock types has its own strictly determined sulfide assemblage. Phoscorite is the earliest rock type of the carbonatite series in the Turiy complex; it does not contain primary sulfide mineralization, and only during the later stages of alteration do the secondary minerals and low-temperature sulfides appear. The earliest types of carbonatites are characterized by their own high-temperature sulfide mineralization, whereas the later types have a low-temperature sulfide mineral assemblage.

In all the phoscorite-carbonatite rocks of the Turiy complex studied, the sulfides crystallized after the main carbonate minerals, i.e. silicates and apatite. The sulfide aggregates fill spaces between the carbonates, silicates and apatite, or impregnate them along cracks and fractures. The general sequence of sulfide formation is: pyrrhotite → chalcopyrite + sphalerite → galena → pyrite.

3 ORIGIN OF SULFIDE MINERALIZATION

A thermodynamic model of the sulfide formation in carbonatites of the Turiy alkaline complex has been established on the basis of geothermobarometery (Buddington & Lindsley 1964; Hutchison & Scott 1981) and physico-chemical methods of calculation (Garrels & Christ 1965). As the result of our calculations we constructed the potential-pH diagram (Karchevsky 2000) showing the stability fields of sulfide minerals in the carbonatites from Turiy complex and general evolution of the chemical conditions during the sulfides formation (Fig. 1).

Figure 1. Model of sulfide formation in the carbonatites of Turiy alkaline complex

Legend: Mgt – magnetite, PO – pyrrhotite, Pyr – pyrite, CP – chalcopyrite, Hem – hematite.

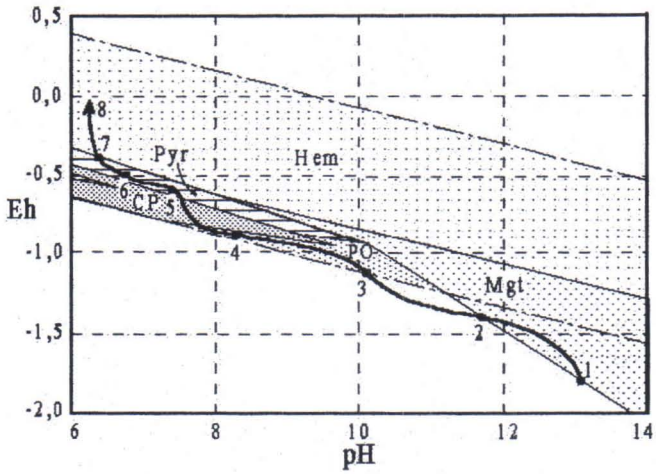

Phoscorites do not contain sulfide minerals but have large amounts of magnetite. They formed at a temperature of 550 °C, a pressure of 3-3.5 kBar, under fo_2 around $10^{-21.5}$, pH more than 10 and sulphur activity below 10^{-6} (Fig.1, segment 1-2). High-temperature sulfide mineralization appears as the sulphur activity increases up to $10^{-4} - 10^{-2}$, at approximately 350 °C and under pH values corresponding to reducing conditions (Fig. 1, segment 3-4). The main part of this mineralization corresponds to 7.8<pH<8.2, when Eh values sharply increase and the processes of amphibolization and tetraferriphlogopitization occur (Fig. 1, segment 4-5). Low-temperature sulfide minerals formed at neutral pH conditions, under conditions of higher Eh and temperatures below 250 °C (Fig. 1, segment 6-7). Oxidation of pyrrhotite occurs during the final stages of carbonatite evolution in the Turiy complex, in conjunction with an increase of Eh and the formation of baryte and hematite occured (Fig. 1, segment 7-8).

4 CONCLUSIONS

There are different suggestions concerning the origin of the sulfide minerals in the carbonatite complexes. On the basis of our data on the morphology of sulfide aggregates and results of the thermodynamic calculations we attribute sulfide mineralization in carbonatites of Turiy alkaline complex to a hydrothermal origin.

5 ACKNOWLEDGEMENTS

This work was completed with INTAS support, grant 97-0722.

6 REFERENCES

Bell, K., Dunworth, E.A., Bulakh, A.G. & Ivanikov, V.V. 1996. Alkaline rocks of Turij Peninsula, Russia, including type-locality turjaite and turjite: a rewiev. Canadian Mineralogist, 34, 265-280.

Buddington, A.F. & Lindsley, D.H. 1964. Iron-titanium oxide minerals and syntheic equivalents. Journal of Petrology, 5(2), 310-357.

Garrels, R.M. & Christ C.L. 1965. Solutions, Minerals and Equilibria. New York.

Hutchison, M.N. & Scott, S.D. 1981. Sphalerite geobarometry in the Cu-Fe-Zn-S system. Economic geology, 76, 143-153.

Karchevsky, P.I. 2000. Thermodynamic model of sulfide formation in the carbonatites of Turiy alkaline complex, Kola Peninsula (Russia). Abstract volume "Carbonatites Workshop, 2000", Saint-Etienne (France), 23.

Platinum-group element mineralogy of the Channagiri layered complex, Karnataka, India

R.J. Kaukonen
University of Oulu, Dept. of Geosciences, Linnanmaa, FIN-90014, Oulu, Finland
risto.kaukonen@oulu.fi

ABSTRACT. The Archaean Channagiri Layered Complex in Karnataka, India contains a promising, mainly silicate-hosted PGE mineralization that was discovered in the early 1990's. There are actually several mineralized zones which can be divided into four types based on the PGE mineralogy and the associated rock types. These are in a descending order of PGE content 1) silicate-hosted Pd mineralization, 2) silicate-hosted Pt mineralization, 3) sulfide-hosted Pd mineralization and 4) oxide-hosted PGE mineralization. The most important platinum-group minerals are sperrylite and various Pd-Te-Bi and Pd-Sb minerals.

1 INTRODUCTION

The occurrence of platinum-group elements (PGE) in the Channagiri Layered Complex was first reported in 1994 by Devaraju et. al., but it wasn't until in 1998 when drilling of the PGE-bearing intrusion commenced. So far several cores have been obtained and a lot of various analyses have been made from that material. The results have been somewhat encouraging as best whole rock PGE values indicate several ppm's of Pt+Pd.

This paper concentrates on the PGE mineralogy of the deposit by describing the characteristics of the various platinum-group minerals (PGM) and/or mineral groups, i.e. what they are and how they occur in this particular deposit.

2 GEOLOGIC SETTING

The Channagiri Layered Complex is composed of several tectonically separated blocks, together spanning about 30 km in length with thicknesses ranging from about 0.2 to 1 km. The block hosting the Magyatahalli PGE Reef is about 3 km long and 0.3 km wide.

According to field relations the complex is of Archean age and has been thoroughly metamorphosed (Jayaraj et. al, 1995; Radhakrishna & Vaidyanadhan, 1997). Hence the list of the main rock-forming minerals is rather short comprising generally just amphibole, chlorite and magnetite along with the more confined occurrences of carbonate, epidote and talc.

3 PGE MINERALOGY

3.1 *Samples and analytical techniques*

All samples used in this study were taken from one drill core only (DH-1). Continuous sampling has been applied to almost the entire drill core for whole rock lead fire-assay PGE analysis. Polished thin sections were then made from samples with anomalously high PGE concentrations for identifying and studying the PGM's with an optical microscope as well as a SEM/EDS system.

3.2 *Grouping of PGM's*

Due to the small grain size, which is commonly < 5 μm as shown in figure 1. and the limitations of the energy dispersive analytical method and hardware the actual analyses are usually semi-quantitative and hence some interpretation is required to identify the mineral. Also the actual formulae of many PGM's are so close to each other that the differences often fall within reasonable analytical errors. Then there

is also the probability of yet to be proven solid-solution series between several possible end-members. All these problems become very evident particularly when dealing with the various Pd-Sb and Pd-Te-Bi minerals.

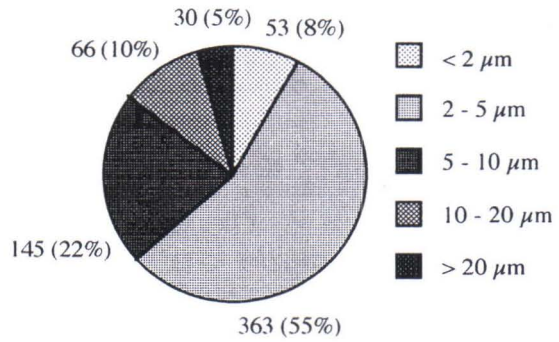

Figure 1. Grain sizes of the PGM's in DH-1.

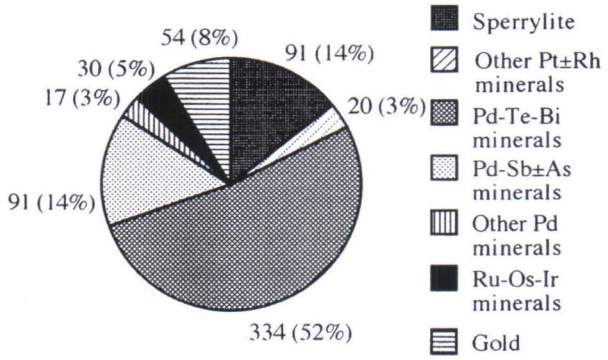

Figure 2. Distribution of the PGM's in DH-1.

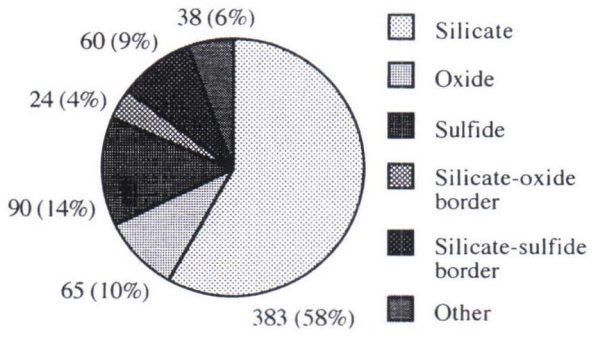

Figure 3. Hosts of the PGM's in DH-1. The last section termed "other" includes the association of PGM's with carbonates as well as three or more of the other groups at a time.

So far over 650 PGM's have been analysed from the first drill core and they have been grouped as shown in figure 2. into sperrylite, other Pt±Rh minerals, Pd-Te-Bi minerals, Pd-Sb±As minerals, other Pd minerals and Ru-Os-Ir minerals. Gold grains have also been documented. This division is based on statistics, chemical affinities of PGE's and the association of certain minerals with some of the main rock-forming minerals. Figure 3. gives a generalized representation of how the PGM's relate to other minerals.

3.3 *Pt-bearing minerals*

Sperrylite ($PtAs_2$) is by far the most common Pt-bearing mineral in the analyzed samples. Sperrylite grains are often euhedral or subhedral and they are usually associated with silicates.

More than half of the group "other Pt±Rh minerals" is actually hollingworthite (RhAsS) and it was added to this group mainly for the sake of simplicity. However, because sperrylite may often contain a few percent of Rh and also hollingworthite may contain significant amounts of Pt and/or Ir it fits reasonably well into this group. The other minerals in this group are moncheite ($PtTe_2$), cooperite (PtS), braggite ((Pt,Pd)S) and platarsite (PtAsS) and all of them tend to occur in silicates.

3.4 *Pd-bearing minerals*

About one third of all PGM grains found from DH-1 so far are kotulskite (PdTe) and a vast majority (over 80 %) of them are hosted by silicates. Also in the case of kotulskite it can best be seen that as the occurrence of the mineral gets more frequent the grain size also increases. Although a large portion of kotulskite grains still fall within the 2-5 μm range the occurrence of much larger grains does indeed become more frequent. Kotulskites in DH-1 usually contain several percent of both Sb and Bi.

Merenskyite ($PdTe_2$) and michenerite (PdTeBi) are common too but with them the association with sulfides becomes more apparent for they are often found either inside the base metal sulfides or at the border between a sulfide grain and some other mineral (silicate, carbonate or oxide). In addition to these the group "Pd-Te-Bi minerals" contains a few grains of keithconnite ($Pd_{3-x}Te$), testibiopalladinite (Pd(Sb,Bi)Te) and some

apparently unnamed phases. Figure 4. shows a ternary plot of all Pd-Te-Bi minerals so far analyzed from DH-1.

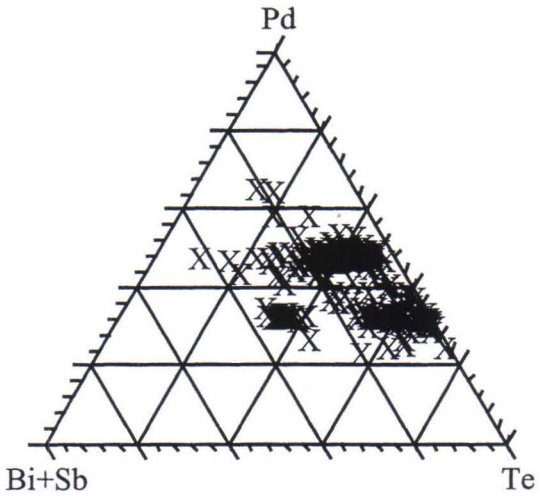

Figure 4. Compositions of the various Pd-Te-Bi minerals analyzed from DH-1 on a ternary diagram.

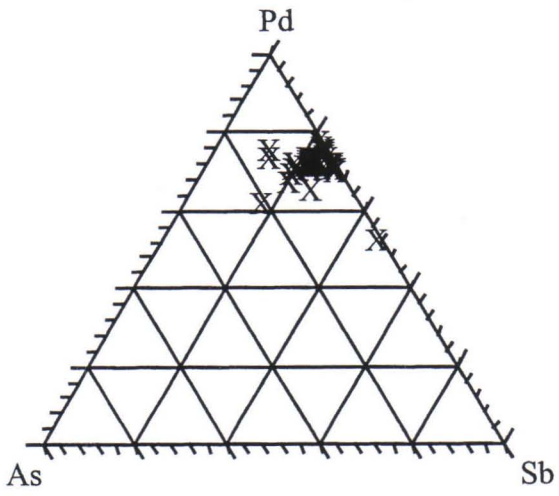

Figure 5. Compositions of the various Pd-Sb±As minerals analyzed from DH-1 on a ternary diagram.

Pd-Sb minerals may often be difficult to distinguish from each other. As a rule of thumb along with the element percentages the distinction is often based on the presence of As in the analysis, although that alone may not always validate the name for one way or another. The most common Pd-Sb±As minerals in DH-1 are mertieite-II (Pd_8Sb_3), stibiopalladinite (Pd_5Sb_2) and mertieite-I ($Pd_5(Sb,As)_2$) and they are most often found to occur as inclusions in silicates. Other minerals in the group "Pd-Sb±As minerals" include isomertieite ($(Pd,Cu)_{11}(Sb,As)_4$), sudburyite (PdSb) and some presumably unnamed phases. Figure 5. shows a ternary plot of all Pd-Sb±As minerals so far analyzed from DH-1.

The small group of "other Pd minerals" comprises temagamite (Pd_3HgTe_3), paolovite (Pd_2Sn), sopcheite ($Ag_4Pd_3Te_4$) and some unnamed phases.

3.5 *Ru-Os-Ir minerals*

Despite the name of the group the individual mineral grains don't necessarily contain all of those elements. What is common to them all in DH-1, however, is that they tend to be closely associated with oxide minerals, namely chromite or Cr-rich magnetite. The minerals in this group are laurite (RuS_2), anduoite ($RuAs_2$), ruarsite (RuAsS), erlichmanite (OsS_2), osarsite (OsAsS) and irarsite (IrAsS).

3.6 *Gold*

The highest gold values from DH-1 are a few hundred ppb. Gold forms alloys with silver and the metal ratios vary a lot from nearly pure gold to about 90% silver. The grain sizes are usually very small. Gold grains are usually found from base metal sulfides, but they do occur quite often in magnetite too and sometimes in silicates as well. Often when gold is associated with silicates it forms composite grains with some PGM's.

4 CONCLUSIONS

The whole rock Pt+Pd analyses (due to be published at a later date) indicate that there may actually be several different PGE mineralizations within the intrusion at different stratigraphic levels. When combined with the mineralogical data, this information leads us to distinguish four different types of PGE mineralization. They are in a descending order of PGE content 1) silicate-hosted Pd mineralization, 2) silicate-hosted Pt mineralization, 3) sulfide-hosted Pd mineralization and 4) oxide-hosted PGE mineralization. Preliminary studies of other drill cores seem to support this conclusion, but more data is needed yet and that work is currently in progress.

5 REFERENCES

Devaraju, T.C, Alapieti, T.T, Halkoaho, T.A, Jayaraj, K.R & Khanadali, S.D, 1994. Evidence of PGE Mineralization in the Channagiri Mafic Complex, Shimoga District, Karnataka, Jour. Geol. Soc. India, Vol. 43, pp. 317-318.

Jayaraj, K.R, Khanadali, S.D, Devaraju, T.C & Spiering, B, 1995, A Study of Hogbomite in the V-Ti-Fe Deposits of Karnataka, Jour. Geol. Soc. India, Vol. 45, pp. 57-64.

Radhakrishna, B.P & Vaidyanadhan, R. 1997. Geology of Karnataka, 353 p.

Mineral recovery modeling in flotation: combining data from image analysis and laboratory tests

P. Lamberg, P. Sotka, M. Lyyra and J. Liipo
Outokumpu Research, P.O. Box 60, 28101 Pori, FINLAND
pertti.lamberg@outokumpu.com

ABSTRACT. The behavior of minerals in flotation was studied by combining data from image analysis and laboratory tests. Recovery of each particle type can be modeled using the first order flotation kinetics equation, where the flotation rate of the particle is the average of mineral flotation rates weighed by mineral areas. Modeling requires i) exact mineralogical data of each particle in the feed, and ii) flotation rate constants of the minerals. Practical solution to approximate the flotation rates of minerals from flotation tests and a prototype of a modeling program were developed.

1 INTRODUCTION

Image analysis studies related to mineral processing aim to determine the mineralogical characteristics that affect the behavior of minerals and ores in processing (Lastra et al. 1998). Image analysis can reliably and accurately characterize the mode of occurrence of minerals in process products. This is quite often enough to solve 'mineralogical problems' in process plants (see examples in Lastra et al. 1998). More versatile data and interpretation is, however, needed when considering different process alternatives e.g. in the flowsheet development; or when process parameters are adjusted as new ore types come into production. Optimization in these cases requires that the mutual relationships between different properties of each process product could be expressed in the form of equations. For example, one might be interested in the consequences in mass flows, grades and recoveries when Fe-sulfides are depressed to upgrade the concentrate. These kinds of cases have been solved by additional laboratory testing and simulating alternative processes with modeling programs such as USIM PAC 2. From the mineralogical point of view, the problem is that modeling programs are not capable of utilizing the exact and precise liberation data provided by image analysis, and therefore the number of different alternatives studied is quite small, and consequently optimization is defective. For the metallurgist, liberation data is undoubtedly precise, and it is good for comparing different feed materials for example, but it is far too complicated to be used in modeling.

This paper describes a technique which combines precise image analysis data acquired from ore samples or process products and mineral process modeling. The technique is applied here in flotation, but it can be equally well utilized in other mineral separation processes such as gravity and magnetic separation and even leaching. Only the kinetic equations presented here would have to be replaced with equations appropriate for the process in question.

2 MATHEMATICAL MODELS OF FLOTATION

The behavior of particles in flotation is usually described by the following well-known flotation kinetics equation (Huber-Panu et al. 1976):

$$R = \Psi \cdot \left(1 - e^{Kt}\right) \qquad (1)$$

where R is the recovery of a valuable mineral; Ψ is the fraction of valuable mineral in the

feed, which is floatable; K is the flotation rate constant, and t is the flotation time (for other models see Dowling et al. 1985, Villeneuve et al. 1995, and Yuan et al. 1996). Modeling with equation 1 has to be done in size fractions, since floatability varies from one fraction to another. In the middle fractions (say from 20 μm to 120 μm, depending on the case) selectivity is the best and floatable minerals float quickly whereas in fine (<20 μm) and coarse (>120 μm) fractions selectivity is poor and floatable minerals need more time to be floated. Generally equation 1 does not correspond very well with flotation results (Fig. 1). Therefore more variables have been introduced. In the USIM PAC 2 model 2A each particle type is divided into three sub-populations: i) a fast-floating sub-population, ii) a slow-floating sub-population and iii) a non-floating sub-population, and the recovery of particle (in froth) is defined as (modified after BRGM 1993, see also Villeneuve et al. 1995):

$$R = \Psi \cdot \left(\phi \cdot \left[1 - e^{K_S t} \right] + (1 - \phi) \cdot \left[1 - e^{K_F t} \right] \right) \quad (2)$$

where R is the recovery of particle type i, Ψ is the fraction of particle type i in the feed, which is floatable, ϕ is the proportion of particle type i capable of floating and which shows slow floating behaviour, K_s the slow-floating kinetic constant, and K_F the fast-floating kinetic constant. When applying equation 2 a reasonable fit can be achieved with laboratory flotation tests and models (Fig. 1). Additional modifications have been proposed for the kinetic constant to take into account the entrainment of particles by water (Villeneuve et al. 1995, BRGM 1993).

Modeling of the flotation circuit with equation 2 requires that parameters are determined for each mineral and each size fraction. The disadvantage of equation 2 is that it is applicable only for those specific feed and flotation conditions where constants were determined. For example if the feed grade or grinding fineness changes, the constants of equation 2 have to be redetermined for each mineral and each fraction.

A study was made of the relationship between the sub-populations of equation 2 and different particle types determined by image analysis in a set of laboratory flotation tests and corresponding feed. The feed material was a representative ore sample of a sulfidic nickel ore. Successful rougher flotation tests with different flotation times were selected, and mineral recoveries were determined from chemical analyses by mineral mass balancing (Lamberg et al. 1997). Liberation of sulfide minerals (pentlandite, chalcopyrite and pyrrhotite) and gangue minerals (serpentine, chlorite, amphibole and some minor phases) were determined by the SEM-EDS method using the liberation program of Link eXl. Fitting the test data into equation 2 gave the result that 11% of pentlandite is non-floating, 67% fast-floating and 22% slow-floating (Fig. 1). When these figures are compared with the liberation data of the feed the non-floating sub-population corresponds to particles containing less than 10% pentlandite, the slow-floating sub-population to grains where the pentlandite content is between 10 and 20% and the fast-floating population to grains where the pentlandite content is more than 20%. Observations indicate that different sub-populations used in flotation models correspond to different particle types in the feed, as concluded also by Petruk and Lastra (1993), Morizon et al. (1997) and Penberthy et al. (2000). Particle types of any sample can be determined exactly by image analysis and expressed as the liberation of minerals.

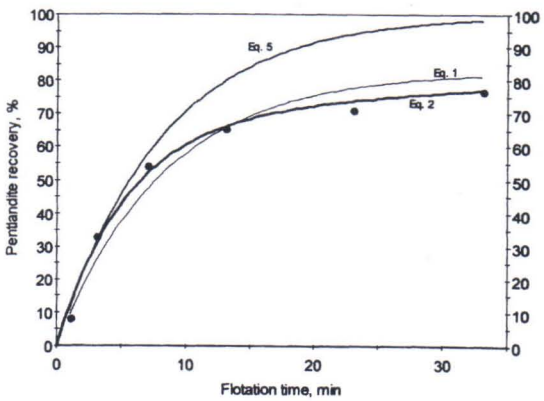

Figure 1. Cumulative recovery of pentlandite as a function of flotation time in one flotation test with sulfidic nickel ore (dots). Model curves according to equations 1, 2 and 5.

3 COMBINING IMAGE ANALYSIS AND MATHEMATICAL FLOTATION MODELS

The floatability of a single mineral particle in given conditions (certain flowsheet, flotation reagents, mineral surface properties, flotation

machine, pulp transport characteristics etc.) is dependent on its mineral composition and the floatability of these minerals. For simplicity in this paper it is assumed that all grains of similar type have identical floatability.

If the floatability of free mineral particles is known, the floatability of the particle can be expressed as follows:

$$K_{tot} = \sum_{i=1}^{n} (A_i^s \cdot K_i) \qquad (3)$$

where A^s_i is the surface area of mineral i in the particle and K_i is the flotation rate constant of mineral i when occurring as a liberated particle. To simplify the measurement and calculations, the surface area can be replaced by the particle volume, which equals the area in a section, thus

$$K_{tot} = \sum_{i=1}^{n} (A_i \cdot K_i) \quad (4);$$

since there is no need to have different sub-populations the term $\Psi=1$ and equation 1 becomes very simple

$$R = 1 - e^{Kt} \quad (5)$$

Equations 4 and 5 show that the recovery of the particle can be determined using the first order kinetic phenomenon, and the flotation rate of the particle is the average of mineral flotation rates weighed by mineral areas as illustrated in Fig. 2.

4. PRACTICAL APPLICATION OF THE TECHNIQUE

The application of equations 4 and 5 in the optimization of some process requires i) exact mineralogical data of each particle in the feed, and ii) flotation rate constants of the minerals (i.e. liberated mineral particles). For accurate results the examination has to be done in size fractions.

The mineral composition of each particle type in the feed can be determined routinely by image analysis. Instead of 'liberation tables' (see Tables 1-3 in Lastra et al. 1998) raw particle data is used, i.e. row-wise data that lists for each particle the size and areal fractions of each identified mineral (Table 1). In some special cases minerals can occur as a coating on particles, when floatability should be determined on the basis of the outer pixels of the particles (equation 4), but particle composition should be determined from areal fractions.

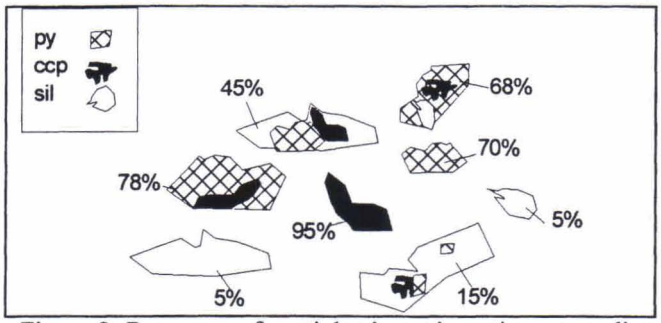

Figure 2. Recovery of particles in a given time according to equations 4 and 5, when recoveries for liberated particles are pyrite (py) 70%, chalcopyrite (ccp) 95% and silicate (sil) 15%.

Table 1. Example of particle data required for modeling according to equations 4 and 5. The figures are volume percentages of the mineral in the particle.

Particle	py	ccp	sil	Other
1	12	55	33	0
2	67	12	20	1
3	0	100	0	0

The determination of the flotation rate constant for each mineral requires liberation measurements for the feed and concentrate after which recoveries of liberated particles can be determined. Thus, it seems that if equation 2 is replaced by equations 4 and 5, modeling requires even more detailed data and practical application becomes more remote. Examination of the nickel sulfide ore flotation test and the liberation data of the corresponding feed reveals that some simplifications can be used. Recovery vs. flotation time curves of the flotation tests normally follow equation 5 at short flotation times after which the curve becomes flatter. This flattening has been overcome in equation 2 by dividing the population into fast-, slow- and non-floating. The first points equal the fast-floating population, which approximately corresponds to liberated particles, when floatable minerals are concerned. Thus, the flotation rate constant of a floatable mineral can be determined by fitting equation 5 along the first two flotation times. In the case of depressed minerals, the fast-floating population equals particles locked with fast-floating minerals, and the flotation rate constant can be determined by fitting equation 5 along points with a long flotation time.

The advantage of equations 4 and 5 compared with equation 2 is that the flotation rate constants determined for the minerals are not so strongly dependent on grain size as they are in equation 2. Different ore types with almost similar mineralogy (but for example a different grade) of the same ore should have similar flotation rate constants. Therefore the modeling of different ore types, different grinding fineness, or different flowsheets may require only the liberation measurements of the corresponding feed. Naturally flotation rate constants are dependent on flotation conditions (reagents, equipment, flowsheet, etc.).

5. PREDICTING THE BEHAVIOR OF MINERALS IN PROCESSING

In general the prediction of mineral behavior in processing requires i) exact knowledge of the mineral composition of the particles (i.e. liberation data), and ii) separation equations of the liberated particles. A particle behaves in processing according to the weighed average of the single minerals it is composed of; in flotation according to equations 4 and 5. When the behavior of the particle is controlled by its surface properties (flotation, leaching) then the outer pixel of the particles should be determined. In leaching both solid and liquid phases have to be considered (shrinking core model; Levenspiel, 1972).

When the above-described data is available, then the behavior of a given mineral in the process can be predicted by modeling. For example in flotation the time is set and recoveries of each particle are calculated from the liberation data according to equation 4 and 5. When the recovery of each particle and the weight fraction of the minerals in the particles is known, then the weight fraction of the mineral in the product can be calculated. The equations and calculations themselves are simple, but the difficulty is that for reliable prediction the number of particles measured has to be in the thousands and the calculations are laborious to make. Due to the lack of such a program a prototype has been designed and built by Outokumpu Research Oy (Lamberg et al. 2000).

4 REFERENCES

BRGM, 1993. USIM PAC 2 for Windows, Advanced Guide. BRGM. 186 p.

Dowling, E.C., Klimpel, R.R. & Aplan, F.F., 1985. Model Discrimination in the Flotation of a Porphyry Copper Ore. Mineral & Met. Processing, 2, 87-101.

Huber-Panu, I., Ene-Danalache, E. and Cojocariu, D. G. Mathematical models of batch and continuous flotation. In: Fuerstenau, M. C. (editor) Flotation A.M. Gaudin memorial volume vol. 2. New York: American Institute of Mining, Metallurgical and Petroleum Engineers, 1976, p 675-724.

Lamberg, P., Hautala, P., Sotka, P. and Saavalainen, S., 1997: Mineralogical balances by dissolution methodology. COM/IMA Short course on ore and environmental mineralogy. Modern Approaches to ore and environmental mineralogy. 8-10 September, 1997, Laboratorio do IGM, S. Mamede de Infesta, Portugal.

Lamberg, P., Sotka, P. and Lyyra, M., 2000. Mineralogian ja panoskokeiden ennustemallit –Loppuraportti. Unpublished report (in Finnish) of Outokumpu Research, 00013-ORC-T, 20.1.2000, 56 p.

Lastra, R., Petruk, W., Wilson, J., 1998. Image-analysis techniques and applications to mineral processing. In Cabri, L., J., and Vaughan, D.J., 1998, Modern Approaches to Ore and Environmental Mineralogy, Mineral. Assoc. Canada, Short Course Series, Vol. 27.327-366.

Levenspiel, O. 1972. Chemical Reaction Engineering, Chapter 12: Fluid - Particle reactions.

Morizot, G., Conil, P., Durance, M.V., and Gourram Badri, F., 1997. Liberation and its role in flotation-based flowsheet development. Int. J. Miner. Process. 51, 39-49.

Penberthy, C.J., Oosthuyzen, E.J., and Merkle, R.K.W., 2000. The recovery of platinum-group elements from the UG-2 chromitite, Bushveld Complex - a mineralogical perspective. Mineral. Petrol. 68, 213-222.

Petruk, W. and Lastra, R., 1993. Evaluation of the recovery of liberated and unliberated chalcopyrite by flotation columns in a copper cleaner circuit. Internat. J. Mineral Process. 40, 137-149.

Villeneuve, J., Guillaneau, J.-C., Durance, M.-V., 1995. Flotation modeling: a wide range of solutions for solving industrial problems. Miner. Eng. 8 (4/5), 409-420.

Yuan, X.-M., Pålsson, B.I., and Forssberg, K.S.E., 1996. Statistical interpretation of flotation kinetics for a complex sulphide ore. Miner. Eng. 9, 429-442.

Semiquantitative extraction of chrome spinel from Quaternary till - perspective for discriminative analysis, a case study from Lapland.

Marja Lehtonen
Geological Survey of Finland, P.O.Box 96, FIN-02151 Espoo, Finland
Marja Lehtonen@gsf.fi

ABSTRACT. In 1998 the Geological Survey of Finland (GTK) collected Quaternary till samples from a region in Eastern Lapland. The aim of the study was to locate potential diamondiferous kimberlites and/or lamproites based on the indicator mineral distribution in till. The samples were preconcentrated with a GTK modified 3" Knelson concentrator and subsequently processed by standard laboratory methods. The only indicator mineral studied was chrome spinel. More than 600 grains were analysed by electron microprobe. The fundamental problem turned out to be how to tell the difference between regionally and more locally derived chrome spinel populations. The result from this preliminary discriminative analysis was encouraging.

1 INTRODUCTION

Since 1996 Geological Survey of Finland (GTK) has carried out regional sampling of Quaternary till in Lapland. The aim of the study is to locate potential areas for diamond deposits i.e. kimberlites and/or lamproites based on the indicator mineral distribution in till. Apart from a sound understanding of Pleistocene glaciation events, there are two major aspects emphasized in this study: 1st, the know how of quantitative sample processing methods and 2nd, the ability to discriminate between regional (e.g. voluminous mafic layered intrusions) and more local (e.g. kimberlites/lamproites and small ultramafic bodies) chrome spinel populations.

2 PROCESSING METHODS

The study material was collected in summer of 1998. The till samples ca. 80 kg in weight were taken by excavator at a depth of 2.5-4.5 m allowing at the same time the till stratigraphy to be studied. The samples were preconcentrated with a GTK modified laboratory scale 3" Knelson concentrator originally designed for extracting gold (Chernet et al. 1999). Subsequent processing methods included heavy medium separation, high and low intensity magnetic separation and dry sieving. The final heavy mineral concentrates were hand picked for kimberlitic (and lamproitic) indicator minerals: eclogitic and chrome pyrope garnet, chrome diopside, high Cr-Mg chrome spinel and picroilmenite. The extracted grains were analysed by electron microprobe. The analyses were conducted in the GTK microanalysis laboratory with a Cameca Camebax SX50.

3 RESULTS AND CONCLUSIONS

All of the till samples turned out to be quite homogenous in terms of grain size and heavy mineral distribution. Most probably they all represented the same till bed.

More than 600 chrome spinel grains were analysed, overwhelmingly from the grain size fraction 0.25-0.5 mm. The main focus was on the content of the following elements: Cr, Mg, Ti, Zn and Ni. Based on widely used classifications

(Smith et al. 1991, Fipke et al. 1995, Griffin et al. 1994) the number of the grains suggestive of diamond potential was 20-30. For regional mantle derived rock formations reference material was searched from previously published chrome spinel analyses.

In this study the samples have been divided into either positive or negative groups depending on whether or not they contain diamond field chrome spinels. In Fig. 1 all of the chrome spinel grains which were found in positive samples are shown in a Cr_2O_3-MgO-diagram (Smith et al. 1991). The negative samples are shown in Fig. 2. Comparing these figures, it can be seen that the low- Zn and high Cr-Mg chrome spinel population plotting in the diamond stability field is associated with another population with the same MgO contents but with lower Cr. The other chrome spinel populations that occur in both diagrams are most probably grains derived from other sources than kimberlites or lamproites. These populations are interpreted to be regional. The positive samples (20 of 32) were concentrated in three localities within the 20 * 45 km study area. This is strong evidence for a local source of the diamond field grains.

The results from this preliminary study are encouraging; in addition to the local chrome spinel population possibly suggestive of diamond potential, another regional chrome spinel population, corresponding to a Proterozoic mafic layered intrusion (Mutanen 1997), can be recognized in the study material.

In the absence of G10 field chrome pyrope (Dawson 1984) or chrome pyrope in general, the interpretation of diamond potential based solely on chrome spinel is difficult if not impossible. Hanski (1997), for instance, has described a discontinuous belt of Paleoproterozoic ophiolitic rocks that contain chrome spinels plotting into the diamond field on a Cr_2O_3-MgO-diagram by Smith et al. (1991).

The most important result of this study - regardless of the source for the high Cr-Mg chrome spinel grains: kimberlites, lamproites or small ultramafic bodies- is to show that the methodology described here can be used to distinguish between regional and the local heavy mineral signatures.

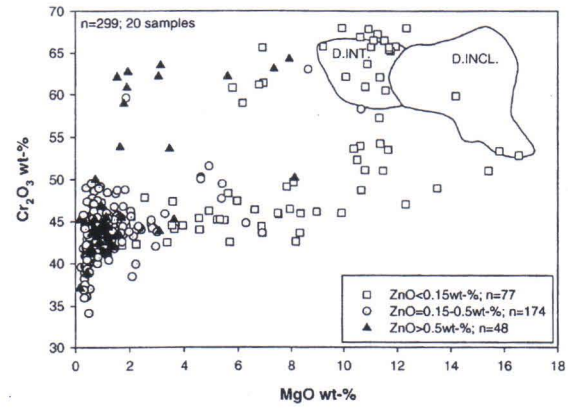

Figure 1. The chrome spinel analyses of the positive samples in Cr_2O_3-MgO-diagram redrawn after Smith et al. (1991). The analyses are divided into three classes based on their ZnO-content. D.INT.=diamond intergrowth field, D.INCL.=diamond inclusion field.

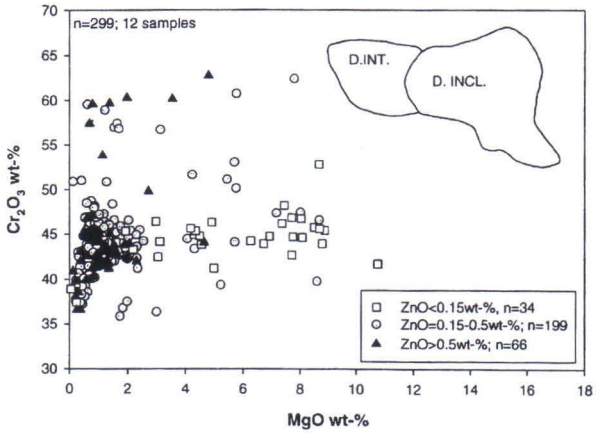

Figure 2.The chrome spinel analyses of the negative samples in Cr_2O_3-MgO-diagram redrawn after Smith et al. (1991). The analyses are divided into three classes based on their ZnO-content. D.INT.=diamond intergrowth field, D.INCL.=diamond inclusion field.

4 ACKNOWLEDGEMENTS

This study was conducted at the GTK. I would like to thank especially Dr Jukka Marmo for the innovation of this work, and Mr Lassi Pakkanen and Mr Bo Johanson for the excellent microanalytical data. I'm also grateful to Dr Hugh O'Brien, Mr Ahti Nissinen, Mr Pekka Huhta and Mr Pertti Hakala and to the personnel

of the GTK heavy mineral laboratory.

5 REFERENCES

Chernet, T., Marmo, J. & Nissinen, A. 1999. Technical Note. Significantly improved recovery of slightly heavy minerals from Quaternary samples using GTK modified 3"Knelson preconcentrator. Minerals Engineering, Vol.12, 1999, 1521-1526.

Dawson, J.B. 1984. Petrogenesis of kimberlite. In: Glover, J.E. and Harris, P.G. (edit.). Kimberlite Occurrence and Origin: A Basis for Conceptual Models in Exploration. Geol. Dep. and Univ. Ext., Univ. of West Aust., Publ. No 8, 104-105.

Fipke, C. E., Gurney, J. J. & Moore, R. O. 1995. Diamond exploration techniques emphasing indicator mineral geochemistry and Canadian examples. Bulletin / Geological Survey of Canada ; 423: , 86 p.

Griffin, W.L., Ryan, C.G., Gurney, J.J., Sobolev, N.V. & Win, T.T. 1994. Chromite macrocrysts in kimberlites and lamproites: geochemistry and origin. In: Meyer, H.O.A. & Leonardos, O.H. (edit.): Kimberlites, Related Rocks and Mantle Xenoliths. CPRM Spec. Publ. 1A/93, 366-377.

Hanski, E.S. 1997. The Nuttio Serpentinite Belt, central Lapland: an example of Paleoproterozoic ophiolitic mantle rocks in Finland. Ofioliitti, 1997, 22 (1), 35-46.

Mutanen, T. 1997. Geology and ore petrology of the Akanvaara and Koitelainen mafic layered intrusion and the Keivitsa-Satovaara layered complex, northern Finland. Geological Survey of Finland, Bulletin 395, 233 p.

Smith, C.B., Lucas, H., Hall, A.E. & Ramsay, R.R. 1991. Diamond prospectivity and indicator mineral chemistry: a Western Australian perspective. In: Fifth International Kimberlite Conference, Brazil. Comphania de Pequisa de Recursos Minerais, Special Publication 2/91, 380-382.

Environmental impact of sulfide-rich formations

K. Loukola-Ruskeeniemi
Geological Survey of Finland, Betonimiehenkuja 4, 02150 Espoo, Finland
kirsti.l-r@gsf.fi

ABSTRACT. Sulfide-rich formations are encountered both in nature and in industrial wastes. A major problem associated with sulfide-rich formations is acid rock drainage (ARD). Sulfide-rich bedrock has an impact on the pH and chemical composition of surface waters and groundwater even under natural conditions, but more so if the bedrock is exposed and blasted, for example during road construction. Geochemistry of graphite- and sulfide-rich shales in Finland was studied with some 2000 drill core samples. Environmental studies were done in five localities. Graphite- and sulfide-rich formations have been compiled to a 1 : 1 000 000 map and database. The map is used in regional planning, exploration, bedrock mapping and environmental studies. In addition to natural sulfide-rich formations, new sulfide-rich formations are formed during mining of sulfide ores. Common sources of ARD are mine water, waste rock piles and tailings ponds.

1 INTRODUCTION

Abundant sulfides are encountered both in the natural formations and in industrial wastes. Sulfide-rich bedrock has an impact on the pH and chemical composition of surface waters and groundwater even under natural conditions, but more so if the bedrock is exposed and broken. Anthropogenic sulfide-rich formations include the tailings of sulfide mines. Sulfides are originally formed in reducing environments and they become unstable in oxygen-rich environments at the Earth's surface. Sulfide oxidation is part of the natural weathering process.

2 ACID ROCK DRAINAGE

A serious problem associated with sulfide-rich formations is acid rock drainage (ARD), also known as acid mine drainage. Primary requirements for ARD are the presence of 1) sulfides, 2) water or humid atmosphere, and 3) an oxidant, usually oxygen. There are several rate-determining factors in ARD generation, including pH, temperature, particle size of sulfides (surface area) and bacterial activity. *Thiobacillus ferro-oxidans*, for example, catalyses the oxidation of pyrite, producing ferric and hydrogen ions. The rate of ARD is temperature dependent: a tailings pile that oxidizes completely at 25°C in 200 years will do the same at 0°C in 500 years (Dave and Blanchette, 1999).

3 NATURAL CONTAMINATION

Geochemistry of the bedrock is reflected in the geochemistry of the surrounding environment. Calcium and magnesium concentrations in groundwater are higher, for example, in gabbro, peridotite and carbonate rock areas than in granite areas, and fluorine concentrations are high in groundwater in rapakivi areas (Lahermo and Backman, 2000). Elevated uranium concentrations are associated with certain granites, and these in turn are responsible for the high radon concentrations in wells drilled into the bedrock (Juntunen and Backman, 1996). The natural background levels for ore forming elements such as the heavy metals tend to be high in the surroundings of ore deposits compared with the average values. For example, a nickel ore deposit may be reflected

in elevated nickel concentration in surface waters, organic stream and lake sediments and till. These elevated concentrations have been used as a tool in exploration.

4 ENVIRONMENTAL IMPACT OF BLACK SHALES

Sulfide-rich black shales have caused environmental problems in South Korea, Canada and Finland (Kim and Thornton, 1993, Pasava et al., 1995, Piispanen and Nykyri 1997). Even though black shales contain abundant sulfides, they seldom constitute ore deposits, since the concentrations of Ni, Cu, Zn, Au, As, PGE, U, Mo etc. usually are too low. However, concentrations of potentially harmful elements often are high enough to cause pollution, especially if the black shale is exposed and broken. If the geological formation contains abundant carbonate-rich layers in the vicinity of black shales, carbonates may suffice to neutralise the low pH produced by sulfide oxidation.

Geochemistry of black shales in Finland was studied with some 2000 drill core samples during 1989-1999 (Loukola-Ruskeeniemi and Heino, 1996, Loukola-Ruskeeniemi et al., 1997, Loukola-Ruskeeniemi, 1999). In addition, environmental studies were done in five localities. For example, elevated nickel concentrations in black shales at Sotkamo were found to be reflected in elevated nickel concentrations in till, organic stream and lake sediments, surface waters, groundwater and moss (Loukola-Ruskeeniemi et al., 1998). Even the chemical composition of crayfish muscle is different in lakes in black shale areas than in lakes underlain by granitic or quartzitic bedrock (Halonen, unpubl. data).

Arsenic-bearing bedrock in Finnish Lapland is reflected in elevated As concentrations in till, organic stream sediments, stream water, in wells drilled into bedrock and especially in spring waters (up to 34 µg/L, Loukola-Ruskeeniemi et al., 1999).

5 COMPILATION OF MAPS OF SULFIDE-RICH FORMATIONS

Studies on black shales have shown that forestry, drainage programs and road construction have a more disturbing environmental impact in sulfide-rich areas than other areas. It is inadvisable to carry out earthmoving or forestry activities in black shale areas that might lead to erosion and extensive exposure of bedrock. Bedrock distributions can also be used directly in delineating areas suitable for obtaining groundwater, since it is unwise to drill wells into sulfide-rich bedrock. To assist in this, maps are needed that show the distribution of sulfide-rich formations.

In Finland, graphite- and sulfide-rich formations have recently been compiled to a 1 : 1 000 000 map and database (Arkimaa et al., 1999). The map will find applications in addition to regional planning, also in exploration and bedrock mapping, and in studies on the natural background levels in the environment.

6 ENVIRONMENTAL IMPACT OF SULFIDE MINES

In addition to natural sulfide-rich formations, described in the sections above, new sulfide-rich formations are formed during mining activities. In particular, the tailings of sulfide mines are rich in sulfides.

The main environmental impacts of the mining industry are air pollution (dust, gaseous emissions), accumulation of pollutants in plants, soil, groundwater and surface waters, disturbance of landscape and blasting vibration.

Sources of ARD are mine water, waste rock piles and tailings ponds. The resulting drainage water is usually highly acidic and contains large amounts of dissolved heavy metals and may cause damage to groundwater and ecosystems in the downstream environment.

The least costly and most efficient method of controlling ARD is to prevent its initial formation. Water covers and underwater disposal of sulfide tailings have been confirmed as the best technology for preventing ARD from unoxidized sulfide-bearing tailings. Collecting and treating mine effluents before they discharge to the environment should be normal practice, but also passive treatments like wetlands are useful means of controlling ARD.

7 REFERENCES

Arkimaa, H., Hyvönen, E., Lerssi, J., Loukola-Ruskeeniemi, K. and Vanne, J. 1999. Compilation of

maps of black shales in Finland: applications for exploration and environmental studies. Geological Survey of Finland, Current Research 1997-1998. Geological Survey of Finland. Special Paper 27, 111-114.

Dave, N.K. and Blanchette, M. 1999. Role of cold climate conditions in management of reactive mining waste in northern Canada. Mining in the Arctic, Udd & Keen (eds). Balkema, Rotterdam.

Juntunen, Risto; Backman, Birgitta 1996. Uraani ja radon pohjavedessä. Abstract (p. 46): Uranium and radon in groundwater. Vesitalous 37 (2), 7-11.

Kim, K.W. and Thornton, I. 1993. Influence of uraniferous black shales on cadmium, molybdenum and selenium in soils and crop plants in the Deog-Pyong area of Korea. Environmental Geochemistry and Health 15, 119-133

Lahermo, P. and Backman, B. 2000. The Lahermo, Pertti; Backman, Birgitta 2000. The occurrence and geochemistry of fluorides with special reference to natural waters in Finland. Geologian tutkimuskeskus. Tutkimusraportti 149. 40 p.

Loukola-Ruskeeniemi, K. 1999. Origin of black shales and the serpentinite-associated Cu-Zn-Co ores at Outokumpu in Finland. Economic Geology

Loukola-Ruskeeniemi, K. and Heino, T. 1996. Geochemistry and genesis of the black shale-hosted Ni-Cu-Zn deposit at Talvivaara, Finland. Economic Geology 91, 80-110.

Loukola-Ruskeeniemi, K., Kuronen, U. and Arkimaa, H. 1997. Geochemical comparison of metamorphosed black shales associated with the Vihanti zinc deposit and prospects in western Finland. Geological Survey of Finland, Current Research 1995-1996. Geological Survey of Finland, Special Paper 23, 5-13.

Loukola-Ruskeeniemi, K., Uutela, A., Tenhola, M. and Paukola, T. 1998. Environmental impact of metalliferous black shales at Talvivaara in Finland, with indication of lake acidification 9000 years ago. Journal of Geochemical Exploration 64, 395-407.

Loukola-Ruskeeniemi, K., Tanskanen, H. and Lahermo, P. 1999. Anomalously high arsenic concentrations in spring waters in Kittilä, Finnish Lapland. Geological Survey of Finland, Current Research 1997-1998. Geological Survey of Finland. Special Paper 27, 97-102.

Pasava, J., MacInnis, I., Graves, M., Zentilli, M. 1995. Black slates - a source of acid drainage at the Halifax International Airport, Nova Scotia, Canada. In: Pasava, J., Kribek, B., Zak, K. (eds.), Mineral Deposits: from their Origin to their Environmental Impacts. Proceedings of the Third Biennial SGA Meeting, 28-31 August, Prague. Balkema, Rotterdam, pp. 785-788.

Piispanen, R. and Nykyri, T. 1997. Acidification of groundwater in water-filled gravel pits - a new environmental and geomedical threat. Environmental Geochemistry and Health 19, 111-126.

The structure pattern image analysis of Au-bearing Witwatersrand conglomerates: discrimination between productive and barren reefs

I. Maximiouk, A. Kremenetsky
IMGRE, 15 Veresaeva ul., Moscow, 121357, Russia
krem@imgre.iitp.ru

A. Danil'chenko, A. Makavetskas
OOO NVP Tsentr-ESTAgeo, 4 Leninsky prosp., 117936, Russia
nvpcentr@online.ru

ABSTRACT. Geometry and optical properties using the image analysis method, along with chemistries of trace elements and organic matter were studied in samples from auriferous parts of reefs and their barren analogs from Witwatersrand, South Africa. The image analysis demonstrated that quartz pebbles from auriferous varieties are more homogeneous with respect to optical properties, have higher optical density, are better ordered and stronger elongated relative to the barren analogs. These features favor in situ formation of 'pebbles' in auriferous parts of reefs from a homogeneous siliceous substance. The image analysis data, in combination with our observations on the trace element, gas, and organic matter chemistries, favor the notion on the formation of the Au mineralization in Witwatersrand as a result of destruction of the parent SEDEX-type ('smoker'-related) mineralization.

1 INTRODUCTION

Witwatersrand is the world's largest (approx. 350 by 100 km) auriferous paleo-basin with gold resources about 80 Kt. Eight gold fields are located mainly along its northern and northwestern flank. In the ore-bearing sequence of the Central Rand gold field, potentially ore-bearing conglomerate constitutes 10—15 continuous horizons. Thickness of each horizon may vary from several meters to several tens meters. Exposures of these horizons occur along N and NW flanks of the paleo-basin, as well as near the Vredefort dome at the center of the basin. In the former case, these are economic Au-bearing quartz conglomerates, whereas in the latter—polymictic conglomerates, barren or carrying poor mineralization.

Discussions on the origin of the Witwatersrand gold have a long history. First, the metamorphosed placer hypothesis (Ramdohr, 1955) was introduced and dominated. Later, the idea on hydrothermally altered placers came to front (Robb *et al.*, 1989). The oppositionists were Davidson (1960) with his hydrothermal hypothesis that employed an endogeneous Au source related to the Bushveld Complex development, along with Phillips and Myers (1989) who assumed hydrothermal gold remobilization from the conglomerate-hosting rock and basement. Newer concepts associate Au resources with submarine exhalations (Hutchinson, Viljoen, 1988; Kremenetsky *et al.*, 1997), multiple sources and mechanisms (Shcheglov, 1993), or lasting SEDEX-dominated deposition (Kremenetsky, 1998).

2 ANALYTICAL METHODS

We employed an optical geometric method in morphostructural studies of the barren and economic conglomerates. Data processing employed the VIDEO-MASTER image processing system equipped with Scannex-2 input system (Russia). The image analyzer enhances the operations in the optical geometric studies aimed at delineation of objects in the digital images, measurements of optical and morphometric parameters of the objects thus obtained, and calculation of relevant statistics. The source images were analyzed using the harmonic and kepster structural analyses with secondary images as results.

The parameters of pebbles measured in the polished sections were as follows: (1) cross-section area, (2) perimeter, (3) length (the longest chord), (4) width (the longest normal), (5) orientation, (6) relative brightness, and (7) the curvature index of the pebble contour, along with other derivative characteristics.

3 RESULTS

To test our concept on the leading role of SEDEX process similar to that related to recent submarine 'smokers' (Kremenetsky *et al.*, 1997), we compared productive and barren conglomerates from the same horizons. These were sampled in different sites of the paleobasin (50—70 km apart). The horizons (reefs) studied were as follows (top to bottom): the Black Reef, the Ventersdorp Contact Reef (VCR), Kloof, the Bird Group (Vaal), Carbon Leader, and Dominion.

The VCR case history exemplifies the differences in chemistries and structures of barren and economic conglomerates. This reef is one of the major economic members. It is constituted by oligomictic quartz conglomerate. Pebbles of homogeneous milky quartz are elongated and rounded, occasionally, dumbbell-like. Quartzite pebbles and chert fragments are less frequent in conglomerate. Pebbles are cemented by fine-grained mass of quartz, chlorite, pyrite, pyrrhotite, and minor chalcopyrite. Small pyrite pebbles (max. 0.5 by 0.7 mm) are present in the matrix. The pebble/cement ratio is approximately 2:1.

Color of quartz varies from milky white (prevails) to grayish white and smoky gray; zonal or spotted color patterns are observed. Color of quartz is controlled by fine impregnations of chlorite and sericite along fissures, abundant gas-and-liquid micro-inclusions, and unevenly distributed organic matter. Our studies using the laser spectral analyzer demonstrated that the source quartz is optically pure and contains negligible amounts of C_{org} (0.01%), gold, and other trace components. These are concentrated in microfissures, which cut quartz, and in the cement. The organic compounds are quite variegated in quartz. The latter is saturated with methane and ethane. Heptane, octane, and hexene is found here; these are not typical of the vein quartz varieties. This fact indicates special conditions, which favor polymerization of simple hydrocarbons into more complex varieties. High He contents we observed in the quartz pebbles (0.7—1.82 g/cm^3) are inherent in 'smokers' located in the oceanic zones (Lisitsyn, 1983). All these facts, plus weak zoning of optically pure quartz pebbles, witness the authigene hydrothermal (SEDEX-related) nature and post-depositional re-distribution of the organic and mineral matter.

Pebbles of variegated composition (chert, quartzite, schist, and quartz) constitute barren conglomerate varieties. Usually, pebbles are intensely fissured, well rounded, and poorly sorted. Quartz, micas, and pyrite are major components of the matrix. The pebble/cement ratio is approximately 4:1.

Features of pebbles from productive *versus* barren conglomerate determined statistically are as follows. In auriferous parts of reefs, the percentage share of pebbles with the cross-section area less or equal to 100 mm^2 is 45%. The cross-section area ranges here from 13 to 1614 mm^2. Barren conglomerate bears smaller pebbles: 42% of them ranges in cross-section from 30 to 50 mm^2; the total extent is 17–187 mm^2. Small pebbles from the barren and auriferous varieties do not differ in length and width, but large pebbles are more frequent in the latter. Variability of the cross-section area in productive varieties is higher relative to the barren ones. Mineralized varieties carry more elongated pebbles relative to the barren one. The curvature (unevenness) of the pebble contours is characterized by uni-modal statistical distribution in auriferous zones, what is not the case in the barren ones (Figure 1a). The inner structure is more homogeneous in mineralized parts of reefs, and its variations are more smooth relative to the barren ones where both quartz and quartzite pebbles occur. In the latter case, the pebbles may originate from different sources. Pebbles from mineralized zones are more rounded (Figure 1b), and the span of their roundness index is more narrow relative to the barren parts. This fact is another confirmation of greater homogeneity of quartz pebbles from the auriferous parts of reefs. Optical density of pebbles in barren zones is lower (Figure 1c) because of frequent presence of quartzite as the pebble material (optical density of this rock is lower). In addition, pebbles in auriferous zones are more orderly oriented (Figure 1d).

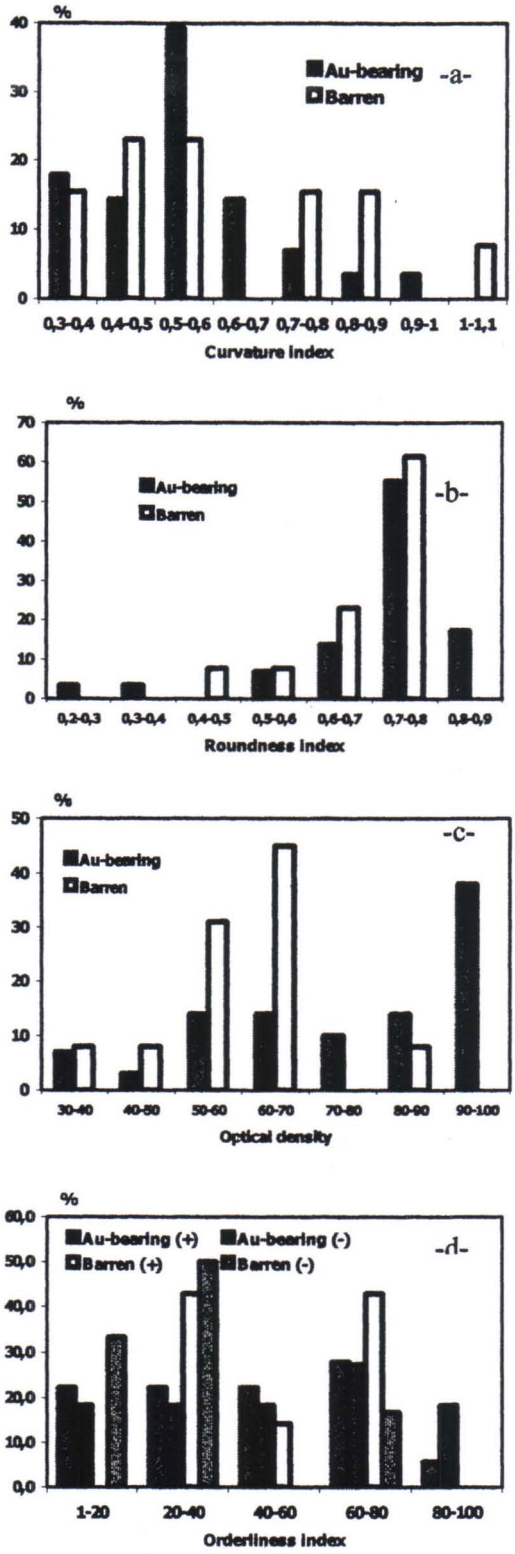

Figure 1. Auriferous *versus* barren parts of reefs: frequency curves of geometric and optical parameters. (a) curvature index, (b) roundness index, (c) optical density, (d) orderliness index.

4 CONCLUSIONS

The image analysis data show characteristic features of quartz from auriferous parts of the reefs: homogeneous inner structure, absence of the basement rocks (granite, amphibolite) as pebble materials, elongated contours, uni-modal statistical distribution of the curvature index, high roundness grade and optical density, and orderliness in orientation. All these features favor the notion on the formation of the Au mineralization by way of destruction of the crystallized parent siliceous gel produced by a SEDEX-type process. Data on the S-isotope composition of sulfides from auriferous parts of reefs, along with increased Hg content in gold (max. 4 wt%) and He in quartz typical of recent SEDEX deposits, match the results of the image analysis.

Structurally and chemically, the auriferous parts of reefs are similar over the Central Rand, what favors the idea on the continuous exhalation activities during the period when the mineralized parts of reefs were formed.

4 REFERENCES

Davidson, G.F. 1960. The present state of the Witwatersrand controversy. Mining Magazine, 102, 2-4.

Hutchinson, R.W., Viljoen, R.P. 1988. Re-evaluation of gold source in Witwatersrand ores. South African Journal of Geology, 91 (2), 157-173

Kremenetsky, A.A. 1998. Gold giants of the world: a new genetic geological concept. In: Gold deposits of Uzbekistan: Geology and Economic types. Scientific Conference Abstracts, Tashkent, 46-49 (in Russian)

Kremenetsky, A.A., Yushko, N.A., & Maksimyuk, I.Ye. 1997. Hydrothermal formation of Precambrian auriferous conglomerates. In: H. Papunen (ed.), Mineral Deposits Research and Exploration: Where Do They Meet? Rotterdam, Balkema, 221-224.

Lisitsyn, A.P. 1983. Biogeochemistry of the ocean. Moscow, Nauka (in Russian).

Phillips, G.N. & Myers, R.E. 1989. The Witwatersrand Gold Fields: part II. An origin of Witwatersrand gold during metamorphism and associated alteration. In: Keays, R.R., Ramsay, W.R. & Croves, D.J. (eds.) 1989. The geology of gold deposits: the perspective in 1998. Economic Geology, Monograph 6, 598-608

Ramdohr, P. 1955. Neue Beobachtungen an Erzen des Witwatersrand in Süd Africa und ihre genetische Bedeutung. Berlin, Acad. Verlag

Robb, L.J., Charlesworth, E.G., Drennan, G.R., Gibson, R.L. & Tongu, E.L. 1997. Tectono-metamorphic setting and paragenetic sequence of Au-U mineralization in the Archean Witwatersrand Basin, South Africa. Australian Journal of Earth Sciences, 44, 353-371

Shchegov, A.D. 1993. On the origin of Au deposits of Witwatersrand, RSA. Doklady RAN, 333 (1), 79-82.

Sulfosalt mineralogy today

N.N. Mozgova
Institute of Geology of Ore Deposits, Petrography, Mineralogy and Geochemistry, RAS, Staromonetny 35, 109017, Moscow, Russia
mozgova@igem.ru

ABSTRACT. The following points are considered: scientific and practical significance of sulfosalt minerals; definition of "sulfosalts" in mineralogy; general features of sulfosalts and their "mysterious" pecularities, which are explained from the nonstoichiometry standpoint; general features of non-stoichiometric compounds; development of the conception of non-stoichiometry and homologous series of sulfosalts; principles of classification of sulfosalts.

1 INTRODUCTION

Sulfosalts represent the most complex ore minerals, which are often discussed at International Geological Congresses and Sessions of International Mineralogical Association. This interest is caused by the following:

1) sulfosalts as minerals with complex composition and structure can be used as a model in many respects and their investigation can shed light on some general relationships of mineral constitution;

2) a lot of sulfosalts are sources of important industrial components of ores (Ag, Cu, Bi, Hg and others);

3) some sulfosalts display semiconducting properties, which are usable in science and technology;

4) sulfosalts sensitively respond to changes of environment and may be used as its indicator.

Definition "sulfosalts" is the longstanding problem in mineralogy. Although the term "sulfosalts" has long been in use, no generally accepted definition exists up to now. In chemistry, sulfosalts (thiosalts) are known as derivatives of sulfoacids (thioacids) [$H_3(AsS_3)$, $H_3(SbS_3)$, $H_3(BiS_3)$ etc]. In a broad sense, sulfosalts are regarded in mineralogy as compounds of metals and semi-metals with sulfur, which can be partially replaced by Se, rarely by Cl and O. The general formula commonly accepted for these minerals is $A_mB_nX_p$, where A - metallic elements, usually Pb, Ag and Cu and less frequently Zn, Hg, Tl etc., B - semi-metallic (formally trivalent) elements As, Sb and Bi (partly Te^{4+}) only, X - S, partly Se, more rarely Cl and O.

Some structural restrictions were proposed later in the definition of sulfosalt minerals. For example, the structure of sulfosalts has to contain the BS_3 pyramidal groups (Takeuchi & Sadanaga 1969; Wuensch 1974 and others). Now, variable coordinations of the B elements (especially of Sb and Bi) have been established as well as a number of mixed sites of the A and B elements in sulfosalt structures (e.g. Pb and Bi in lillianite, Pb and Sb in boulangerite and so on). But in all cases, direct Me-SMe bonds are absent in sulfosalts. So, sulfosalt minerals can be considered as compounds with formula given above, which have not Me-SMe bonding in the structure.

2 GENERAL CHARACTERISTIC OF SULFOSALTS

List of sulfosalts contains about 200 mineral species. Among them there are very common minerals (e.g., tetrahedrite, boulangerite, jamesonite etc.) and very rare ones occurring only as very tiny grains in single deposit. On the basis of sulfoanions, three main general groups of sulfosalts are recognized: sulfoantimonites, sulfobismutites and sulfoarsenites. Sulfosalts with mixed sulfoanions are more rare.

Complex crystal structures of sulfosalts show a relationship to simple structures of some sulfides from which they can be derived through various sudstitutions, omissions or additions of atoms, or through distortion ("derivative structures"). A large number of sulfosalts have "composite structures", containing blocks of simpler structures jointed in various orientation by twinning or shear, or via non-commensurate interfaces. Some sulfosalt structures represent intergrowths of two simpler structure types on unit-cell scale.

Morphology of the minerals is diverse: prismatic and acicular crystals (the most common). Short and elongated platy and tabular crystals, thin laths, bladed crystals, and irregular grains. Subparallel or acicular aggregates (rarely rings), fibrous, massive, granular and compact masses are observed. Most of the sulfosalts belong to the low symmetry (monoclinic, orthorombic, triclinic) system. The cubic variety is rare.

Sulfosalts are very similar in physical properties. They are usually opaque in visible light but many of them are transparent in near-infrared light. Minerals are commonly lead-gray (with various tints) with a metallic (sometimes adamantine) lustre. They have low and moderate hardness (2-4) and rather high density (4 –7 g/cm^3, increasing from Cu-sulfosalts to Ag- and Pb-sulfosalts). As a rule, reflectance of sulfosalts is moderate. Semiconductors, semiconductor-segnetoelectrics, solid electrolites are known among them.

Sulfosalts occur in various types of hydrothermal deposits. Sulfoantimonites and sulfoarsenites are abundant in low- and moderate-temperature deposits; sulfobismutites occur in high- and moderate-temperature ones. Sulfoantimonites and sulfoarsenites have been recently discovered in modern hydrothermal formations on the ocean floor (so-called "black and white smokers", T about 450° and 230°C, respectively). Sulfobismutites occur in fumaroles (T 500 - 700 °C). It should be stressed that tiny size of sulfosalt grains and the resemblance of their properties create problems for researchers.

Sulfosalt minerals have some general "mysterious" pecularities. The main of them are the following:

a) Many minerals have questionable formulas. Real compositions of minerals do not often suit their stoichiometric formulas. Sometimes different stoichiometric formulas are given for the same mineral.

b) Some sulfosalt minerals are very close to each other in composition. They have the same two unit cell parameters and differ only in the third one. The relevant interplanar spacings change incrementally from one such mineral to another.

c) Regular intimate microintergrowths of very similar sulfosalt phases are usual. Therefore, the history of many natural sulfosalts is confused: valid mineral species were discredited as mixtures and were established later with the same name (e.g. lillianite) or with new name (e.g. ashamalmite and heyrovskiite).

These pecularities were sometimes attributed to accidental reasons (in particular to instrumental errors). But actually, they are related to the non-stoichiometry of sulfosalts.

3 GENERAL FEATURES OF NON-STOICHIOMETRIC COMPOUNDS

Evolution of the conception of non-stoichiometric compounds (berthollides) in chemistry goes back to the very beginning of the XIX century to the famous dicussion between Proust and Bertholle. This conception was elaborated in different sciences - chemistry, crystal chemistry and chemical physics. Therefore, the term "non-stoichiometric compounds" have different definitions, e.g., (1) "Compounds, which do not conform with Dalton's laws of constant and multiple proportions, i.e., their elements are not

combined in a simple whole number ratio" (with defenition is usually accepted in chemistry); (2) "Defective phases with changeable number of atoms in unit cell" (Makarov 1973) - in crystal chemistry.

In 1964 Wadsley suggested five types of crystal-chemical reasons of non-stoichiometry:

1) a substitution (cation and anion occupy partly same sites in the structure);
2) interpolation (cations or anions occupy normally vacant sites);
3) subtraction (variable amounts of either or both cation and anion are absent from the structure);
4) shear structures (adjacent blocks of the structure are "out of step" with each other, reducing the number of anions);
5) mixed or intergrowth structures composed by the fragments of related structures of different composition.

The major feature of berthollides is the capacity to change their composition field and to exsolve into separate, structurally related, ordered homologous phases under the influence of changing physico-chemical conditions (usually when temperature decreases). Every phase is characterized by a less wide range of homogeneity (sometimes almost "line"). As a result, exsolution structures, consisting of isochemical phases, appear instead of the homogenic berthollide. The newly formed phases are very close each other in structure and composition. All phases formed from one non-stoichiometric compound represent homologous series, the structure and composition of which change regularly from one member to another (Magnelli 1953). These series bear similarities to polymer homologous series of organic compounds. It should be noted that there are others terms describing such series, such as ordering series (Marfunin 1962), polysomatic series (Thompson 1978), structural series (Parthe et al. 1985), modular series (Makovicky 1989 and others). But the term "homologous series" is connected with the ordering transformations of non-stoichiometric compounds and refers only to isoelemental series.

One can see resemblance between general features of non-stoichiometric compounds and the pecularities of sulfosalts given above. Wadsley (1964) was the first who discussed sulfosalts among the other examples of berthollides, not distinguishing homologous series. Composite structures and mixed structural sites of cations and anions of various valency are the main causes of non-stoichiometry and homologous series of sulfosalts.

4 DEVELOPMENT OF THE CONCEPTION OF NON-STOICHIOMETRY AND HOMOLOGOUS SERIES OF SULFOSALTS

From a non-stoichiometry standpoint the "mysterious" pecularity of sulfosalt minerals is coming to light. In particular, questionable stoichiometric formulas of some sulfosalts are evidently due to their variable composition (non-stoichiometric composition fields). These pecularities have an informative value to recognize the homologous series of these minerals.

Based on consideration of the results of our long standing investigations of sulfosalts as well as published data, the indicators of the sulfosalt homologous series have been revealed (Mozgova 1974). The fine intergrowths of chemically and structuraly related sulfosalt phases are the most illustrative among them (Mozgova 1977). It was shown that the first homologous sulfosalt series was described as the plagionite morphotropic group by L. Spencer in 1899. On the basis of indicators revealed, about 10 homologous series were established in sulfosalt groups of different chemical compositions. All members of a homologous series can be characterized by single general formula although every member of such series can have certain chemical formula, unit cell parameters and symmetry. Two lattice parameters remain constant throughout the series; one parameter (and the relevant interplanar spacing) changes with the change of composition. (Mozgova 1974, 1977, 1984 , 1985 and others).

The sulfosalt homologous series conception was later elaborated by Makovicky (1989) from the structural point of view in his numerous excellent papers. But his interpretation of such term differs from that accepted in chemistry.

Makovicky considered homologous structures as those that have certain structural units in common, and a homologous series as a series of homologous structures that can be theoretically derived from one basic structural unit. He classified homologous series into two categories: accretional and variable-fit homologous series. The members of the former category differ in the sizes of common structural building fragment of the parent structure, the latter are composed of two kinds of alternating mutually non-commensurate layers (or possibly columns, etc.). These series usually include minerals that are similar in structure but not always in composition (for example, the lillianite homologous series includes both Bi-sulfosalts and Sb-sulfosalts, synthetic $Pb_4In_4S_{17}$ is considered as a homologue of cosalite $Pb_2Bi_2S_5$ and so on). Hence such homologous series do not characterize the composition field of a non-stoichiometric compound.

5 PRINCIPLES OF CLASSIFICATION OF SULFOSALTS

Considerable attention has been given to classifications of sulfosalts but up to now this problem remains unsolved. Systematics of sulfosalts can be divided into chemical, structural, and crystal-geochemical ones (reviews see Mozgova 1984; Makovicky 1989). A lot of attention was paid to structural classifications of sulfosats on a basis of sulforadical. Members of a sulfosalt homologous series are often devided into different units in such classifications.

The structural classification on the basis of homologous series was recently elaborated by Makovicky (1989). In fact, it is a classification of ideal homologous structures, but not sulfosalt minerals, because chemical factors are not given enough consideration and a homologous series combines often chemically different minerals with the same topology of structure. It should be stressed that the structural systematics on a basis of geometrical arrangements of structural fragments were criticized previously (Berry 1942; Belov & Pobedimskaja 1966; Kostov 1980, Kostov & Min eva-Stefanova 1981). Such systematics could not be considered as mineralogical ones, since chemical approach accepted in mineralogy was subordinated in them to dimensional.

Mineralogical systematics should reveal natural relationships between minerals and have some predicative power. It was shown above that such relationships exist in isoelemental homologous series of sulfosalts with interrelation of composition, structures and properties of members of the series. Such homologous series can provide the basis for a rational classification of sulfosalts. But since minerals are natural chemical compounds, sulfosalts are proposed to be devided first of all on a chemical basis (at first on the basis of sulfoanions and then after metals). Homologous series with related derivative structures should be recognized as a classification unit in isoelemental sulfosalt groups. A homologous series, containing the same chemical elements, was recommended to be considered as a mineral species and its members as structural varieties. According to rational nomenclature, individual mineral name was proposed to be given only to homologous series, adding the correspondig symbols to names of its members. (Mozgova 1984; Mozgova 1985 and others)

Non-stoichiometry of sulfosalts allows to define them as a class of ore minerals intermediate between natural alloys and sulfides.

6 REFERENCES

Belov, N.V. & Pobedimskaja, E.A. 1966. Characteristic pecularities of crystal chemistry of sulfides, sulfosalts and their analogues. Mineralogical annual proceeding (Mineralogitschesky sbornik) of the Lvov university, 3, 20, 326–340 (in Russian).

Berry, L.G. 1942. Studies of mineral sulphosalts: VII. A systematic arrangement on the basis of cell dimensions. Contribution of Canadian Mineralogist, 47, 9-30.

Kostov, I. 1980. Crystal chemistry and systematics of th sulfosalt minerals. In: Sulfosalts, platinum minerals and ore mycroscopy. Proceedings of XI IMA General Meeting, Moscow, 7-15.

Kostov I. & Min eva-Stefanova, J. 1981. Sulfide minerals: Crystal chemistry, paragenesis and systematics. Sofia, 211p.

Magnelli, A. 1953. Structures of the ReO_3–type with recurrent dislocations of atoms: "Homologous series"

of molybdenum and tungsten oxides. Acta Crystallography, 6, 495- 500.
Makarov, E.S. 1973. Isomorphism of atoms in crystals. Moscow. Atomizdat. 288 p. (In Russian)
Makovicky, E. 1989. Modular classification of sulphosalts - current status. Definition and application of homologous series. Neues Jahrbuch für Mineralogie. Abh., 160, 3, 269-297.
Mozgova, N.N. 1974. Homologous series of sulfosalts (complex sulphides). IX IMA meeting-74. Collected Abstracts, 116.
Mozgova, N.N. 1977. Regular microintergrowths as a characteristic feature of homologous series of sulfosalts. 25th International Geological Congress. Abstracts, vol.2, section 14, Mineralogy, 586-587
Mozgova, N.N. 1984. Principles of classification of sulfosalts. 27 th International Geological Congress. Proceedings, section C.10, Mineralogy, 53-65.
Mozgova, N.N. 1985. Non-stoichiometry and homologous series in sulfosalts. - Moscow. Nauka. 264 p. (in Russian).
Marfunin, A.S. 1962. Feldspar – phase relations, optical properties, geological distribution.. Moscow, Proceedings of IGEM, 78, 275p.
Parthé, E., Chabot, B.A. & Cenzual, K. 1985. Complex structures of intermetallic compounds interpreted as intergrowth of segments of simple structures. Chimia 39.164-174.
Spencer, L.I. 1899. Plagionite, heteromorphite and semseyite as members of a natural group of minerals. Mineralogical Magazine. 12. 55. 55-68.
Takeuchi, Y. & Sadanaga, R. 1969. Structural principles and classification of sulfosalts. Zeitschriftm für Kristallographie. 130. 346-368.
Thompson , J.B. Jr.1978. Biopyriboles and polysomatic series. American Mineralogist. 63. 239 – 249.
Wadsley, A.D. 1964. Inorganic non-stoichiometric compounds. In: Non-stoichiometric compounds. Academic press, 99 –209.
Wuensch, B.J. 1974. Sulfide mineralogy: Short course notes. - Washington. 1. 1-43.

A new occurrence of schwertmannite

T. P. Pedersen
Store Mølle Vej 24, 4.th, Dk-2300 KBH. S, Denmark
rie.thomas@get2net.dk

C. B. Koch
Dept. of Chemistry, The Royal Veterinary and Agricultural University
Thorvaldsensvej 40, DK-1871 FRB. C, Denmark
cbk@kvl.dk

ABSTRACT. A new occurrence of schwertmannite as a weathering product of ancient iron and iron-nickel alloys has been investigated. Schwertmannite, formally $Fe_{16}O_{16}(OH)_y(SO_4)_z$ *nH_2O, where 16-y=2z, 2<z<3.5, has hitherto been found exclusively as an extremely fine grained alteration product in Acid Mine Drainage (AMD) areas. The common morphology of schwertmannite in AMD occurrences is as needles with a diameter in the range of a few tens of nanometres, and a length of a few hundred nanometers, whereas schwertmannite in weathering iron may display crystallites up to a few tens of microns in width and a few hundred microns in length, sizes approximately 3 orders of magnitude larger than those described hitherto.

1 INTRODUCTION

The existence of an iron oxyhydroxysulfate with the formula $Fe_{16}O_{16}(OH)_y(SO_4)_z*nH_2O$, where 16-y=2z and 2<z<3.5, was first suggested by Bigham et al. (1990). Bigham et al. (1994) proceeded to name it schwertmannite. Schwertmannite as a mineral has exclusively been found to occur as a alteration product of sulfide mine tailings in the so-called acid mine drainage areas, where it may exist metastably in the pH range of 2.8 to 4.5 (Bigham et al., 1996).

Schwertmannite is considered to be largely isostructural with akaganéite, which has the β-FeOOH structure (Post & Buchwald, 1991). Akaganéite has Cl^- occupying central cavities in the structure, which in schwertmannite are filled by SO4-groups. The large size of an SO4-group relative to a Cl^- ion dictates that the SO4-group must share at least two oxygens with the neighboring iron octahedra, in order to be accommodated in the central cavities (Bigham et al, 1990). The bonding of the SO4-groups probably leads to a severe deformation of the structure, which may be what causes the extremely small grain size of both natural and synthetic schwertmannite, the morphology of which is generally small needles or aggregates of needles ("pin-cushions"). The individual needles fall in the range of a few tens of nanometers in diameter and a few hundred nanometers in length.

This abstract reports on the finding of schwertmannite as a weathering product in ancient iron and iron-nickel alloys.

2 OBSERVATIONS

While performing a study on the long-term weathering products and processes in iron meteorites and archaeological iron, a phase with a composition much like that of schwertmannite was encountered (table 1). The phase was found primarily in an iron meteorite, Ider (found in Alabama, U.S.) and in a sample of archaeological iron, Sorte Muld from Denmark.

2.1 Ider, Alabama

Ider, a group IIIA medium octahedrite, has a terrestrial age of 3.1±0.4 Ma. The investigated samples contain abundant schwertmannite throughout, both as surface alteration products and in depth as colloidal bands in cracks and along the widmanstätten pattern, together with

goethite and hydrous goethite. On the surface it may take on striking textures, consisting of intergrown platelets and needles (fig. 1). In thin section it is virtually indistinguishable from goethite, except for displaying deep red internal reflections.

Another interesting feature of Ider is the absence of akaganéite, otherwise known as the main corroding agent of iron meteorites (Buchwald & Clarke, 1989), in the investigated samples.

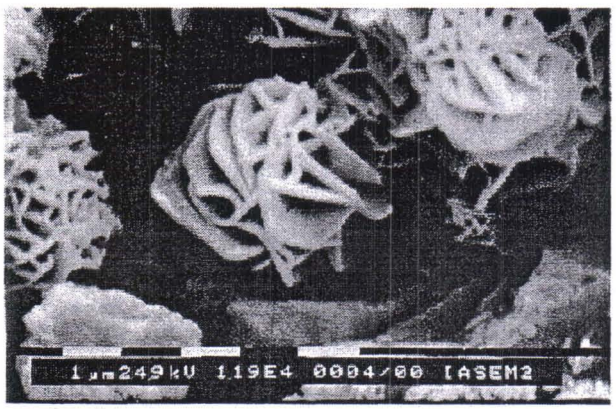

Figure 1. Morphology of schwertmannite from the surface of the Ider, Alabama iron meteorite. Scale bar = 1 µm.

2.2 *Sorte Muld*

Sorte Muld is a sample of a Viking age sword from approximately 1300 yrs. BP. It contains abundant chlorine-bearing weathering products, primarily hibbingite, a rare Fe(II) hydroxy-chloride (Saini-Eiducat et al., 1994). Schwertmannite in this setting occurs as a well crystallized phase with a needle- or bundle-like morphology, usually overgrowing hibbingite into preexisting cavities in the iron. The size of the individual crystallites may reach up to tens of micrometers in width and hundreds of micrometers in length, sizes three orders of magnitude larger than those usually observed for schwertmannite of the AMD type.

Table 1. Analyses of schwertmannite. Comparison of data from Ider, Alabama (IA), Sorte Muld (SM) and a theoretical stoichiometric schwertmannite (schwert.).

Sample	IA	SM	Schwert.
No. Anal.	22	14	-
FeO	65.66	67.82	74.37
NiO	5.68	-	-
CoO	0.39	-	-
Cl	-	1.78	-
P_2O_5	0.47	-	-
SO_3	4.85	6.82	10.36
Total	77.05	76.42	84.73

Kindly note that the main part of the deviation of the totals from 100% is caused by the analyses being performed measuring for FeO instead of Fe_2O_3.

3 DISCUSSION

Work is in progress in order to verify the structure of the occurring schwertmannite. Due to the scarcity of the material, conventional XRD has not yet been attempted. Electron diffraction has however produced promising results, which will be presented. Attempts towards determining the Raman spectrum of schwertmannite have until further been inconclusive, as it seems to have essentially the same spectrum as goethite.

The occurrence of schwertmannite as a weathering product of iron has not been recognized previously. The scarcity of native iron in nature is one explanation for this, however the increasing human use of iron and iron alloys will no doubt lead to more occurrences of this type. The large variations in the size of the different types of schwertmannite may be hypothesized to be due to slow kinetics of formation, giving the slowly formed (1.000-3.000.000 yrs.) weathering schwertmannite a chance to grow to much larger sizes than the synthetic and AMD varieties. Differences in the morphology of the weathering schwertmannite may be explained in terms of the nature of the iron in which it formed. The slow kinetics of formation may also explain why so little schwertmannite usually forms compared to akaganéite.

4 REFERENCES

Bigham, J.M., U. Schwertmann, S.J.Traina, R.L. Winland & M. Wolf. 1996. Schwertmannite and the chemical modelling of iron in acid sulphate waters. Geochimica et Cosmochimica Acta, vol. 60, nr. 12, p. 2111-2121.

Bigham, J.M., L. Carlson & E. Murad. 1994 . Schwertmannite, a new iron oxyhydroxysulfate from Pyhäsalmi, Finland, and other localities. Mineralogical Magazine, vol. 58, p. 641-648.

Bigham, J.M., U. Schwertmann, L. Carlson & E. Murad. 1990. A poorly crystallized oxyhydroxysulfate of iron formed by bacterial oxidation of Fe(II) in acid mine waters. Geochimica et Cosmochimica Acta, vol. 54, p. 2743-2758.

Buchwald, V.F. & R.S. Clarke. 1989. Corrosion of Fe-Ni alloys by Cl-containing Akaganéite (Beta-FeOOH): The Antarctic meteorite case. American Mineralogist, vol. 74, p. 656-667.

Post, J.E. & V.F. Buchwald. 1991. Crystal structure of Akaganéite. American Mineralogist, vol. 76, p. 272-277.

Saini-Eidukat, B., H. Kucha & H. Keppler. 1994. Hibbingite, gamma-$Fe_2(OH)_3Cl$, a new mineral from the Duluth complex, Minnesota, with implications for the oxidation of Fe-bearing compounds and the transport of metals. American Mineralogist, vol. 79, p. 555-561.

The AutoGeoSEM: A programmable fully-automatic SEM for rapid grain-counting and heavy mineral characterisation in exploration.

B.W. Robinson, G.J. Hitchen, M.R. Verrall
CSIRO Exploration and Mining, Floreat Park, Western Australia 6014
B.Robinson@per.dem.csiro.au, G.Hitchen@per.dem.csiro.au, M.Verrall@per.dem.csiro.au,

ABSTRACT. A modern low-vacuum scanning electron microscope (SEM) is being modified to allow fully-automated grain-counting in addition to its routine manual use. The manual low-vacuum mode of operation is ideal for much mineralogy, as no sample coating is required. We refer to this mode as the "GeoSEM", and to the programmable mode as the "AutoGeoSEM". We are investigating applications in exploration for mineral sands, diamonds and oil, and other areas where precise heavy-mineral assemblage information is likely to be useful. The technique has been used on polished sections of mineral grains, and on rough grains mounted on adhesive tape. When the minerals can be readily identified from the energy-dispersive X-ray spectrum, we can identify grains at rates of up to two per second. Currently the SEM can accommodate 36 sample mounts, each of 25 mm square, so large numbers of grains can be identified and counted overnight. Examples of some of the possibilities and difficulties of the technique are discussed.

1 INTRODUCTION

Low-vacuum SEM (GeoSEM) has proven to be very useful in a range of mineralogical tasks (Robinson and Nickel 1979, Nickel 1981, Robinson, 1998). Experience with manual operation on repetitive tasks indicates a substantial need for automation. Unattended computer control of the SEM/EDX has the potential of considerably expanding existing uses for the GeoSEM. Some mineralogical grain-counting tasks which are far too labour-intensitive when undertaken manually will become practical with the AutoGeoSEM.

Modern SEMs are now designed for manual control via computer interfaces. The mouse and a graphical user interface have replaced the traditional knobs and switches. This provided windows of opportunity for CSIRO Exploration and Mining to specify automation capabilities when replacing an old GeoSEM. The computer interfaces which allow the operator to use the mouse and on-screen menus also allow straightforward user-written programs to control the SEM for unattended operation. The standard EDX spectrometer supplied with the SEM also runs under full computer control, and can be similarly programmed. The EDX spectrometer can not only collect X-ray spectra but it can also control the SEM beam via the interfaces normally used for X-ray mapping.

We make the simplifying assumption that the target heavy mineral assemblages are composed very largely of mono-minerallic grains. Where the detection and identification of inclusions and composite grains is important to the outcome, our current technique is inappropriate.

2 METHODS

The mineral grain counting strategy we are using has a number of simple logical steps. The strategy outlined here is designed for uncoated or coated polished sections. The sample mounts need to be representative of the bulk sample, but poorly polished sections can be tolerated. Indeed sectioned but unpolished sample mounts have been used. Rough grain sample mounts require some slightly different strategies to those outlined here.

The basic steps used in the AutoGeoSEM are:

1. The SEM moves to a sample mount and collects and stores an electron image of a field of view containing perhaps 100 or more grains (Fig. 1).

2. Image analysis (using routines from a commercial package) is used to examine the image and to recognise the grains. It can distinguish pairs of grains which may be touching from cracked or irregularly-shaped grains with a relatively low error rate.

3. The location of the centroid of each grain is calculated by the image analysis routines, as are other parameters such as area, size and shape if needed.

4. The electron beam is placed on the centroid of each grain in turn, and the X-ray spectrum is collected for between 0.1 second and 1 second, and the spectrum stored (Figs. 2 and 3).

5. The X-ray spectrum is interpreted to allocate that grain into one of a number of groups, based on the relative heights of element peaks observed in the spectrum. These groups may be predetermined from a list of expected minerals. They may also be allocated automatically during the run by grouping together observed spectra with similar characteristics as they are encountered. A combination of both strategies promises to prove very useful.

6. Some of the groups can be assigned unambiguously to specific minerals. For instance, zircon has a simple unique X-ray spectrum. Other groups may cover a number of minerals with a broadly similar chemical composition (Fig 4.).

7. Depending on the task requirements, a second longer X-ray collection period can be used on grains which fall into specified groups. This will provide data for a semi-quantitative or quantitative EDX analysis. These analyses can be used to resolve important ambiguities in the grain identification. Those ambiguities which are not important to the task in hand can be ignored rather than devoting extra counting time to collecting non-essential data.

8. When X-ray data have been collected from all the grains in the field of view, the program moves the sample stage to the next field-of-view, and those grains are imaged and identified.

9. This is repeated for all the desired sample mounts that are loaded in the SEM sample chamber. Our sample stage is 150 mm square, so a considerable number of sample mounts can be accommodated and examined before operator intervention is required for a sample change. The area required on each sample mount will depend on the grain size and the number of grains to be examined.

The current version of the software allows for the optional post-processing of the mineral classification step. Data already collected and archived can be re-evaluated if the classification strategy needs to be refined. This may occur either if minerals not initially expected are found, or if one or more of the initial classes prove to have been poorly defined.

The spectrum from each grain in a given group can be displayed easily for the user to check for errors in classification. Individual grains can be located on the stored images, and the associated spectra examined. The SEM can also return to individual grains on request to allow manual checking. This may be to examine closely a discovered grain of a mineral for which one was searching. It can also be used to refine procedures and explain apparent errors.

It is possible to select a subset of grains by nominating the backscattered electron reflectance levels to be included in the grain count. For instance, low electron-reflectance grains like quartz could be ignored or high reflectance grains like zircon could be specified to save time in certain specific tasks.

We have some other related programs which allow manual selection of the points for X-ray collection (Fig. 5), and for semi-quantitative EDX analysis. These have considerable

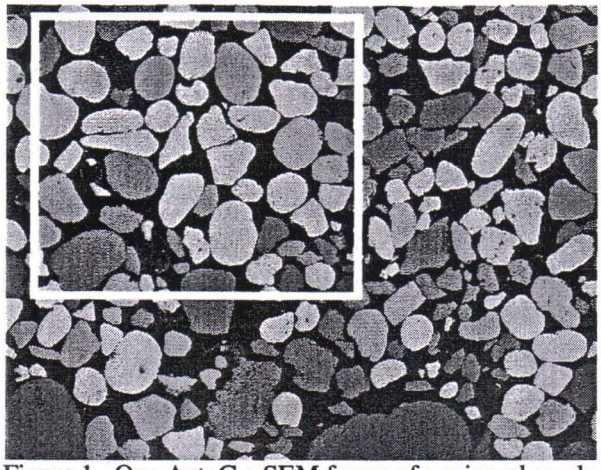

Figure 1. One AutoGeoSEM frame of a mineral sands non-magnetic fraction, showing area of Figure 2.

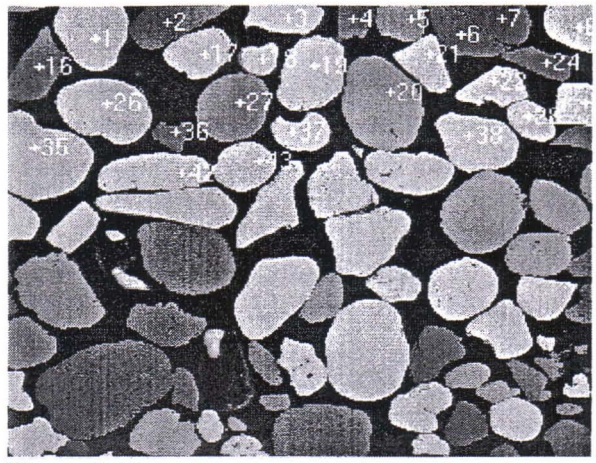

Figure 2. Part of a screen snapshot as the computer puts the electron beam on the centroid of each grain in turn. Part only of the frame shown in Figure 1.

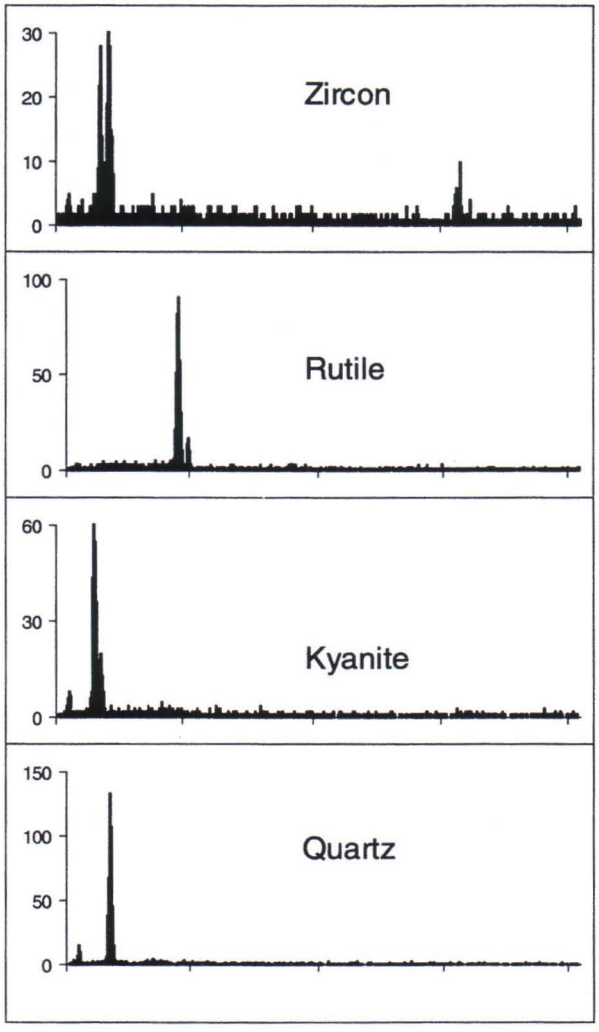

Figure 3. X-ray spectra from the points on grains 3,5,6 and 16 in Fig 2. 10 eV/channel, 20 KeV wide, 0.1 sec collection time, 30kV, circa 4 nA beam current.

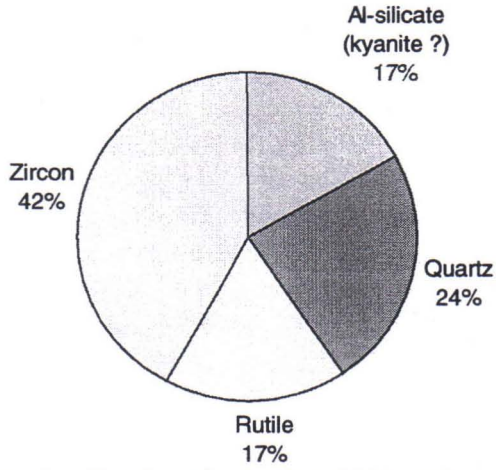

Figure 4. Results of counting 3154 grains of a mineral sands non-magnetic fraction.

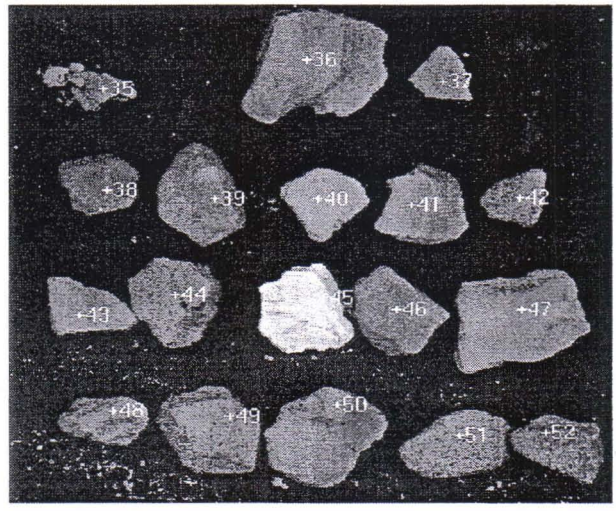

Figure 5. Computer display of manually selected points later used for automatic rapid X-ray collection on uncoated rough diamond indicator minerals

potential to improve the efficiency of GeoSEM use in diamond indicator mineral identification.

We also have a microprospecting program to search for and classify rare grains of gold or platinum-group minerals down to a size of 0.5 micrometre. The microprospecting program is a commercial gun-shot residue analysis program designed initially for forensic science, but suitable for other rare-phase searches.

3 CONCLUSIONS

One major aim of our AutoGeoSEM design is to include a substantial degree of flexibility and programmability so suitable strategies can be chosen and optimised for different tasks.

The project is at an initial prototype stage and we have been using locally available samples for instrument testing and development. We are seeking advice from mineralogists and potential users on the future development of the AutoGeoSEM.

Suggestions of grain identification tasks of importance to exploration and mining companies which may be suitable for the AutoGeoSEM technique will be welcomed.

In a broad sense the techniques outlined here are common to all modern SEM/EDX systems. Specific details depend on particular hardware configurations. Ideally there would be much greater efficiency and progress if SEM and EDX manufacturers would agree to move towards a common set of computer control protocols. This would make the transfer of programs between different instruments much easier. It would also reduce the costs of developing and using application-specific mineralogical programs.

4 ACKNOWLEDGEMENTS

Our development of the AutoGeoSEM is based on the examples of a wide range of previous SEM and electron microprobe automation projects. The pioneering work of the CSIRO QEM*SEM team has been one major inspiration. Invaluable assistance has been provided by Ken Mason of Eastern Analytical Pty Ltd, Grahame Rosolen of CSIRO Telecommunications and Industrial Physics and Nick Ware, of the Australian National University, Research School of Earth Sciences. Staff from Tiwest Pty Ltd, Peter de Broekert of CSIRO Exploration and Mining, and Lynda Frewer of Diatech Heavy Mineral Services have provided test samples, ideas and encouragement.

5 REFERENCES

Nickel, E.H. 1981 The application of the scanning electron microscope in gossan research. Bulletin de Minéralogie 104 292-297

Robinson, B.W. and Nickel, E.H. 1979 A useful new technique in mineralogy: the backscattered-electron/low vacuum mode of SEM operation. American Mineralogist 64 1322-1328

Robinson, B.W. 1998 The "GeoSEM" (Low-vacuum SEM): An underutilized tool for mineralogy. In Modern Approaches to Ore and Environmental Mineralogy Ed. L.J.Cabri and D.J.Vaughan. Mineralogical Society of Canada, Short Course 27 139-151

The origin of the fine-grained rocks and PGE mineralization in the Lukkulaisvaara Layered Intrusion (Northern Karelia, Russia)

V. Semenov & S. Klepinin
Institute of Precambrian Geology and Geochronology, St.Petersburg, Russia
tur@ad.iggp.ras.spb.ru

A. Koltsov & S. Semenov
Department of Geology, St Petersburg State University, Russia

ABSTRACT. The origin of the fine-grained rocks could be explained by injections of new magma portions. Magmas of additional intrusive phases had the chemical composition close to the primary magma and DM isotope-geochemical signatures (ε_{Nd} =-0.7 ~ -3.9 for rocks of the layered series, ε_{Nd} =+3.0 ~ +3.9 for fine-grained rocks). The chilled crystallization of the fine-grained rocks could be due to rapid loss of volatiles (decompression effect) and temperature difference between residual and additional melts. At least some portions of new magmas were trapped in the solidificated part of the layered mafic intrusion and the pressure 9.0-12.0 kbar is related to the shock pressure of a new magma injection. The richest Fe-Ni-Cu sulfide and platinum metal mineralization is related to the potholes. The secondary mineral composition and zoning of the ore bearing rocks with (M1) assemblages are well reproduced by a model of the diffusive grain interaction. The formation of ore bearing (M2) mineral assemblages is described by the model of a metasomatic decompression.

1 STRUCTURE OF THE INTRUSION

The Lukkulaisvaara intrusion is located in the east of Paanajärvi rift structure. The intrusion was dated with U-Pb method at 2442±1 Ma. The Lukkulaisvaara intrusion forms an irregular ellipse in plan and has been traced along the strike not more than 10 km. The width of the intrusion is up to 4.6 km; gravity surveys have shown it to be 1.5 km in depth and with a real thickness of about 4.5 km. The strike of layering and trachytoid fabric is 0-15° ENE in the western and central parts and 40-45° NE in the eastern part of the intrusion. The angles of dip of the layering structures vary within 45-70° to the N. Within the layered complex lenticular bodies of fine-grained gabbro-norites and norites of different thickness oriented along the magmatic layering are identified. The presence of these gabbro-norites and norites is a typical feature of the intrusion. The primary role of crystallization differentiation in the process of massive formation is confirmed by the vertical sequence of cumulative paragenesis and can be presented as follows: (1) Low marginal zone – up to 150 m thick, (2) Ultrabasic zone – up to 450 m, (3) Norite-I zon – more than 900 m, (4) Gabbro-norite-I zone – up to 700 m, (5) Norite-2 zone – variable thickness with an average of 160 m, (6) Gabbro-norite-2 zone – up to 1670 m, (7) Upper marginal zone made up of gabbro-norites – up to 620 m. According to the chemical data we calculated the mean weighted composition of the layered complex: SiO_2 = 51.02, TiO_2 = 0.28, Al_2O_3 = 15.35, FeO = 7.82, MnO = 0.16, MgO = 12.69, CaO = 9.61, Na_2O = 2.00, K_2O = 0.33, P_2O_5 =0.03. Comparison of mean weighed composition of the intrusion with compositionally different magmas points to a consistency with magmas of the boninite - marianite series (Camerron et al., 1979). However, this does not solve the problem concerning the composition of parental magma because of the possible multiphase structure of

the intrusion. The structures are similar in morphology with the Merensky Reef structures known as "potholes" in the Bushveld Complex (Kruger and Marsh, 1985; Balihaus and Stumpfl, 1986; Ballhaus, 1988) were mapping. Many authors (Campbell et al., 1983; Campbell, 1986; Kruger and Marsh, 1985) relate the origin of the potholes to injection of new portion of magmas. The character of the structures is emphasized by a similar set of the forming rocks, namely, spoted anorthosites, gabbro-pegmatites, and poikilitic bronzitites and norites. The presence of fine-grained rocks is a peculiarity of the potholes-like structure. The fabric of these rocks suggests rapid crystallization of new melts. Two main genetic types of sulfides and PGE minerals occur with largest fine-grain rock bodies: a) sulfides and PGE minerals of magmatic stage occur in the veins bronzitites and gabbro-norites within the bodies of fine-grained gabbro-norites, b) sulfides and PGE minerals of a metasomatic stage occur along the internal angular unconformity of the pothole-like structures and near the contact of fine-grained lithologies with the underlying layers. Sulfides (type a) with secondary minerals (talc + anthophylite + actinolite) fill the space between magmatic minerals or form microveins which crosscut both plagioclase and bronzite. Sulfides (type b) occur as fine disseminations and form segregations with secondary minerals (actinolite + hornblende + clinozoisite + chlorite; scapolite, K-feldspar, garnet, biotite, quartz, albite and muskovite may be present). Unaltered or weakly altered rocks make up about 30% of the layered series. A high degree of alteration is typical for sulfide-bearing rocks with PGE-mineralization.

2 ORIGIN OF THE FINE-GRAINED ROCKS

The fine-grained gabbro-norites and norites form large and small lenticular bodies. The mean weighted composition of the largest bodies of fine-grained rocks are: (a) *First body* (thikness about 100 m) - SiO_2- 51.88, TiO_2- 0.17, Al_2O_3- 16.74, FeO- 5.35, MnO- 0.14, MgO- 11.20, CaO-13.33, Na_2O-1.06, K_2O-0.09, P_2O_5- 0.03; (b) *Second body (thikness about 80 m)* - SiO_2- 50.97, TiO_2-0.10, Al_2O_3- 15.75, FeO- 6.81, MnO- 0.14, MgO- 12.32, CaO-12.20, Na_2O-1.54, K_2O- 0.13, P_2O_5- 0.04. The mean weighed composition of the Lukkulaisvaara intrusion is chemically close to the mean weighed composition of the large lenticular bodies of fine-grained rocks. There are some differences in CaO-content. Concentrations of Cr are above 300 and 800 ppm in the first and second bodies respectively. That is typical for low-evolved mantle melts. The TREE concentrations in the fine-grained rocks have the primitive character and the TREE patterns are subhorizontal with a slight TREE enrichment up to 8 times chondritic. Symmetrical distribution of rock-forming elements, Cr, Ni along the profile through the fine-grained rock bodies characterize the last as independent magmatic formations, crystallization of which took place under conditions of closed system. Isotope investigations also support this conclusion. No mixing or only negligible mixing rate can be suggested from for 3 reasons: (1) the difference in physical properties of new and resident melts (Semenov et al, 1996), (2) the fine-grained rocks are distinctly characterized by positive $\varepsilon_{Nd}(T)$ from +3.04 to +3.94 ($\varepsilon_{Nd}(T)$=-0.7 ~ -3.9 for rocks of the layered series), (3) primary character of composition and chilled structure of the fine-grained rocks). The injection of melt into the chamber suggest that the melt was under higher pressure - P_m (including partial pressure of the fluid for wet system) than the pressure in the magmatic chamber. That is why the chilled crystallization of the fine grained rocks could be due to rapid loss of volatile (decompression effect) and temperature difference.

3 CONDITIONS OF A NEW MAGMA INJECTION

Garnet-bearing mineral assemblages with occusion kyanite and orthoclase were found around some large bodies of fine-grained rocks. Fine-grained garnet (less than 0.01 mm) form isometric aggregates up to 0.2 mm across, or skeleton crystals enclosing small plagioclase grains. The garnet also occurs in the axial parts of hornblende segregations. Garnet was discovered in the assemblages with sulfides. In

the totally recrystallized lithologies, aggregates of the garnet-bearing mineral assemblages replace the primary plagioclase. The assemblage hornblende + garnet + secondary plagioclase under dry conditions was used for the P-T estimation. Equlibria were calculated with TWEEQU program (Berman 1988, 1991). There is 5 possible equilibrium that can be written for the selected end-member phases. The results gave P=8.5-12.0 kbar, T= 550-900°C for the samples taken near to the contact with the body of fine-grained rocks (in the place where kyanite, orthoclase and garnet were found), and P= 2.6 -7.6 kbar, T=500-750°C for the sample taken at some distance from the body of the fine-grained rocks (Fig. 1, c). The P-T conditions of metamorphism received from garnet assosiations can be a result (influence) of the additional magma injection in case of a fresh magma intrusion into the crystallized (solidificated) part of the chamber: maximum pressure (P_m=12.0 kbar) obtained from exocontact zone of the fine-grained rock bodies has to correspond to conditions of the fresh magma intrusion, but the minimum one (P_m=8.0 -- >3.0 kbar) may be connected with the distance of the sample from the place of new magma injection and/or with the relaxation of the P_m in the rocks. T=800-900°C reflects the temperature condition of the solidificated part of layered intrusion at a cooling stage.

4 ORIGIN OF THE PGE MINERALIZATION

The results of the study of the Lukkulaisvaara ore-bearing rocks are following: a) discovery of the relations between the PGE-rich ore deposits and altered rocks of the pothole-like structures. We suppose that the potholes play the role of "traps" or geochemical buffer for highly mineralized fluid; b) coexistence of sulfide minerals and minerals of precious metals with the secondary silicate minerals and calcite in all studied cases; c) conditions of the formation of ore-bearing mineral associations are: T= 660-800°C and P=1.5-3.0 kbar (Fig.1,a - talc + anthophylite (M1) assemblages); T=320-450°C and P=1.5-2.5 kbar (Fig.1,b - actinolite + hornblende + clinozoisite + chlorite (M2) assemblages); d) the fluid of the ore-bearing rocks was enriched with chlorine; e) the M1 association developed in the veins of pyroxenites and gabbro-norites located in the middle part of the large bodies of fine-grained rocks and the M2 association developed in leucocratic gabbro–norites and anorthosites overlaying the fine-grained gabbro-norites of norite-II zone. They are characterized by the richest sulfide and platinum mineralization. Theoretically, it has been proved that the bodies of fine-grained rocks should cause deformation of the host rocks at the stage of intrusion cooling. Such a deformation caused local decompression, which in turn increased the porosity of the rock and might have acted like a "pump" for the fluid. The formation of the ore-bearing mineral assemblages (M2) near the contact of large bodies of fine-grained rocks with the underlaying rocks was the result of local decompression.

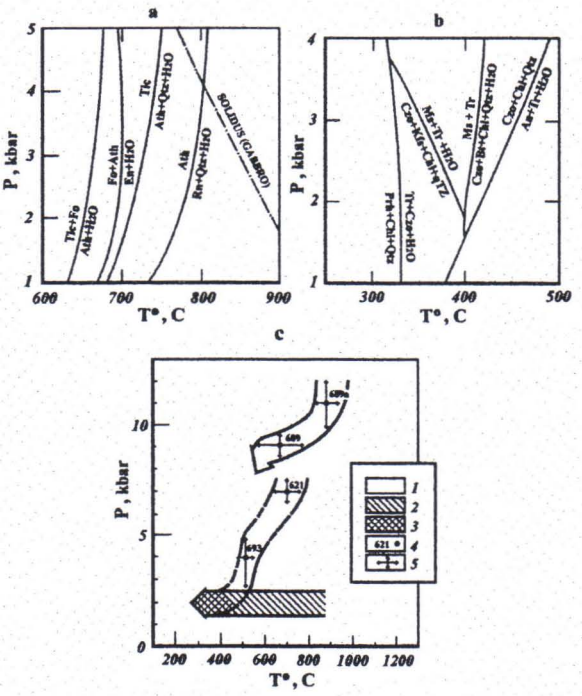

Fig.1. P-T diagrams for secondary mineral assemblages: Ore-bearing mineral associations: (a) talc+anthophyllite assemblages – T = 660 - 800° C, P = 1.5 - 3.0 kbar; (b) clinozoisite + tremolite + chlorite + quartz ± biotite ± muskovite assemblages - T= 320-450°C, P= 1.5-3.0 kbar; (c) Metamorphic P-T path for the rocks of the Lukkulaisvaara Intrusion: (1) P-T conditions obtained by TWEEQU method; (2) P-T conditions constraints on the base of the paragenetic analysis; (3) P-T conditions constrains on the base of gas-water inclusions examination (Semenov et al.,1998), 4 - number of samples, 5 - precision of the P-T measuring.

The models of ore mineral redeposition discussed by Ballhaus and Stumpfl (1986), and Boudreau and McCallum (1992) deal with the high temperature metasomatic fluid alteration (about 730°C and >1000°C). The source of this fluid, as proposed by Boudreau and McCallum (1992) could be the intercumulus liquid. Within the Lukkulaisvaara massive, the redeposition of the precious metals took place at temperature 660-880°C (M1) and 320-450°C (M2). The isotope data also show that the age of the secondary mineral associations does not differ (within the uncertainties) from the age of the intrusion itself, and that the metasomatic fluid with ε_{Nd} =+2.1 (initial 87Sr/86Sr=0.7028) exhibits mantle characteristics (Semenov et al., 1998). These can be the result of a less degree of fluid contamination. Three versions of the alteration processes were studied by means of computer modeling using the method of step-by-step multiwave reactor with various water/rock ratios (W/R): bimetasomatic interaction of different minerals; 2) metamorphic alteration; 3) metasomatic alteration by fluid flow cooling and decompression. The secondary mineral composition and zoning of the rocks with (M1) assemblages are well reproduced by a model of the diffusive grain interaction. Minimum W/R values for starting orthopyroxene substitution are by 1.5-2.0 orders of magnitude lower than for Pl, corresponding to much wider reaction rims around Opx grains in these rocks. Na-rich amphibole forming after plagioclase is also characteristic. Integral W/R is near 0.01 and is determined by fluid stock in the remaining melt. The formation of (M2) mineral assemblages is described by the model of a metasomatic decompression process. The development of such process is favored by low temperature conditions when brittle deformation becomes leading to the formation of fluid conduits.

5 CONCLUSIONS

1. The presence of the fine-grained rocks is a peculiarity of the potholes-like structure of the Lukkulaisvaara intrusion. The origin of the fine-grained rocks could be explained by injections of new magma or melts portions because magmas of additional intrusive phases had the chemical composition close to the primary magma and mantle isotope-geochemical signatures (ε_{Nd} =-0.7 ~ -3.9 for rocks of the layered series, ε_{Nd} =+3.0 ~ +3.9 for fine-grained rocks). The chilled crystallization of the fine-grained rocks could be due to rapid loss of volatiles (decompression effect) and temperature difference between residual and additional melts. At least some portions of new magmas were trapped in the solidificated part of the layered mafic intrusion and the P=9.0-11.5 kbar is related to the shock pressure of a new magma injection.

2. The richest Fe-Ni-Cu sulfide and platinum metal mineralization is related to the potholes. The secondary mineral composition and zoning of the ore bearing rocks with (M1) assemblages are well reproduced by a model of the diffusive grain interaction. The formation of ore bearing (M2) mineral assemblages is described by the model of a metasomatic decompression process.

3. The formation of ore-bearing mineral associations occurred at T=660-800°C, P=1.5-3.0 kbar (associations M1) and T = 320-450°C, P =1.5-3.0 kbar (associations M2). Ore-bearing rocks were formed under the influence of highly mineralized reducing hydrothermal solutions 2442 Ma ago due to reworking of the intrusive rocks and an influx of a new portion of the mantle fluid with ε_{Nd}=+2.1 and initial $^{87}Sr/^{86}Sr$=0.7028.

This work is supported by grant RFBR 00-05-65168.

REFERENCES

Ballhaus, C. G., Stumpfl, E.F. 1986. Sulfide and platinum mineralization in the Merensky Reef: evidence from hydrous silicates and fluid inclusions. Contr. Mineral. Petrol., 94: 193-204.

Ballhaus, C. G. 1988. Potholes of the Merensky Reef at Brakspruit Shaft. Rustenburg Platinum Mines: Primary disturbances in the magmatic stratigraphy. Econ. Geol., v. 83, No.6, 1140-1158.

Berman, R.G. 1988. Internally consistent thermodynamic data for minerals in the system Na2O-K2O-CaO-MgO-FeO-Fe2O3-Al2O3-SiO2-TiO2-H2O-CO2. J.Petrol., 29: 445 522.

Berman, R.G. 1991. Thermobarometry using multi-equilibrium calculations: a new technique, with petrological applications. Canadian Mineralogist, 29, 833-855.

Boudreau A. E., McCallum, I. S. 1992. Concentration of Platinum-Group Elements by Magmatic Fluids in Layered Intrusions. *Econ. Geol.*, 87, p. 1830-1848.

Camerron, W. E., Nisbet, E. G., Dietrich, V. J. 1979., Boninites, komatiites and ophiolite basalts. Nature 280, 550-3.

Campbell, I. H., Naldrett, A. I., Barnes, S. I. 1983. A model for the origion of the platinum rich horizons in the Bushveld and Stillwater Complexes. J. Petrology., v. 24, 133-165.

Campbell I. H. 1986. A fluid dynamic model for the potholes of the Merensky Riff. Econ. Geol., v. 81, 1118-1125.

Kruger F. I., Marsh I. S. 1985. The mineralogy, petrology and origin of the Merensky cyclic unit in the Western Bushveld Complex. Econ. Geol., vol. 80, 958-974.

Semenov, V.S., Shalaev, V.S., Kolychev, E. V., Berkovsky, A. N. 1996. The Lukkulaisvaara intrusion – multiphase layered complex: Program and abstracts,. IGCP project 336 symposium in Rovaniemi, Finland, August 21-23.

Semenov,V.S., Beljatsky,B.V., Baltibaev, Sh.K., Glebovitski V.A., Koltsov, A.B., Koptev-Dvornikov, E.V. 1998. Fe-Ni-Cu sulfide and platinum mineralisation in the Lukkulaisvaara layered mafuc intrusion (Northen Karelia, Russia). International Platinum., Theophrastus publications, St-Petersburg-Athens, pp.63-78.

Environmental mineralogy in the international Kola and Barents Projects

E.F. Stumpfl, A. Felfernig, D. Gregurek*
Institute of Geological Sciences, University of Leoben, Austria
stumpfl@unileoben.ac.at
** present address: Naintsch Mineralwerke, Graz, Austria*

ABSTRACT. The international Kola Project (Norway-Finland-Russia; mineralogy: Austria) has accumulated a vast amount of analytical data from various media to determine quantitatively the environmental impact of the Russian nickel mining industry in the Kola Peninsula. Mineralogical investigations of snow and soil samples reveal a wide spectrum of geogenic and anthropogenic components, including sulphides, oxides, alloys, silicates and slags. First mineralogical results are also presented from the international Barents Project, which extends the limits of the Kola Project to include an area of 1.5 million km^2 in NW-Russia, Finland and Norway.

1 INTRODUCTION

Selected data and information from two major international projects are presented in this note. The main aim is to show that mineralogical investigations in reflected (and sometimes transmitted) light, combined with quantitative microprobe analyses should form an integral part of any project concerned with metal contamination in the environment. It is not only the presence of potentially hazardous elements in snow, soils and sediments which need to be determined and analysed, but also the mineralogical form and the textural setting in which these elements occur. The protection of Ni-Co-Cu sulphide globules, emitted from smelter smoke stacks, by a layer of silicate slag or oxides may render such grains relatively harmless, while sulphides without protective cover can easily be attacked by circulating waters in soils and sediments (Gregurek et.al., 1998). This leads to release of Ni, Co and Cu, and contamination of ground water, streams, rivers and plants. It thus depends on the mode of accommodation of potentially hazardous elements in the crystal lattice of minerals and alloys or on adsorption onto organic particles, whether these elements are available for distribution in the environment or whether they remain immobilised. These questions are of crucial importance in environmental damage assessment; they cannot be answered if chemical data only are considered. Mineralogical investigations must be included in the respective programmes.

2 THE PROJECTS

The international Kola project has been planned and executed jointly by the Geological Surveys of Norway (NGU) and Finland (GTK), and by the Kola Geological Expedition, Russia (CGE). The considerable amounts of emitted SO_2 (300.000 t/year) and metals (several thousand t/year) by the nickel industry in the Kola Peninsula were at the root of the Kola project. It comprised a comprehensive study of the distribution of 40 elements in an area of 185.000 km^2 in the Russian, Finnish and Norwegian parts of the Kola Peninsula, with special emphasis on major sources of pollution, i.e. the nickel mining and processing centres of Zapoljarnij, Nikel and Monchegorsk (Tommervik et.al., 1995). A large number of media, including snow, rainwater, soils, sediments, river and lake waters, plants and animals have been investigated (Äyräs & Reimann, 1995; Caritat et.al., 1996a,

b; Reimann et.al., 1998). Mineralogical studies of snow melt water filter residues and soil samples at the Institute of Geosciences, University of Leoben, Austria, have been supported by the Austrian Research Fund (FWF).

The international Barents project can, to some extent, be considered an extension of the Kola project to an area of about 1.5 million km^2 from the Northern Urals to the North Cape, and to the area of St. Petersburg in the south. In an initial step of this four-year project, soils samples from 9 catchments in this vast area have been taken during a sampling campaign using a fixed-wing aircraft in summer 1999. Mineralogical investigation of mineral concentrates from these samples are presently underway at the Institute of Geological Sciences, Leoben.

3 THE KOLA PROJECT

Three aspects have been selected for inclusion in this report:

Mineralogy of snow samples; correlation of snow mineralogy with chemical analyses of snow samples; correlation of snow and soil mineralogy

- Snow samples have been taken during the 1995/96 winter in the vicinity of the main emitters, Zapoljarnij, Nikel and Monchegorsk. They were processed at the laboratories of the Geological Survey of Finland and meltwater filter residues were sent to Leoben for mineralogical investigation. These snow samples represent atmospheric deposition of the 1995/96 winter.

The filter residues contain grains in the 3 to 50 µm grain size range. These have been embedded in araldite resin, and polished on a Rehwald machine finishing with 0.5 µ diamond polishing paste. Microprobe analyses and SEM imaging war performed on ARL, respectively JEOL instruments at Leoben.

Reflected light microscopy of filter residues revealed varying proportions of geogenic and anthropogenic components depending on the location. In Zapoljarnij higher proportions of geogenic grains were observed, in Monchegorsk anthropogenic grains dominate.

Geogenic components comprise silicates (olivine, pyroxene, amphibole, plagioclase) as well as oxides (magnetite, chromite) and sulphides (pyrrhotite, pentlandite, chalcopyrite, pyrite). Fragments of ore samples from the operating nickel-copper mines near Zapoljarnij (Pechanga (Pechanga area ; Abzalov & Both, 1997), with typical intergrowths textures, showing networks of ino- and phyllosilicates in a sulphide matrix, have been well preserved in snow samples.

The most conspicuous anthropogenic components are well-rounded globules in the 20-60 µ grain size range, derived from smelters at Nikel and Monchegrosk. There are both, sulphide and slag globules; both may also contain oxides in a variety of textural positions. These globules cover a wider compositional field in the Cu-(Ni, Fe, Co)-S-system. Slag particles are mostly of Fe-Mg slicate composition. Alloys also occur; Fe tends to be a major component. PGE alloys are extremely rare and have only been observed in samples form Monchegorsk.

- Routine analyses of 40 elements were performed at GTK in Rovaniemi, Finland. The analytical spectrum included the platinum group elements (PGE). Their distribution patterns reveal distinct differences between samples from Nikel, where mostly low-PGE Pechenga (average 1 ppm Pd) ores are processed, and samples from Monchegorsk where Pechenga ores are mixed with ores from the PGE rich (total ≈ 6 ppm) Norilsk deposits in northern Siberia.

- Soil samples have been taken at all Kola localities from exactly the same points (GPS monitoring) from which the snow samples had been derived. Soil samples represent about 60 years of industrial input; nickel mining and processing in the Kola peninsula commenced in the 1930ies (Boyd et.al., 1997). Mineralogy of samples from both media show many similarities; the major difference is the advanced stage of oxidation observed in many sulphides, both geogenic and anthropogenic (Gregurek et.al, 1999). Unless individual grains are embedded in silicates or slag, or covered by a slag or oxide rim, alteration to Fe-oxides and hydroxides has advanced significantly. Frequently sulphates and, especially, melanterite ($FeSO_4 . 7H_2O$) has been formed. PGE in soils seem to be rather "static"; compared to snow samples PGE in soils are significantly higher, i.e. 7µg vs 189 µg in snow and soil from a locality near Monchegorsk.

4 THE BARENTS PROJECT

This international project may b e considered an extension and continuation of the Kola project, covering a much larger area and focussing on

differences between pristine areas without any industrial activity and areas contaminated by varies industries. Comprehensive geochemical analyses (40 elements, ICP-MS) have already been performed by the Geological Survey of Finland (GTK), Rovaniemi. Representative soil samples from the O-horizon of the nine catchments have been processed at Leoben; magnetic and non-magnetic mineral fractions have been obtained after removal of organic matter by H_2O_2; some samples have been treated by heavy liquids (tetrabromethane, $\rho = 2.96$)) to obtain fractions with $D > 3$. Polished sections, as well as polished thin sections, have been prepared from these concentrates. Pristine areas are characterised by opaque mineral associations linked to bed-rock compositions, i.e. widespread oriented ilmenite-hematite and hematite-ilmenite intergrowths in areas dominated by gneisses and granitoids. A wider spectrum of primary rock components, including chromite and magnetite, can be observed in areas dominated by river sediments, i.e. Narjan Mar. Various anthropogenic components, including slags, coke particles, alloys and globules have been identified. Detailed evaluation of the results aims at correlating mineralogical compositions as revealed by reflected light microscopy with distinct types of industrial activity, and with the results of geochemical analyses. This will facilitate recognition of mineral carriers of potentially hazardous elements.

5 CONCLUSIONS

Reflected light microscopy and microprobe analyses of geogenic and anthropogenic components in snow filter residues, soil samples and heavy mineral concentrates obtained from soils and sediments have emerged as a powerful tool in environmental investigations. Carriers of potentially hazardous elements can be identified as, either, unstable (sulphides) or stable (oxides, silicates) in soils and sediments. Distinct mineral and phase associations can be attributed to geological environments (rock types, operating mines) or to sources of industrial pollution (smelters, thermal power stations, cement plants etc.).

6 ACKNOWLEDGEMENTS

The Austrian Research Fund (FWF, Vienna) generously supported the mineralogical investigations through grant No. 11 983 CHE to E.F. Stumpfl. H. Mühlhans and H. Seiser, both of the Leoben Mineralogy Group, prepared excellent thin and polished section of snow filtrates and mineral concentrates.

7 REFERENCES

Abzalov, M.Z., Both, R. (1997) The Pechenga Ni-Cu deposits, Russia: data on PGE and Au distribution and sulphur isotope compositions. Mineral Petrol 61: 119-143

Äyräs, M., Reimann, C. (1995) Joint ecogeochemical mapping and monitoring in the scale of 1:1 million in the west Murmansk region and continuous area of Finland and Norway-Field handbook. Nor Geol Unders Report 95.111, 33pp

Boyd, R., Niskavaara, H., Kontas, E., Chekushin, V.A., Pavlov, V., Often, M., Reimann, C. (1997) Anthropogenic noble-metal enrichment of topsoil in the Monchegorsk Area, Kola Peninsula, northwest Russia. J Geochem Explor 58: 283-289

Caritat, P.de, Reimann, C., Äyräs, M., Niskavaara, H., Chekushin, V.A., Pavlov, V. (1996a) Stream water geochemistry from selected catchments on the Kola Peninsula (NW Russia) and neighbouring areas of Finland and Norway. 1. Element levels and sources. Aq Geochem 2: 149-168

Caritat, P.de, Reimann, C., Äyräs, M., Niskavaara, H.,Chekushin, V.A., Pavlov, V. (1996b) Stream water geochemistry from selected catchments on the Kola Peninsula (NW Russia) and neighbouring areas of Finland and Norway 2. Time-series. Aq Geochem 2: 169-184

Gregurek, D., Reimann, C., Stumpfl, E.F. (1998) Trace elements and precious metals in snow samples from the immediate vicinity of nickel processing plans, Kola Peninsula, northwest Russia. Environ Pollution 102: 221-232

Gregurek, D., Melcher. F., Pavlov, V., Reimann, C.,Stumpfl, E.F. (1999) Mineralogy and mineral chemistry of snow filter residues in the vicinity of the nickel-copper processing industry, Kola Peninsula, NW Russia. Mineral Petrol 65: 87-111.

Neinavai, H., Pirkl, H. (1996) Bewertung von Schwermetallverteilungen in Böden und Flußsedimenten mit Hilfe angewandter mineralogischer und geostatistischer Werkzeuge. Berichte der Geologischen Bundesanstalt 34, 67 pp

Reimann, C., Boyd, R., Caritat, Pde., Halleraker, J.H., Kashulina, G., Niskavaara, H., Bogotyrev, I. (1997) Topsoil (0-5 cm) composition in eight Arctic catchments in Northern Europe (Finland, Norway and Russia), Environ Pollution 95: 45-56

Reimann, C., Äyräs, M., Chekushin, V.A., Begotyrev, I., Boyd, R., Caritat, P. de, Dutter, R., Finne, T.E., Halleraker, J.H., Jaeger, O., Kashulina, G., Lehto, O., Niskavaara, H., Pavlov, V., Räisänen, M.L., Strand, T., Volden, T. (1998) Environmental geochemical atlas of the central Barents region. CKE-GTK-NGU Spec. Publ. Trondheim, Norway 745 pp

Tommervik, H., Johansen, B.E., Pedersen, J.P. (1995) Monitoring the effects of air pollution on Nikel-Pechenga (Russia) using remote sensing. Sci Total Environment 160/161: 753-767

The Environmental benefits of reprocessing metalliferous spoil

M. Thornhill
Institutt for geologi og bergteknikk, NTNU, 7491, Trondheim, Norway
maria.thornhill@geo.ntnu.no

ABSTRACT. Wales has had a history of non-ferrous metal mining since the Bronze Age, with the major mining period being during the Nineteenth Century, the legacy of which are some 1 300 former metal mining sites. Of these, 200 have a serious impact on the environment, particularly with regard to the contamination of water sources due to the leaching of residual heavy metals. Reprocessing of metalliferous spoil attempts to achieve overall reductions in metal content and where possible, conversion of metals to a form less susceptible to removal through leaching. Neither of these concerns are addressed by the currently used encapsulation and covering techniques, where the spoil remains untreated with the possibility that a future event will result in further pollution. Successful reprocessing leads directly to an improvement in the site's conditions. Profits from the sale of reprocessed minerals can be used to offset the costs of the remediation program. Other end benefits are improved water quality, prevention of airborne pollution from tailings and increased vegetation. This leads to greater aesthetic and amenity value and compliance with environmental legislation.

1 INTRODUCTION

Reclamation of metalliferous spoil associated with disused non-ferrous metal mines presents a broad spectrum of environmental problems. It is particularly relevant to Wales, which has historically been a major mining area for non-ferrous metals, where mining activities ceased long before statutory controls on mining were in place. However, this topic also has global significance and it's application to sites in Norway is currently under investigation by the author.

The main period of lead mining in Wales was during the Nineteenth Century and until 1870 Wales was one of the world's major lead producers. Inadequate processing methods were responsible for large metal losses and it is estimated that 1 to 1.6 tons of lead were released to the environment for every ton reported in official statistics.

Approximately 1300 former metal mines have been identified in Wales by the Welsh Environmental Protection Agency. Of these, some 200 have a serious impact on the environment, in particular from contamination due to the leaching of residual heavy metals to the aquatic environment and the release of fines. In this study, 11 mines were investigated in order to represent a typical cross-section of Pb-Zn minespoil types.

Physical, chemical and bacterial mineral processing techniques were utilised in this study, together with a range of standard environmental leaching tests. Reprocessing of metalliferous spoil attempts to achieve overall reductions in metal content and where possible, conversion of metals to a form less susceptible to removal through leaching. Neither of these concerns are addressed by the currently used encapsulation and covering techniques, where the spoil remains untreated with the possibility that a future event will result in further pollution.

2 AIMS

- Assessment of the quality of Pb-Zn spoil in a wide range of sites.
- Investigation of the potential for metal removal using mineral processing techniques.
- Consideration of environmental acceptability of raw spoil and processed tailings.
- Production of guidelines for decontamination applicable to other sites.

3 CONCLUSIONS

Successful reprocessing leads directly to an improvement in the site's conditions. Profits from the sale of reprocessed minerals can be used to offset the costs of the remediation program. Other end benefits are improved water quality, prevention of airborne pollution from tailings and increased vegetation. This leads to greater aesthetic and amenity value and compliance with environmental legislation.

Characterisation has proved that spoil at these sites is highly heterogeneous in terms of both size and metal assay. Significant reductions may be made in spoil heavy metal content and reduction in the volume of the contaminated material, reducing the cost of disposal for the latter.

Separation of the fine material from the spoil, which would otherwise be a source airborne contamination, is achieved by successful reprocessing. Tailings produced by successful reprocessing are highly resistant to leaching of residual heavy metal to the aquatic environment. Gravity separation techniques are preferable. No single technique will completely decontaminate a site, due to the extreme heterogeneity in metal assay and size of such spoil. This required that mineral processing techniques applied to spoil from each site were site specific.

4 REFERENCES

Thornhill, M. 1996. A technological appraisal of the reclamation of metalliferous spoil. PhD. Thesis. Division of Materials and Minerals, Cardiff School of Engineering, Cardiff University, Wales, U.K.

Characterization of iron ochre deposits formed by the oxidation processes of sulphides in pyrite and stibnite deposits in the Malé Karpaty Mts.

S. Trtíková
Geological Institute of Slovak Academy of Sciences, Dúbravská cesta 9, 842 26 Bratislava, Slovakia, trtikova@gu.bb.sanet.sk

J. Madejová
Institute of Inorganic Chemistry, Slovak Academy of Sciences, Dúbravská cesta 9, 842 26 Bratislava, Slovakia, uachjmad@savba.savba.sk

M. Chovan
Department of Mineralogy and Petrology, Comenius University, Mlynská dolina G, 842 15 Bratislava, Slovakia, chovan@fns.uniba.sk

J. Lipka
Department of Nuclear Physics, Slovak Technical University, Ilkovi ova 3, 812 19 Bratislava, Slovakia, lipka@elf.stuba.sk

ABSTRACT. The iron ochre deposits formed from mine waters in the region of pyrite and stibnite mines in the Malé Karpaty Mts. in western Slovakia have been investigated. Goethite, opal and jarosite occur as crusts and coatings on the dumps and tailings impoundments. Jarosite, poorly crystalline schwertmannite, goethite, ferrihydrite(?), a mixture of iron arsenates and sulphates, hydrated Fe^{III} silicate(?), amorphous SiO_2 and Al_2O_3 phases precipitate in mine waters and effluents from dumps and tailings impoundments.

1 INTRODUCTION

The pyrite and stibnite deposits in the Malé Karpaty Mts. lie in the western part of Slovakia, between towns Pezinok and Pernek in a nature reserve of the Malé Karpaty Mts. The mineralizations are bound to lenses of black shales in actinolitic shists and amphibolites and are associated with a large tectonized zone. Pyrite of the exhalation and sedimentary *pyrite-pyrrhotite mineralization* was mined (Augustín, Michal, Pernek-Krí nica deposits), its exploitation flourished between 1850 and 1896. The hydrothermal *Sb-As-Au mineralization,* with arsenopyrite, pyrite, stibnite and gudmundite as dominant ore minerals, cuts through the pyrite-pyrrhotite one and is connected with intense carbonatization process as well. Two Sb deposits were exploited: Pernek-Krí nica deposit (1790 – 1922) where several abandoned dumps remained, and the Kolársky Vrch deposit (1790 – 1991) where the waste after flotation processing was deposited in three tailings impoundments since 1906. All mining activities on these deposits have ended and the tailings impoundments are now inactive.

The weathering of ore-bearing rocks and the production of secondary minerals in the pyrite and stibnite deposits in the Malé Karpaty Mts. are intensified by mining activities. A wide variety of secondary minerals has been reported: allophane, azurite, cervantite, chapmanite, destinezite, gypsum, halloysite, hematite, jarosite, kaolinite, kermesite, limonite, malachite, Mn oxides and hydroxides, opal, Sb ochre, schafarzikite, scorodite, senarmontite, siderite, stibioconite and valentinite (for complete overview of mineral inventory see Kod ra ed., 1990 and Uher et al., 2000).

2 ANALYTICAL TECHNIQUES

Freshly precipitated iron oxyhydroxides were sampled for further processing and water pH was measured in mine drainage and effluents from tailings impoundments. Samples of mine drainage waters and HCl (1M) extracts of iron oxyhydroxides were analysed for Fe_{tot} (AAS with atomization in air-acetylene flame), Al (atomic emission spectroscopy with inductively coupled plasma), As, Sb (AAS with hydride generation), SO_4 (gravimetry), Cd, Cu, Mn, Pb, Si, Zn, Na and K (AAS) (Chemical laboratories of analytic methods of the Faculty of Natural Sciences, Comenius University, Bratislava and the Slovak Academy of Science, Banská Bystrica). Oxalate soluble Fe (Fe_o) was determined after dissolution in ammonium oxalate (Schwertmann 1964; van Reeuwijk et al. 1995). Minerals have been identified and characterized by X-ray powder diffraction (XRD), transmission electron micrography (TEM) coupled with analytical electron microscopy (AEM), infrared spectroscopy (IR), Mössbauer spectroscopy (MS), differential thermal and thermogravimetric analyses (DTA, TGA). Munsell colour chart for colour determination of dried samples was used. Identification of chemolithotrophic bacteria in mine waters was accomplished by isolation tests. Polished sections of hard pans of Fe oxide minerals were studied by means of optical microscopy, scanning electron microscopy (SEM), electronprobe microanalysing and XRD.

3 RESULTS AND DISCUSSION

Iron oxyhydroxides of the hard pans from sulphide-containing dump rocks – especially actinolitic schists – and from the vadose zones and paleosurfaces replace sulphide grains (mainly pyrite, arsenopyrite and gudmundite) and cement rockforming material. Goethite, opal and jarosite occur as main mineral species in these crusts and coatings.

Jarosite was identified in the samples of fresh iron ochre precipitates formed in acid conditions (pH = 2.5-3) of mine dump effluents in the pyrite deposit at Augustín. The samples collected from identical sampling points eight months later contained schwertmannite. This change is likely to be a consequence of temporal depletion of S and a slight increase of pH in the mine drainage. However, iron ochre precipitates from the pyrite deposit of Augustín exhibit a low mole ratio Fe_{tot}/S_{tot}. Therefore, the main component is poorly crystalline nonsulphate compound, probably goethite. Microbial activity of *Thiobacillus ferrooxidans, Th. thiooxidans* and *Leptospirillum ferrooxidans* has been recognized.

Schwertmannite was detected also in fresh ochres, precipitated from weakly acidic water in the opening of an adit at the pyrite – stibnite deposit at Pernek-Krí nica. Ferrihydrite could be also formed in these precipitates, however, its presence has not been proved reliably. In the overlying adit at Zubau goethite is present besides other non-specified oxyhydroxides. Fresh iron ochre sediments from this deposit accumulate Si (4.72 – 8.96 wt.%) and Al (1.98 – 4.70 wt.%), but their speciation is not determined. Poorly-ordered hydrated ferric silicate was identified by IR absorption spectroscopy.

In weakly acidic to neutral mine waters of the pyrite deposit at Michal fresh ochres of yellow-brownish colour are formed, with low contents of S and high concentrations of Al and Si. Their mineral composition is unclear due to their amorphous character. Several species of bacteria *Bacillus* were identified in the marsh, filled by these young ochres.

Samples of yellow-red ochre accretions produced in tailings effluents of the Sb-Au deposit at Kolársky vrch are exceptional because of their high contents of As (13.99 wt.% – 15.73 wt.%) and S (5.00 – 5.32 wt.%). Freshly precipitated accumulations are extremely poorly crystalline and most likely consist of iron arsenate and sulphate compounds. Precipitates of similar composition have been described by several authors (Leblanc et al. 1996; Pichler et al. 1999). However, As-S-rich iron ochres from the Malé Karpaty Mts. are formed at higher pH (7.45 - 7.90) than ochres described by these authors.

Fresh iron ochre deposits formed by the oxidation of sulphides in the deposits of the Malé Karpaty Mts. accumulate a number of toxic elements. Because of their continuing

production and generally low stability in changing conditions the iron oxide and related minerals are a potential source of pollution.

4 REFERENCES

Kod ra, P. (Ed.) 1990. Topographic mineralogy of Slovakia (in Slovak). Vol. 2, 1st edn. SAV, Bratislava, 1590 pp.

Uher, P., Silvio, M. & Vitáloš, J. 2000. The Pezinok Antimony Mine, Malé Karpaty Mountains, Slovakia. Mineralogical Record 31, March – April, 153-162.

Schwertmann, U. 1964. Differenzierung der Eisenoxide des Bodens durch Extraktion mit Ammoniumoxalat-Lösung. Zeits. Pflanzenernähr. Düng. Bodenk. 105, 194-202.

van Reeuwijk, L. P. (Ed.) 1995. Procedures for soil analyses. International soil reference and information, FAO UN, Wageningen, Netherlands, 125-126.

Pichler, Th., Veizer, J. & Hall, G. E. M. 1999. Natural input of arsenic into a coral-reef ecosystem by hydrothermal fluids and its removal by Fe(III) oxyhydroxides. Environ. Sci. Technol. 33, 1373-1378.

Leblanc, M., Achard, B., Othman, D. B. & Luck, J. M. 1996. Accumulation of arsenic from acidic mine waters by ferruginous bacterial accretions (stromatolites). Appl. Geochem. 11, 541-554.

SEM-EDS studies on the occurrence and mineralogy of gold in a modern, sea-floor massive sulfide deposit, Gorda Ridge, NE Pacific

T.O. Törmänen
University of Oulu, Dept. of Geosciences, Linnanmaa, FIN-90014, Oulu, Finland
tuomo.tormanen@oulu.fi

ABSTRACT. The sediment-hosted massive sea-floor sulfide deposits of southern Gorda Ridge (Escanaba trough) have an average gold content of about 1.3 ppm, with a maximum of about 10 ppm. Elevated gold contents are known to occur in a number of modern sea floor deposits, but in many cases the actual mineralogical host for gold has remained enigmatic, as discrete Au grains have not been found. Careful scanning electron microscope (SEM) investigations of gold-rich samples revealed the presence of minute gold and maldonite grains, ranging in size from < 0.1 μm to about 2 μm. They are mostly associated with various Bi-minerals and, less frequently, with sulfarsenides and galena. This represents a new type of gold paragenesis for sea-foor massive sulfide deposits, where gold is usually associated with sphalerite, pyrite, and chalcopyrite.

1 INTRODUCTION

The first low-temperature sea-floor hot springs and associated hydrothermal mounds were found from the Galápagos Rift in 1977 (Corliss et al. 1979). The first high-temperature vents and massive sulfide deposits were discovered soon after, from the East Pacific Rise (Francheteau et al. 1979, RISE Project Group 1980). Since then sulfide deposits have been found from numerous locations in the Pacific and Atlantic Oceans. Most of these deposits occur on sediment-starved sea-floor spreading centres, but a few sediment-hosted deposits are also known, of which the Escanaba trough deposit at southern Gorda Ridge is one example.

2 GEOLOGIC SETTING

The 300 km long Gorda Ridge is the southern part of the NE Pacific sea-floor spreading system. It is located some 250 km offshore of the northern California-southern Oregon coast-line. Escanaba trough forms the southern, sediment filled part of Gorda Ridge. The ridge is comprised of a relatively wide axial valley and steep flanking ridges that rise up to 1500 m above the valley floor. The sediment fill is locally disturbed and uplifted at centres of igneous and volcanic activity.

3 MASSIVE SULFIDE DEPOSITS

Massive sulfide deposits occur on the flanks of small sediment hills, which were uplifted by the intrusion of basaltic sills in to the underlying sediments. The extent of individual mineralized areas can measure up to hundreds of meters. Massive sulfides occur in the form of mounds, flat lying slabs, breccia, and rubble.

The recovered material can be classified into pyrrhotite-rich sulfides, polymetallic sulfides, and sulfate-rich samples, based on chemical composition and mineralogy. The pyrrhotite-rich type is the most common of the three types.

Sulfate-rich material is mostly made of small barite-rich chimneys and thin crusts covering massive sulfides. In addition, anhydrite-rich sinter occurs at active low-temperature vent sites.

Polymetallic sulfides were recovered from one dredging site.

4 WHOLE-ROCK CHEMISTRY

The average chemical composition of different types of material is presented in table 1. Pyrrhotite-rich samples are characterized by relatively high Cu (up to 20 %), Co (up to 3000 ppm), As (up to 1.5 %), Bi (up to 800 ppm),and Au (up to 10 ppm) concentrations. Polymetallic samples contain lower concentrations of Cu and especially Au (<0.2 ppm), but are strongly enriched in Zn, Pb, As, Sb, Se, Sn, and Ag. Sulfate-rich material contain lower average concentrations of metals, except for Zn, Pb, Ag, and Sb. Some sulfate-rich samples are gold-rich with up to 9.1 ppm of Au.

Compared to other sea-floor sulfide deposits the pyrrhotite-rich sulfides from Escanaba trough are enriched in As, Bi, Se, Co, and Sb, with comparable Au concentrations. In most other sea-floor deposits Au correlates with Zn, Sb, Ag, As, and Pb, whereas at Escanaba trough Au correlates with Cu, Co, Bi, and to lesser extent with As.

Table 1. Average concentrations of selected elements in the sulfide-sulfate samples from Escanaba trough.

Sample	Pyrrhotite-rich	Polymetallic	Sulfate-rich
Cu %	2.4	1.4	0.16
Zn	1.9	22.7	7.2
Pb	0.2	7.2	1.4
As	1.5	2.0	0.2
Au ppm	1.4	<0.2	1.7
Ag	50	725	165
Bi	64	53	2.3
Co	440	2	19
Sb	142	4987	378
Se	207	544	55
Sn	140	946	54

5 ORE MINERALOGY

5.1 *Sulfides and sulfosalts*

Pyrrhotite is the most abundant sulfide mineral, followed by less abundant isocubanite ($CuFe_2S_3$) and sphalerite, although sphalerite is the dominant sulfide in sulfate-rich and polymetallic samples. Pyrite and marcasite are fairly scarce and occur mostly in sulfate-rich samples and as alteration product of pyrrhotite. Galena is minor phase found from all of the sample types, whereas various sulf- and diarsenides occur only in the sulfide-rich types. Analyzed sulfarsenides and diarsenides include arsenopyrite, glaucodot, löllingite, and safflorite. Other minor or rare phases include tetrahedrite, stannite, alabandite, various Pb-sulfosalts, Bi-minerals, gold, and maldonite.

5.2 *Bi-minerals*

The occurrence of a number of different Bi containing phases is typical for the pyrrhotite-rich sulfides of Escanaba trough, and distinguish it from other sea-floor sulfide deposits. The most common phases are native Bi and various Bi-tellurides. The composition of Bi-tellurides show an almost complete range from about 48 to about 82 at. % Bi. In addition some samples contain Bi-sulfides (bismuthinite Bi_2S_3 and possibly ikunolite Bi_4S_3) and various BiTeS-phases (joseite-series) (figure 1).

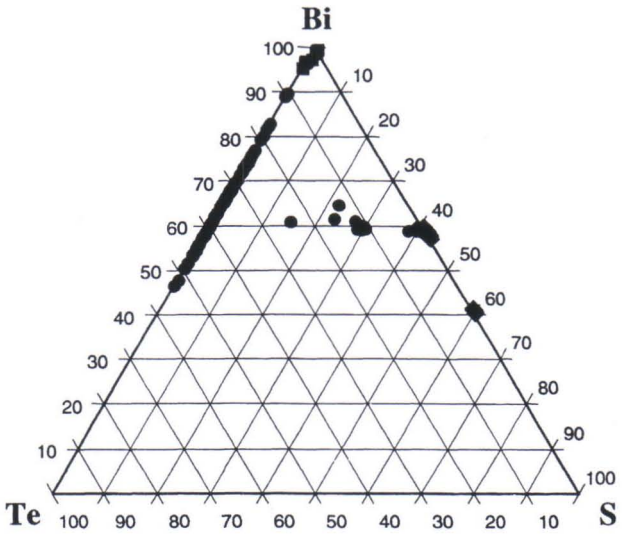

Figure 1. Composition of the different Bi-phases analyzed from Escanaba trough on a Bi-Te-S ternary diagram.

Bismuth minerals occur as small, micrometer-sized grains on the edges of pyrrhotite and isocubanite, and more rarely, as inclusions in base metal sulfides (BMS). Sphalerite does not host any Bi-minerals, and only an a rare occasion do they occur with galena. In addition to pyrrhotite and isocubanite Bi-minerals, mainly native Bi, occur as very small (≤1 μm) inclusions-exsolutions in sulf- and diarsenides. Textures imply that Bi-phases presipitated nearly contemporaneously with pyrrhotite and isocubanite, but preceded galena.

Bismuth minerals and their paragenesis is important as gold (and maldonite) occurs almost exclusively with these phases.

5.3 *Au-bearing phases*

Altogether, more than 500 grains of gold-bearing phases were found from 16 different samples. Most of the grains are native gold (with variable Ag content), but maldonite (Au_2Bi) Is important Au-carrier in some samples. In addition, two grains of a rare $AuBi_5S_4$-phase were also found. The composition of this mineral is almost identical with a $AuBi_5S_4$-phase described by Hamasaki et al. (1986) and Dobosi and Nagy (1989).

There are two different modes of gold occurrence, based on the chemical composition, texture, grain size, and paragenesis. The first and most common group is represented by fine-grained (≤1.0 μm) gold (and maldonite), with variable Ag content, associated with Bi-phases (and sulf- diarsenides). Gold grains belonging to the second group are usually slightly larger, and they have porous, colloidal, or flaky textures. The Ag content is very low, less than 0.5 wt. %. Gold grains belonging to the second type occur with pyrrhotite, which is totally altered/replaced by Fe-sulfates and native sulfur. This type of gold has been named as secondary gold, whereas the first type is called primary gold.

5.4 Primary gold

Gold and maldonite belonging to the so-called primary gold group represent about 78 % of all Au-bearing grains found. The average grain sizes of gold and maldonite are about 0.4 μm and 0.6 μm, respectively, with 75 % of the total population having an average diameter of 0.5 μm or less (figure 2).

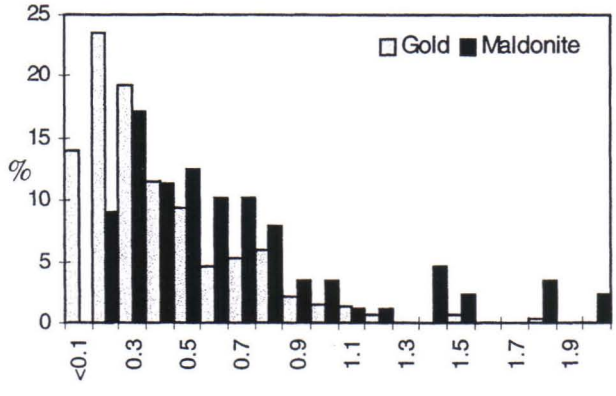

Figure 2. Grain size distribution of gold and maldonite

As can be seen from table 2, 75 % of gold and 53 % of maldonite grains are associated with Bi-phases. In addition, some of the grains that occur with sulf- or diarsenides are also associated with a Bi-phase, especially as native Bi inclusions are common in sulfrasenides. The same applies to the gold-galena association.

Table 2. Distribution (percentages) of gold, maldonite and secondary gold between various host phases

Host phase	Bi-phase	MeAsS MeAs2	Gl (±Bi)	Tetra.	Int. or BMS
Gold	75	14	7	1	3
Au2Bi	53	44			3
Secon-dary Au					100

Gl=galena, Tetra=tetrahedrite, Int.=interstitial

Native Bi and various Bi-tellurides are the most common mineralogical hosts for Au grains. Gold usually occurs as small blebs along the edges of the Bi-grain. In some cases gold occurs as very small grains (≤0.25 μm) scattered through the small (1-5 μm sized) Bi-phase (figure 3).

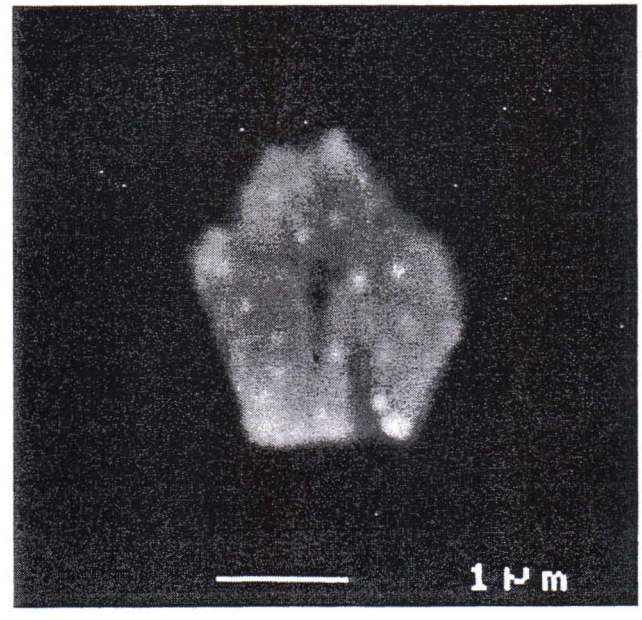

Figure 3. SEM-image (BS) of a small altered native Bi grain with several fine grained Au inclusions.

As seen on table 2, some gold occurs also with galena. However, this type of paragenesis is fairly rare and occurs only in one sample. There is also usually a Bi-phase present, and Au grains occur either in the Bi-phase, or located between Bi and galena. In the Bi-galena case the

composition of the gold varies, depending, at least to some extent, of the host. Gold grains included in a Bi-phase seem to be fairly pure (only semi-quantitative SEM-EDS analyses were possible due to the very small grain size), whereas gold associated with galena is more Ag-rich (up to about 30 wt. % Ag).

Maldonite is fairly rare mineral in the Escanaba trough samples but is more abundant in one sample, which represents a cross section of a narrow, isocubanite lined high-temperature fluid channel. Maldonite occurs mostly with Bi-minerals, especially Bi-sulfides and BiTeS-minerals (joseite group) but also fairly often with sulfarsenides (see table 2).

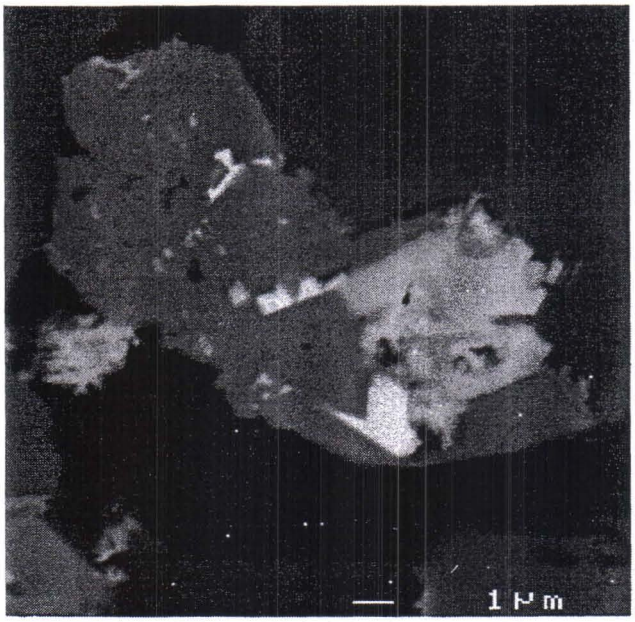

Figure 4. Small maldonite grain (largest white) with altered Bi-phase (light gray) in sulfarsenide (medium gray).

5.5 Secondary gold

Secondary gold forms a separate group from the primary gold-phases. Secondary Au has been found from two samples, both showing extensive pyrrhotite alteration to Fe-sulfates. The average grain size is about 2 µm, largest grains measuring up to about 10 µm. Grain shapes are variable and many grains seem to be made of smaller particles down to 0.1µm or less in size. Grains are often porous and wafer-like, and show strong variation in brightness on backscattered electron images, which is probably due to variation in thickness. Electron microprobe and SEM-EDS analyses resulted in low and highly variable totals. Despite the low totals EPMA analyses indicate that the Ag content of secondary gold is very low (<0.5 wt.%).

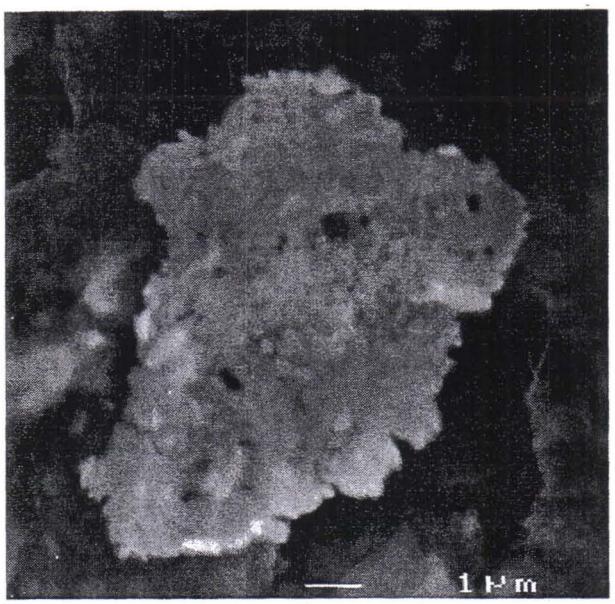

Figure 5. Secondary electron image of a secondary Au grain (FE-SEM).

5 EPMA AND SEM-EDS ANALYSES

Due to the small grain size of gold-bearing phases SEM-EDS system was used for analyses, except for a few trials with electron microprobe.

In practise it proved possible to get quantitative or semiquantitative SEM-EDS analyses of gold and maldonite grains down to about 0.8 µm in size. Altogether 64 analyses were made of gold, maldonite, and $AuBi_5S_4$, of which 24 analyses had totals greater than 96 %. The Ag content of gold grains varies from 0.78 to 32.49 wt. %, with an average of 13.7 wt. %. No other elements, such as Hg were detected within the detection limits of EDS (about 0.3 to 0.5 wt.%)

Maldonite is fairly pure Au_2Bi, some grains analyzed contained small amount of Ag. The two small grains of the $AuBi_5S_4$ phase were both analyzed and the best result is given in table 3, along with some gold and maldonite analyses. All the gold and maldonite grains found occur in the pyrrhotite-rich sulfides. No discrete Au-bearing phases were located from the sulfate-type samples although they also can be enriched in Au. However, some of these samples contain As-rich pyrite, which could contain significant amounts of "invisible" or refrectory gold (Fleet et al. 1993).

Table 3. Examples of SEM-EDS analyses of gold, AuAg (electrum), maldonite and unnamed $AuBi_5S_4$.

	Au	AuAg	Au_2Bi	$AuBi_5S_4$
Au	92.28	65.24	64.13	14.38
Ag	7.12	32.49	n.d.	n.d.
Bi	n.d.	n.d.	35.57	75.44
S	n.d.	n.d.	n.d.	8.79
Total	99.40	96.64	99.70	98.61
Atom. %				
Au	87.65	53.23	65.67	10.31
Ag	12.35	46.77	n.d.	n.d.
Bi	n.d.	n.d.	34.33	50.98
S	n.d.	n.d.	n.d.	38.71

6 CONCLUSIONS

Careful electron microscopy has revealed the presence of discrete gold and maldonite grain in the Au-rich samples from Escanaba trough. Elevated Au contents are known to occur in a number of sea-floor sulfide deposits, but in many cases the exact mineralogical location has remained enigmatic. Where found, gold grains are located in sphalerite, pyrite, chalcopyrite, and more rarely in tetrahedrite-tennantite. The Au-Bi association at Escanaba trough is unique, among the known deposits, and is more resembling of a Au-skarn deposits, than volcanogenic massive sulfide deposit (Meinert 1989).

7 REFERENCES

Corliss, J.B., Dymond, J., Gordon, L.I. et al. (1979). Submarine thermal springs on the Galápagos Rift. Science, 203, 1073-1083.

Dobosi, G. and Nagy, B. (1989). The occurrence of an Au-Bi sulphide in the Nagybšrzsšny hydrothermal ore deposit, northern Hungary. Neues Jahrbuch fur Mineralogie Monatshefte, 1, 8-14.

Fleet, M.E., Chryssoulis, S.L., MacLean, P.J., Davidson, R., and Weisener, C.G. (1993). Arsenian pyrite from gold deposits: Au and As distribution investigated by SIMS and EMP, and color staining and surface oxidation by XPS and LIMS. The Canadian Mineralogist, 31, 1-17.

Hamasaki, S., Murao, S., Koshino, K., Watanabe, M and Soeda, A. (1986). Unnamed Au-Bi sulfide from the Tsugahira mine, southern Kyushu, SW Japan. Neues Jahrbuch fur Mineralogie Monatshefte, 9, 416-422.

Meinert, L.D. (1989). Gold Skarn Deposits - Geology and Exploration Criteria. Economic Geology Monograph, 6, 537-552.

RISE Project Group (1980). East Pacific Rise: Hot springs and geophysical experiments. Science, 207, 1421-1433.

Textural aspects of metamorphosed sulphide ores

F.M. Vokes
Norwegian University of Science and Technology, Trondheim, Norway.
frank.m.vokes@geo.ntnu.no

ABSTRACT. Stratabound, often stratiform, sulphide ores of the VHMS and SHMS types are among the most characteristic metalliferous deposits of orogenic or "fold-mountain" belts, such as, for example the Caledonian-Applachian belt. Their depositional environments were generated during all the stages of a plate-tectonic cycle, with the possible exception of the final collision stage. As a result, ores of these types, together with their host rocks, have been affected to greater or lesser degrees by metamorphic and deformational episodes during the orogenic cycle. The metamorphic effects seen in the ores are generally similar to those seen in the host rocks, though a number of additional features result from the ore minerals' special chemical and physical properties. Perhaps the most striking results of sulphide-ore metamorphism, ones which have been recognised for many years and extensively documented, are the changes in ore textures (Gefüge or fabric) resulting from i) recrystallisation and coarsening of component minerals with increasing grade of metamorphism, ii) deformation, both ductile and brittle, at various stages with respect to i), and iii) remobilisation of ore components, mainly within the ores, but to some extents external to these.

1 INTRODUCTION

The term "ore" means different things to different people, including professional geologists. It is often used in an economic sense to denote accumulations of minerals, generally metallic ones, that are, at least potentially, mineable with profit. The term will not be used in this sense in the following, but will denote rocks with high contents of metallic minerals, mainly sulphides. They may have been formed by processes which differ in many respects from those forming their enclosing lithologies, but like these they are subject to modification by subsequent processes acting on or within the earth's crust.

Ores are rather special kinds of rocks in that they are relatively rare phenomena in the earth's crust as a whole. Also from the point of view of this presentation the rheological properties and chemical reactivities may be very different from those of their enclosing, or host, rocks. These differences govern their responses to processes, such as metamorphism and deformation, which act upon them subsequent to their initial deposition.

In the following, emphasis will be laid almost exclusively on ores of the stratabound, often stratiform, types now occurring in many of the orogenic or fold-mountain belts of the earth, in variably metamorphosed volcanic, sedimentary and mixed lithologies. Present consensus is that they are *syngenetic* in origin, that is, they were deposited (pene)contemporaneously with their enclosing, or host rocks. However, during the last 20 years or so, some workers have questioned the syngenetic, pre-orogenic, nature of a number of large, stratabound, base-metal sulphide deposits in metamorphic terranes, especially in Australia. Their views do not seem to have won wide acceptance in other parts of the world, though interested readers may like to refer to an exhaustive review of the subject which is *in press* at the present time (Marshall & Spry, 2000).

2 STRATABOUND SULPHIDE ORES

The ores are characterised by high contents of pyrite and/or pyrrhotite, together with various combinations of chalcopyrite, sphalerite, and in some types, galena. On the basis of their base-metal contents the ores may be classified as Cu-, Cu-Zn-, or Zn-Pb-Cu-types, though the majority fall into the Cu-Zn category. The aggregation of the ores varies from massive, with sulphides often comprising well over 90% of the total ore volume, through semi-massive, to disseminated with less than 10 vol. % sulphides. The massive ores typically represent the stratiform, syngenetic elements of the deposits, originally deposited on or close to the contemporaneous sea floor. More disseminated types can in some places be recognised as the originally epigenetic feeder zone mineralisation beneath the massive units. Such recognition is dependent on the metamorphic and deformational states of the individual ore bodies and their surroundings. In areas of high deformation, original ore-body morphology is very much modified; in extreme cases the original, pre-orogenic, morphology may not be decipherable.

3 EFFECTS OF METAMORPHISM

Stratabound sulphide ores may be affected by all the forms of metamorphism which affect rocks of the earth's crust. However regional metamorphism is undoubtedly the most important in this respect, due to the enormous areas it affects and to the often high-grade conditions of temperature and of directed, as well as of static, pressure that it involves. It leads to a wide spectrum of changes, both in the ores and their enclosing rocks; not only is recrystallisation induced by temperature changes, both prograde and retrograde, but the dynamic factor leads to deformational movements at all scales, additionally affecting the fabrics of the ores and their host rocks. Superimposed on the recrystallisational and deformational textures may be observed features due to the remobilisation of mineral components originating within the ores or their close surroundings.

The resulting textures of metamorphosed sulphide ores are in general combinations of primary textures inherited from the pre-metamorphic ore, and secondary ones imposed by the metamorphic/deformational processes. The more intensely a deposit has been metamorphosed, the more strongly will the secondary component of texture dominate. At a certain grade, dependent on the type of ore and the degree of deformation involved, the metamorphic component will completely dominate the texture. As King (1958) put it, an ore exposed to conditions of high rank metamorphism "might now have as little resemblance to its original condition as a granite gneiss has to a sandy mudstone". This obliteration of the primary features of sulphide ores by metamorphism has perhaps contributed more than anything else to the past, and present, controversies concerning the origin of massive sulphide ores in high grade terranes.

Currently with the above, there occur certain changes in mineralogy which can effect the fabric of a metamorphosed ore. These include pyrrhotite-pyrite transformations, recombination of trace elements to form new ore minerals, and sulphide-silicate reactions leading to the formation of new gangue minerals.

4 METAMORPHIC FABRICS

The processes leading to the formation of metamorphic texture (fabric) can be discussed under the following headings (after Vokes, 1968,1969).

1). Recrystallisation processes during prograde or retrograde metamorphism. (Crystalloblastesis).

2). Deformation, both of brittle and ductile nature.

3). Remobilization of ore components.

These may act independently of each other, at different times and/or in different parts of an ore body, or they may coincide in time and space. For the purposes of description, the effects of each of the processes will be considered in turn. It must be remembered, however, that the resultant effect on the ore texture will be a compound one, where each of the processes combine in varying proportions to give the final result.

4.1 *Crystalloblastic fabrics.*

As with the non-ore, or gangue, minerals, the ore minerals of massive sulphide ores undergo progressive morphological changes during prograde regional metamorphism. These can be grouped under two headings.

Changes in form or shape. The general result of increasing grade of metamorphism is to produce textures where minerals of high form energy, such as arsenopyrite, pyrite, magnetite,

etc, grow as metacrysts, often as porphyroblasts, in contrast to the surrounding, or *matrix,* minerals of lower form energy, such as galena, chalcopyrite, sphalerite and pyrrhotite. These latter minerals very seldom develop crystal faces and their grain boundary relations are governed by surface tension effects (often expressed as "foam" or "triple junction" texture).

Stanton (e.g., 1972) was was probably the first English-language writer to point out that textures in metamorphosed sulphide ores are not evidence of a paragenetic sequence in which "late" matrix sulphides had infilled early-formed, sub- to euhedral pyrite grains, but expressions of a *crystalloblastic series*, analagous with the classical Becke-Grubemann series for non-sulphide minerals. The degree of idiomorphic development of the high form energy minerals is highly matrix-dependent; pyrite porphyroblasts, for example, reach their greatest size and perfection in a dominantly pyrrhotite matrix. Research on the Appalachian Ducktown ores indicates that such euhedral pyrite grains develop mainly under retrograde conditions when they receive S from pyrrhotite which becomes increasingly more Fe-rich as the temperature wanes (Craig & Vokes, 1993).

Changes in grain size. In general, prograde metamorphism leads to an increase in grain size of massive sulphide ores unless deformation has not caused mechanical reduction of grain size. Over the years, studies from various parts of the world have illustrated this aspect of sulphide ore recrystallisation. For example, Tempelmann-Kluit (1970) after a statistical evaluation of metamorphosed ores from several localities concluded that "the degree of correlation between sulfide grain size (in ore) and metamorphic grade (of host rocks in terms of index minerals) is similar to that between silicate grain size in host rocks and metamorphic grade of host rocks".

In certain parts of the Scandinavian Caledonides it is possible to link increase of grain size in the stratabound pyritic ores rather closely with the increasing metamorphic grade of their enclosing rocks (Vokes, 1968). This may be illustrated by comparing the fine grain size (100-200µm) of the Løkken ore, lying in chlorite-grade rocks, with the coarser-grained (c. 0.2mm) ores in biotite-grade rocks (e.g., Meråker area) and with ores hosted by garnet-grade rocks (e.g., Røros) where the grain size is of the order of 0.5mm or more.

Variations from these general correlations do however occur, even within one and the same ore body. These have been assigned to: a) the so-called matrix effect (see also above) whereby high form energy minerals such as pyrite show a larger grain size in a matrix of low form energy minerals than when they occur as monomineralic aggregates. b) localized pressure effects in different parts of the same ore body, or between different ore bodies in identical metamorphic terranes.

4.2 *Deformational fabrics.*

These are widespread and often very conspicuous in regionally metamorphosed sulphide ores. They vary widely in nature, depending on the relative ductility of the ore mass at the time of deformation (probably a function of the prevailing P and T and the amount of intergranular fluids).

Brittle deformation unaccompanied by recrystallisation is widespread in low metamorphic areas, leading to the formation of cataclastic textures which may be difficult to differentiate from pre-metamorphic (depositional or post-depositional) clastic textures. However, cataclasis of lithified, but unrecrystallised, sulphide ores can be demonstrated in many deposits, as for example in the low metamorphic, extremely fine-grained syngenetic iron sulphide layers known as "vasskis" in the Scandinavian Caledonides. Here, clasts of unrecrystallised pyrite "mudstone" are cemented by new-deposited, coarser, cleaner, pyrite and gangue minerals representing the results of early metamorphic recrystallisation. In other instances, highly-polished, often slickensided, planes cutting fine-grained, unrecrystallised ore provide evidence of brittle deformation without any subsequent metamorphic recrystallisation.

The most obvious evidence of post-recrystallisation brittle deformation are shown by the idioblastic ore minerals of high form energy – such as pyrite, arsenopyrite and magnetite – that are hard and brittle compared with the enveloping matrix minerals. They are frequently cataclastically deformed when the ore mass is subjected to renewed movements, probably under retrograde conditions. Such brittle deformation textures are exemplified by shattered pyrite metablasts, where matrix mineral, especially chalcopyrite, appears to have infilled the shatter cracks and surrounded indi-

vidual pyrite fragments. Such a process implies movement of the matrix mineral, if only over microscopic distances. It is an example of the modification of ore texture by remobilisation. (See also below).

The relatively softer matrix minerals seldom show evidence of brittle deformation, either because they normally react ductilely to deformation (see below) or, because deformational (strain) features have been annealed out during a period of continuing high temperature following deformation. Occasionally, cataclastically deformed or "steel" galena may be observed along late movement planes.

Plastic or ductile deformation is probably the dominant form of deformation in regional dynamo-thermal metamorphism, leading to the development of schistosity and other directed textures in the ores.

Even isometric, high form energy, minerals such as pyrite can be seen to have developed elongated forms, either by distortion of the lattice or by new growth in the direction of minimum strain parallell to the schistosity. Characteristically, such elongated pyrite grains show strain-shadow tails of softer matrix minerals such as pyrrhotite and chalcopyrite - another example of small-scale remobilization. Evidence of mineral growth during deformation is afforded by the spiral fabric often shown by pyrite metacrysts. Such fabrics at Ducktown, Tennessee, have been attributed by Craig et al. (1991) to rotation during metamorphic growth.

Minerals of lower form energy in regionally metamorphosed sulphide ores often show, under the microscope, what may be described as gneissose textures, with undulating extinction being shown by anisotropic minerals such as pyrrhotite. Glide or translational twinning is almost universal in metamorphic sphalerite, while curved or otherwise distorted cleavages are well shown by galena. Perhaps more immediately obvious evidence of the ductile deformation of sulphide ores is afforded by the macro- to mega-scale aspects of fabric. Initial deformation of the ores and their their wall-rocks is shown by the presence of folds varying from more or less open to tight or isoclinal. In ores with silicate- and sulphide-rich interbands, differences of competency during increased intensity of folding – and probably increased temperature of metamorphism - often lead to distinctive deformational fabrics, both at the macro- and micro-scales. Schist bands in the ores may develop detached fold cores, around which the relatively plastic sulphides appear to flow, isolating them in the form of boudins. With continuing deformation these schist boudins, together with clasts of metamorphic "vein" quartz, become rotated in the sulphide mass and take on generally rounded forms. The process may be described as a thorough rotational "kneading" of the whole ore mass, to which the term "Durchbewegung" has been applied. (Vokes, 1973; Marshall & Gilligan, 1989). The non-sulphide clasts in such a "durchbewegt" mass take on a strong resemblance to water-rounded pebbles and acquire a highly polished outer surface due to a thin film or "mirror" of sulphide. In one special example of such a fabric, shown for example by some of the Sulitjelma ores, the "clasts" are highly rounded and polished pyrite porphyroblasts developed prior to the deformational event.

4.3 *Fabrics due to remobilisation*

The role of remobilisation in modifying metamorphic ore textures has already been touched upon in this text. Regional metamorphic remobilisation is a widespread and powerful process which can fundamentally affect the texture (fabric) as well as the gross structure (morphology) and the grade distribution of massive sulphide deposits.

A comprehensive review of the effects of remobilisation is outside the scope of the present abstract. Interested readers are referred to fuller treatments of the subject elsewhere (e.g., Marshall and Gillgan, 1987; Marshall et al. 1999; Marshall et al., 2000). Consensus seems to be that, while solid-state, liquid-state and mixed-state processes are possible for the transfer of components during mobilisation, fluids play a greater role than previously recognised in the modification of the textures of metamorphosed sulphide ores.

In a study of a small deposit in the central Scandinavian Caledonides, Vokes & Craig (1993) documented the veining, and partial replacement, by matrix sulphides, of cataclastic pyrite grains and of partially deformed "foam-textured" pyrite, that had developed in the ore during an earlier phase of metablastesis. In addition, parts of the ore showed patchy quartz grains with replacive relations to both the pyrite and the matrix sulphides. It was concluded that that fluid phase mobilisation of the base-metal sulphides and of the quartz must have played a

dominant role in producing the observed textures. The copper and zinc sulphides were most likely derived from within the ore mass itself; an external source for the quartz seemed most likely.

5 REFERENCES

Craig, J.R. and Vokes, F.M. 1993. The metamorphism of pyrite and pyrite ores: an overview. Mineralogical Magazine 57: 3-18.

Craig, J.R., Vokes, F.M. and Simpson, C. 1991. Rotational fabrics in pyrite from Ducktown, Tennessee. Economic Geology 86: 1737-1746.

King, H.S. 1958. Notes on ore occurrences in highly metamorphosed Precambrian rocks. Australian Institution of Mining Metallurgy, Stilwell Memorial Volume: 143-167.

Marshall, B. and Gilligan, L.B. 1987. An introduction to remobilization: Information from ore-body geometry and considerations. Ore Geology Reviews 2: 87-131.

Marshall, B. and Gilligan, L.B. 1989. Durchbewegung structure, piercement cusps and piercement veins in massive sulfide deposits. Economic Geology 84: 2311-2319.

Marshall. B., Larocque,A.C.L. and Vokes, F.M. 1999. Extensive remobilisation in massive sulphide deposits: A fluid affair! in: Stanley, C.J.et al., (eds.) Mineral deposits: processes to processing. Rotterdam, Balkema: 955-958.

Marshall, B. and Spry, P.G. 2000. Regional metamorphic remobilization and syntectonic emplacement in the genesis of massive sulfide ores: discriminating between them. Reviews in Economic Geology 11: in press.

Marshall, B., Vokes, F.M. and Larocque, A.C.L. 2000. Regional metamorphic remobilization: Upgrading and formation of ore deposits. Reviews in Economic Geology 11: in press.

Stanton, R.L. 1972. Ore Petrology. New York, McGraw Hill: 612-648.

Templelmann-Kluit, D.J. 1970. The relationship between sulfide grain size and metamorphic grade of host rocks in stratabound pyritic ores. Canadian Journal Earth Sciences 7: 1339-1345.

Vokes, F.M. 1968. Regional metamorphism of the Palaeozoic sulphide ore deposits of Norway. Transactions of Mining and Metallurgy, 77: B53-B59.

Vokes, F.M. 1969. A review of the metamorphism of sulphide. Earth Science Reviews 5: 99-143.

Vokes, F.M. 1973. "Ball texture" in sulphide ores. Geologiska Stockholm Förhandlingar 95: 403-406.

Vokes, F.M. & Craig,J.R. 1993. Post-recrystallisation phenomena in metamorphosed stratabound sulphide ores. Mineralogical Magazine 57:19-28.

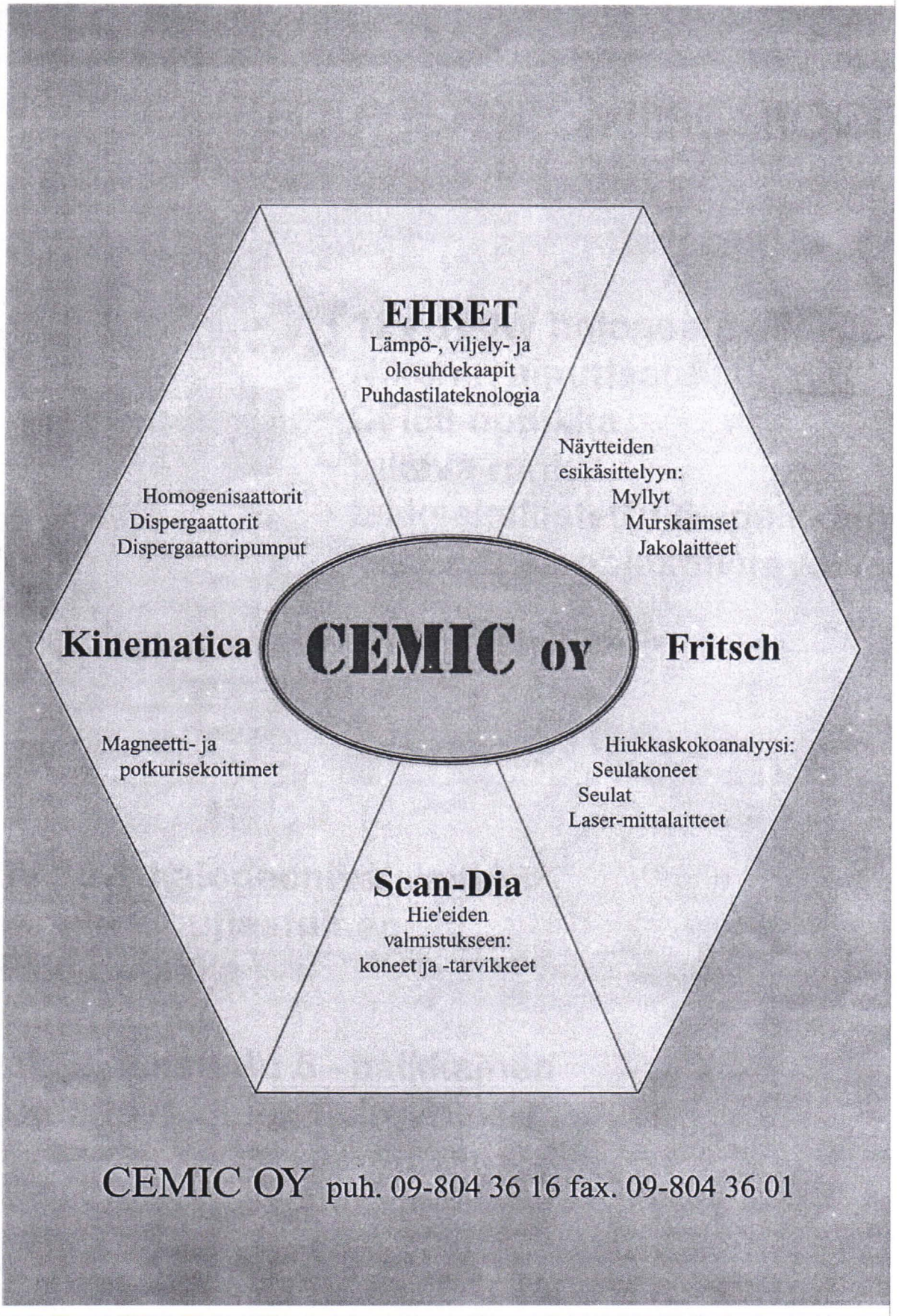

CEMIC OY puh. 09-804 36 16 fax. 09-804 36 01

Nikon ECLIPSE **E600POL**
E400POL

POLARISAATIOMIKROSKOOPIT

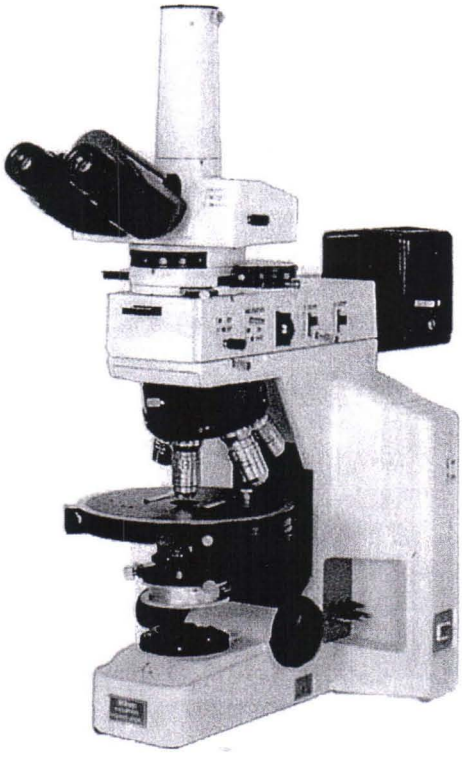

- **12V 100W halogeenivalaisin**
- **Nikonin ainutlaatuinen CFI60 optiikka**
- **tukeva runko**
- **taaksekallistettu 5 –paikkainen keskiöitävä objektiivirevolveri**

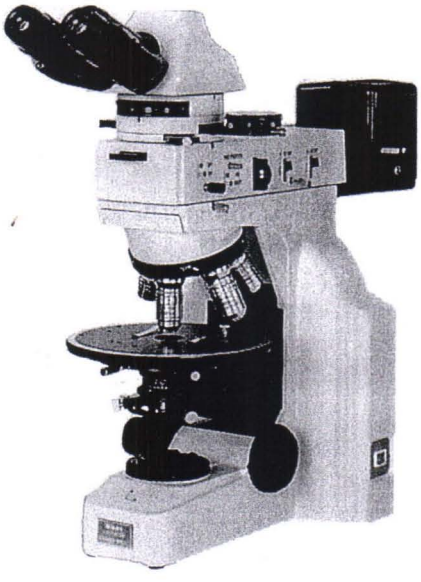

- **60V 30W halogeenivalaisin**
- **Nikonin ainutlaatuinen CFI60 optiikka**
- **tukeva runko**
- **taaksekallistettu 5 –paikkainen keskiöitävä objektiivirevolveri**

FENNOLAB
Tutkimuksesta tuotantoon

Tähtäinkuja 9, 01530 VANTAA
Puh. (09) 2763 6200, Fax (09) 2763 6276

ESEM®

Exceed your Low-Vac SEM expectations

With NEW ESEM gaseous detectors

XL30 ESEM

ONLY ESEM CAN OFFER:

Modes/signal	SE	BSE	EDS
HiVac	✔	✔	✔
LowVac	✔	✔	✔
Environmental	✔	✔	✔

The XL30 ESEM fills the SE/BSE imaging and EDS voids left by the everyday LowVac SEMs. The new Gaseous Backscatter Detector again extends the range of imaging and EDS capabilities for all your applications.

Check out our added value:

- **No compromise in image content (SE for topography, BSE for atomic number difference) in all modes**
- **SE detectors standard for all modes**
- **BSE detectors available for all modes**
- **SE/BSE mixing possible in all modes**
- **Same High Resolution in all modes**

Ask us to show you!

FEI

Tel: +61 2 9413 2889
Fax: +61 2 9413 4619
Email: marcom@nl.feico.com
Web: www.feic.com

PHILIPS

Let's make things better.

Over 60 Years' experience of Geological contracting

* Mineral exploration
* Mining
* Geotechniques, Tunnelling, Civil Engineering
* Groundwater, Aggregates
* Dimension Stones
* Environment

Onram 1000 CCD (Computer Controlled Drill).
Capacity 1200 m size T46 mm.

Geophysical Services

* Survey planning
* Field work
* Data processing
* Map compiling
* Reporting

Drilling Services

Rigs from portable drills to units with capacity of 1500 meters

* Diamond core drilling
* Percussion drillings
* Soil and rock sampling

Geophysical Methods

* Gravity
* Magnetic
* Electromagnetic
* Electrical & IP
* Radiometric
* Seismic
* Radar
* Petrophysics

Auxiliary Drilling Services

* Geological core logging and reporting
* Geophysical hole logging
* Orientated core samples
* Geotechnical test
* 3D deviation surveys
* Directional drilling
* Recording of drilling parameters with computerized rigs

www.smoy.fi

SMOY
SUOMEN MALMI OY

Suomen Malmi Oy (SMOY)
P.O. Box 10, FIN-02921 ESPOO, FINLAND
Tel. + 358-(0)9-8524 010 FAX +358-(0)9-8524 0123
Email: suomen.malmi@smoy.fi

Integrated System

The LEICA Q550IW is an integrated image analysis workstation with a powerful and extensive set of image processing capabilities.

- Ergonomic bench-top unit is designed with the operator's comfort in mind.
- The large, single screen display brings image details to life with astounding clarity and colour.
- Careful attention to the needs of quantitative microscopy ensures the highest possible precision and reliability in your results.
- Compact triple CCD colour cameras are used to obtain high quality RGB images.

Modular and Upgradable

The LEICA Q550IW offers a choice of standard and high resolution CCD TV cameras so the system can be tailored to your needs.

- TWAIN software is available for compatibility with other image sources.
- A range of PC specifications is available to suit your application and budget needs.
- PC based control and data processing assures compatibility with the widest possible range of software and networks.

Note that the capabilities of a particular system will depend on the configuration and options selected. Please refer to the LEICA Image Analysis Systems Product Catalogue for further details of these and the extensive range of advanced applications in life and materials science.

Automation

Automation allows representative samples to be analysed rapidly and consistently, without taxing an operator's endurance and objectivity.

The microscope automation option drives motorised stages precisely and smoothly under program command, while convenient interactive control is always available.

- Focus is automatically maintained while stepping from field to field, such that routine analysis can be performed with minimum intervention from the operator.
- Representative samples are analysed rapidly and consistently.

Image Analysis Software

LEICA QWin is an effective and powerful software suite for image processing and analysis, optimised for quantitative microscopy. The capability of the LEICA Q550IW is defined by the software options selected.

The power of LEICA QWin is made readily accessible to the widest range of potential users through three carefully structured software levels which build on each other's capability.

LEICA QFAB example screen

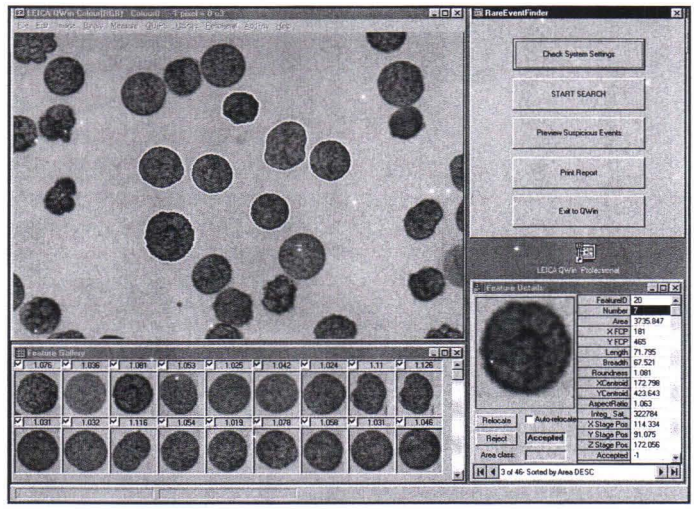

LEICA QWin Lite

- Interactive measurements - draw directly on the screen using the mouse
- Image annotation with arrows, text and calibration scale
- Image printing and documentation
- Storage and image review with LEICA QGallery

LEICA QWin Standard

- Automatic measurement of multiple image features
- Repeatable measuring routines by QUIPS
- Grey and binary image processing
- Image editing and automatic detection
- Results in histogram, scattergram and statistical formats

LEICA QWin Professional

- Advanced grey level morphology
- Fast Fourier Transformation with LEICA QFFT
- Image visualisation and data interpretation through LEICA QFAB
- Customised interface by LEICA QFORM
- Advanced QUIPS for turn-key application development

LEICA LIDA

An impressive image database and archiving system for maintaining, searching, documenting and storing images and data.

Leica

Leica Imaging Systems Ltd
Clifton Road
Cambridge
CB1 3QH UK
Tel: (44) 1223 411101
Fax: (44) 1223 412526
e-mail ia-support@lis.leica.co.uk
Web site: www.leica.co.uk/ia/

Leica Nilomark Oy
Sinimäentie 10 C
PL 111, 02631 Espoo
Puhelin (09) 615 3555
Telefax (09) 502 2398
Email: info@leica.fi
www.leica.com/fi

IA PIB-IA246 - Printed in the UK

LEICA Q550IW

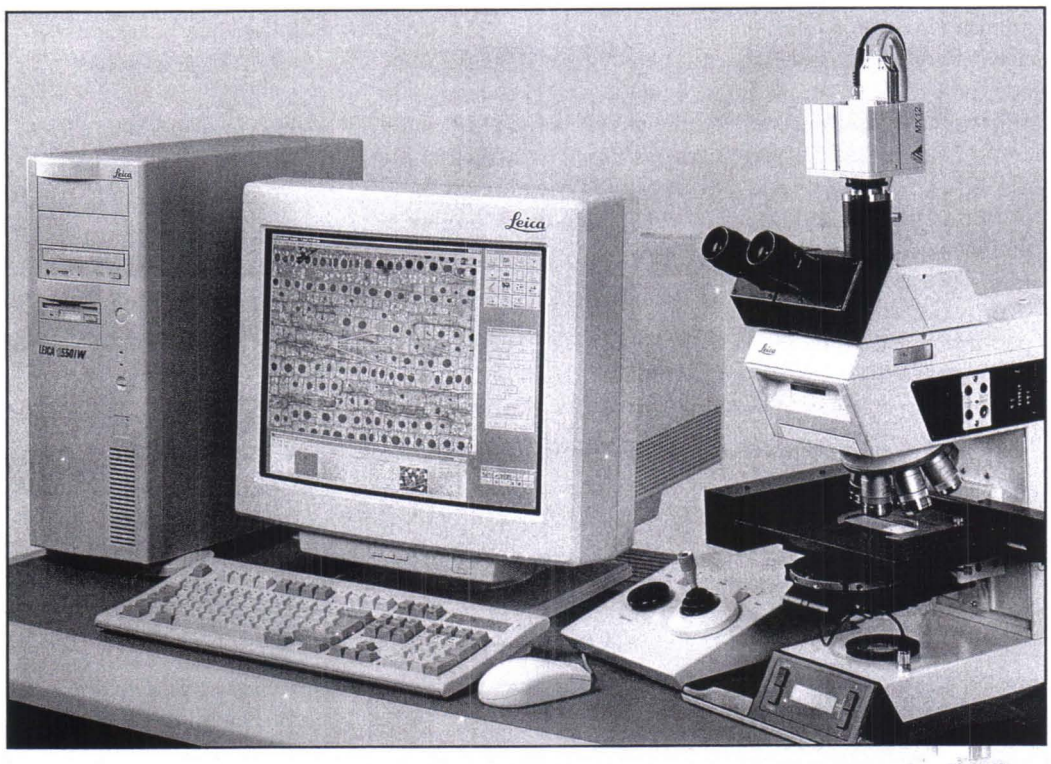

The LEICA Q550IW is a new high resolution, fully integrated image analysis system which builds on the Leica tradition of providing powerful, accurate and user friendly systems at an affordable price.

The LEICA Q550IW leaps ahead with megapixel images and unrivalled performance, speeding through your work; ideal for applications that require fast analysis, high sample throughput and unattended operation.

The LEICA Q550IW combines with LEICA QWin to provide a multitude of image processing and measurement functions.

The richness of image processing functions combined with integrated LEICA QUIPS macro programming software means that the system can solve the most demanding of applications.

Rapidly fitted to any Leica microscope, the full versatility of the system is under your control in moments, yet its potential is unlimited.

Leica Q550 Key Features

- Compatible with a wide range of standard and high resolution CCD TV cameras.
- Modular and adaptable, the PC based systems let you choose the performance and specification.
- In combination with Leica microscopes, the LEICA Q550IW is the ideal tool for accurate and reliable image quantitation.
- Fully automates analysis tasks by moving specimen from field to field.
- The structured LEICA QWin Software Suite allows you to select the level which best meets your requirements in terms of performance and investment.
- Microsoft® Windows™ based graphical user interface, the acknowledged productivity leader.
- Single screen display combines menus and images, making the system a delight to use.

LEICA Q550IW Imaging Workstation
Image Processing and Analysis System

Leica

Tätä julkaisua myy

GEOLOGIAN
TUTKIMUSKESKUS (GTK)
Julkaisumyynti
PL 96
02151 Espoo
☎ 0205 50 11
Telekopio: 0205 50 12

GTK, Väli-Suomen
aluetoimisto
Kirjasto
PL 1237
70211 Kuopio
☎ 0205 50 11
Telekopio: 0205 50 13

GTK, Pohjois-Suomen
aluetoimisto
Kirjasto
PL 77
96101 Rovaniemi
☎ 0205 50 11
Telekopio: 0205 50 14

Denna publikation säljes av

GEOLOGISKA
FORSKNINGSCENTRALEN (GTK)
Publikationsförsäljning
PB 96
02151 Esbo
☎ 0205 50 11
Telefax: 0205 50 12

GFC, Distriktsbyrån för
Mellersta Finland
Biblioteket
PB 1237
70211 Kuopio
☎ 0205 50 11
Telefax: 0205 50 13

GFC, Distriktsbyrån för
Norra Finland
Biblioteket
PB 77
96101 Rovaniemi
☎ 0205 50 11
Telefax: 0205 50 14

This publication can be obtained
from
GEOLOGICAL SURVEY
OF FINLAND (GTK)
Publication sales
P.O. Box 96
FIN-02151 Espoo, Finland
☎ +358 205 50 11
Telefax: +358 205 50 12

GSF, Regional office for
Mid-Finland
Library
P.O. Box 1237
FIN-70211 Kuopio, Finland
☎ +358 205 50 11
Telefax: +358 205 50 13

GSF, Regional office for
Northern Finland
Library
P.O. Box 77
FIN-96101 Rovaniemi, Finland
☎ +358 205 50 11
Telefax: +358 205 50 14

E-mail: info@gsf.fi
WWW-address: http://www.gsf.fi

ISBN 951-690-768-5
ISSN 0781-643X